CLIMATOLOGICAL PATTERNS OF ATLANTA'S URBAN HEAT ISLAND–INITIATED PRECIPITATION

by

PAUL GRADY DIXON

(Under the direction of Thomas L. Mote)

ABSTRACT

Due to Atlanta, Georgia's rapid growth and urbanization over the past few decades, the city has developed a pronounced urban heat island (UHI) that has been shown to enhance and possibly initiate thunderstorms. Therefore, this study attempts to determine if, when, and where the metropolitan Atlanta area induces thunderstorms that might not have initiated otherwise. Land use data, radar reflectivity data, surface meteorological data, upper–air sounding data, and air mass classification (SSC) types are all used to determine if precipitation is initiated by Atlanta. Ultimately, this project illustrates significant spatial and temporal patterns based on a five–year climatology of events. July saw the most events with a diurnal peak just after local midnight. Low–level moisture appears to be the most important factor for UHI induced precipitation, but further research (over a longer time period) is required for more detailed understanding of the primary cause of these events.

INDEX WORDS: Atlanta, Urban Heat Island, Precipitation, Climatology, Climate Change

CLIMATOLOGICAL PATTERNS OF ATLANTA'S URBAN HEAT ISLAND–INITIATED PRECIPITATION

by

PAUL GRADY DIXON

B.S., Mississippi State University, 2000

A Thesis Submitted to the Graduate Faculty of The University of Georgia

in Partial Fulfillment of the Requirements for the Degree

MASTER OF SCIENCE

ATHENS, GEORGIA

2002

CLIMATOLOGICAL PATTERNS OF ATLANTA'S URBAN HEAT ISLAND–INITIATED PRECIPITATION

by

PAUL GRADY DIXON

Approved:

Major Professor:	Thomas L. Mote
Committee:	Andrew J. Grundstein Chor Pang Lo

Electronic Version Approved:

Gordhan L. Patel
Dean of the Graduate School
The University of Georgia
May 2002

ACKNOWLEDGMENTS

I would like to acknowledge the many people who helped me in the completion of this thesis as well as all of my master's work. First and foremost, I would like to thank my wife, Melissa. She was very supportive and tolerant at all times. Also, I must thank those who initially peaked my interest in weather, geography, and research. Thank you Dr. Charles Wax, Dr. Michael Brown, and Dr. Doug Gamble. It was the enthusiasm, encouragement, and friendship from y'all that pushed me to pursue this field as well as graduate study. Likewise, Tim McCarley, thank you for your continued support and motivation…I have learned more from you than I could ever record in a thesis.

A tremendous amount of gratitude is expressed toward my major professor, Dr. Tom Mote. You showed me so much about research and what it takes to be a successful researcher. I now know that your "five–min solutions" to my "all–day problems" are why you "get the big bucks." Also, Dr. Andy Grundstein and Dr. C. P. Lo, thanks for all of your help during my time at UGA. Both of you were always more than willing to answer my many questions no matter how busy you were. In addition, I would like to thank everyone in the Department of Geography who helped me along the way. In particular, the Climate Lab crew of Walker Ashley, Josh Durkee, and Jamie Dyer were all valuable assets while I worked "on the roof."

Part of my funding during my master's work was provided by a USDA Forest Service grant (#SRS 01-CA-11330136-318). Radar reflectivity data was provided by the Global Hydrology Resource Center (GHRC) at the Global Hydrology and Climate

Center, Huntsville, Alabama. Thanks to Dr. Gerritt Hoogenboom, director of the Georgia Automated Environmental Monitoring Network (GAEMN), in Griffin, Georgia for providing GAEMN surface data.

Finally, I want to thank my family and friends who supported me when I decided to stay in school for years and years. Momma, Daddy, Curtis, and Carolyn, your love and support have made life much easier. David Brommer and Buck Bearden, I appreciate your friendship, motivation, and humor as we went through this together.

TABLE OF CONTENTS

Page

CHAPTER

APPENDICES

LIST OF TABLES

LIST OF FIGURES

Page

CHAPTER 1

INTRODUCTION

In the past 30 years, Atlanta, Georgia, has rapidly become the leader among southeastern United States centers for commerce, industry, and transportation. From 1990 to 2000, Georgia was the only state east of the Rocky Mountains to have an increase in population double that of the national rate of 13.2%, and the highest levels of increase were in and around Atlanta. The population of the 20–county area (Figure 1.1), defined by the United States Census Bureau as Atlanta metropolitan statistical area

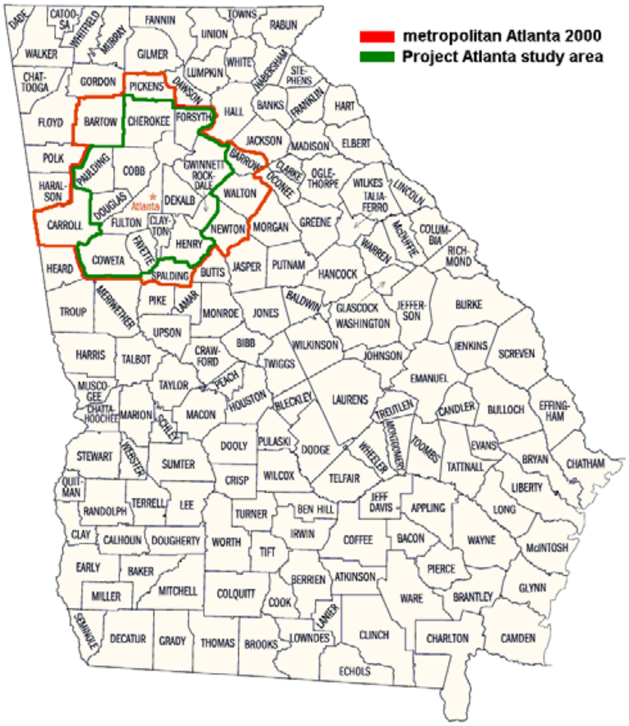

Figure 1.1: County map of Georgia with 20–county Atlanta MSA outlined in red (U.S. Census Bureau 2000) and 13–county Atlanta area used in Project ATLANTA (Daly 2000) outlined in green.

Table 1.1: 15 largest U.S. metropolitan areas ranked by population (U.S. Census Bureau 2000).

Rank	Area Name	Census Population		Change, 1990 to 2000	
		April 1, 2000	April 1, 1990	Number	Percent
1	New York–Northern New Jersey–Long Island, NY–NJ–CT–PA CMSA	21 199 865	19 549 649	1 650 216	8.4%
2	Los Angeles–Riverside–Orange County, CA CMSA	16 373 645	14 531 529	1 842 116	12.7%
3	Chicago–Gary–Kenosha, IL–IN–WI CMSA	9 157 540	8 239 820	917 720	11.1%
4	Washington–Baltimore, DC–MD–VA–WV CMSA	7 608 070	6 727 050	881 020	13.1%
5	San Francisco–Oakland–San Jose, CA CMSA	7 039 362	6 253 311	786 051	12.6%
6	Philadelphia–Wilmington–Atlantic City, PA–NJ–DE–MD CMSA	6 188 463	5 892 937	295 526	5.0%
7	Boston–Worcester–Lawrence, MA–NH–ME–CT CMSA	5 819 100	5 455 403	363 697	6.7%
8	Detroit–Ann Arbor–Flint, MI CMSA	5 456 428	5 187 171	269 257	5.2%
9	Dallas–Fort Worth, TX CMSA	5 221 801	4 037 282	1 184 519	29.3%
10	Houston–Galveston–Brazoria, TX CMSA	4 669 571	3 731 131	938 440	25.2%
11	**Atlanta, GA MSA**	**4 112 198**	**2 959 950**	**1 152 248**	**38.9%**
12	Miami–Fort Lauderdale, FL CMSA	3 876 380	3 192 582	683 798	21.4%
13	Seattle–Tacoma–Bremerton, WA CMSA	3 554 760	2 970 328	584 432	19.7%
14	Phoenix–Mesa, AZ MSA	3 251 876	2 238 480	1 013 396	45.3%
15	Minneapolis–St. Paul, MN–WI MSA	2 968 806	2 538 834	429 972	16.9%

(MSA), has increased by 38.9% since 1990, more than 130% since 1970, and 313% since 1950, to make it the most populated urban area in the southeastern United States. Atlanta was fourth behind Los Angeles–Riverside–Orange County consolidated MSA (CMSA), New York City–Northern New Jersey–Long Island CMSA, and Dallas–Fort Worth CMSA with respect to actual population increase during the 1990s (Table 1.1). However, it should be noted that the Atlanta MSA’s (herewith referred to as *Atlanta*) percentage of population increase during the 1990's (38.9%) was second to only Phoenix–Mesa, Arizona MSA (45.3%) among the 30 most populated urban areas in the United States. More specifically, three Atlanta counties were among the top 10 counties nationwide with respect to percent increase in population from 1990 to 2000. Forsyth County (123.2%) was second, Henry County (103.2%) was fourth, and Paulding County (96.3%) was seventh (Table 1.2). These values show not only the rapid rate at which people have migrated to Atlanta, but due to the fact that Forsyth (northeast), Henry (southeast), and

Table 1.2: Population numbers for Atlanta MSA since 1950 (U.S. Census Bureau).

County	1950 Pop.	1960 Pop.	1970 Pop.	1980 Pop.	1990 Pop.	2000 Pop.	'90–'00 %Change
Metro area	**984 551**	**1 297 989**	**1 746 767**	**2 211 970**	**2 930 229**	**4 066 054**	**39%**
Barrow	13 115	14 485	16 859	21 354	29 721	46 144	55%
Bartow	27 370	28 267	32 663	40 760	55 911	76 019	35%
Carroll	34 112	36 451	45 404	56 346	71 422	87 268	22%
Cherokee	20 750	23 001	31 059	51 699	90 204	141 903	57%
Clayton	22 872	46 365	98 043	150 357	182 052	236 517	29%
Cobb	61 830	114 174	196 793	297 718	447 745	607 751	35%
Coweta	27 786	28 893	32 310	39 268	53 853	89 215	65%
DeKalb	136 395	256 782	415 387	483 024	545 837	665 865	21%
Douglas	12 173	16 741	28 659	54 573	71 120	92 174	29%
Fayette	7 978	8 199	11 364	29 043	62 415	91 263	46%
Forsyth	11 005	12 170	16 928	27 958	44 083	98 407	123%
Fulton	473 572	556 326	607 592	589 904	648 951	816 006	25%
Gwinnett	32 320	43 541	72 349	166 903	352 910	588 448	66%
Henry	15 857	17 619	23 724	36 309	58 741	119 341	103%
Newton	20 185	20 999	26 282	34 489	41 808	62 001	48%
Paulding	11 752	13 101	17 520	26 110	41 611	81 678	96%
Pickens	8 855	8 903	9 620	11 652	14 432	22 983	59%
Rockdale	8 464	10 572	18 152	36 747	54 091	70 111	29%
Spalding	31 045	35 404	39 514	47 899	54 457	58 417	7%
Walton	20 230	20 481	23 404	31 211	38 586	60 687	57%

Paulding (west) Counties are all on the edge of the Atlanta area, they show that the city is expanding outward in many directions.

Such rapid population growth has resulted in unprecedented urbanization rates. Yang and Lo (2002) reported that 1367 km^2 of forest were cleared in a 13–county area surrounding Atlanta between 1973 and 1998 (more than a 20% loss of forested area). In 1973, there were 6537 km^2 of forested land (63% of total area), but this valued declined to 5169 km^2 (50% of total area) by 1997. Yang and Lo (2002) only reported values for a 13–county area instead of the 20–county area defined by United States Census Bureau (Figure 1.1). During that time, commercial development and low–density residential areas (suburbs) both doubled. High–density urban land use increased from 454 km^2 in 1973 to 860 km^2 in 1997, an increase in high–density urban land area of 89%. Low–density urban areas increased from 1214 km^2 in 1973 to 2662 km^2 in 1997—an increase of 119% (Yang and Lo 2000).

The urbanization values listed above were taken from Yang and Lo (2002), reported as part of project ATLANTA (Atlanta Land–use Analysis: Temperature and Air–quality) in which they performed land use/cover change detection for a 13–county Atlanta area using a time–series of Landsat images from 1973 to 1998. More detailed results of the land use changes determined by Yang and Lo (2002) are listed in table 1.3, and three of the Landsat images are shown in Figures 1.2, 1.3, and 1.4. These land use images illustrate the rapid urbanization of Atlanta and locations of the highest density of urban areas.

In 1998, the Sierra Club ranked Atlanta as the “most sprawl–threatened city” in the country among its “30 most sprawl–threatened cities” (Sierra Club 1998). According

Table 1.3: Land use/cover change data for 13–county Atlanta MSA as extracted from a time series of Landsat MSS and TM images, 1973–1998 (Yang and Lo 2002).

Date	Units	High–density Urban	Low–density Urban	Cultivated /Exposed land	Cropland/ Grassland	Forest	Water	Total
4-13-73	**km^2**	454.23	1214.48	99.49	1981.46	6537.29	156.07	10 443.03
	%	4.35	11.63	0.95	18.97	62.60	1.49	100.00
6-11-79	**km^2**	456.72	1590.82	199.14	1687.48	6348.96	159.85	10 442.98
	%	4.37	15.23	1.91	16.16	60.80	1.53	100.00
5-09-83	**km^2**	612.34	1713.68	205.80	1617.47	6139.89	153.17	10 442.36
	%	5.86	16.41	1.97	15.49	58.79	1.47	99.99
6-29-87	**km^2**	740.38	1807.40	186.69	1549.39	5999.73	159.44	10 443.03
	%	7.09	17.31	1.79	14.84	57.45	1.53	100.00
4-23-92	**km^2**	839.87	1320.09	196.55	1374.28	5537.46	174.77	10 443.03
	%	8.04	22.22	1.88	13.16	53.03	1.67	100.00
7-29-97 1-02-98	**km^2**	860.27	2662.22	215.52	1321.68	5169.87	213.47	10 443.03
	%	8.24	25.49	2.06	12.66	49.51	2.04	100.00

to a 1993 report by Research Atlanta, Inc., during the two decades prior to publication of the article, Atlanta had been losing green space to development at a rate faster than any other metropolitan area in world history (Research Atlanta, Inc. 1993).

As more land becomes urbanized, an urban heat island (UHI) develops. This phenomenon occurs when a city remains consistently warmer than its surroundings due primarily to its lack of moisture and vegetation, which reduces evapotranspiration (Myrup 1969). Smaller amounts of moisture within cities enable less solar radiation to become latent heat (energy used to evaporate water); therefore, more energy becomes sensible heat and raises the air temperature. Further, urban building materials tend to have higher specific heat values and be impervious to water. Therefore, city buildings usually emit more energy after sunset. In addition, anthropogenic energy sources (e.g., industrial plants, automobiles) may contribute to the excess urban heat.

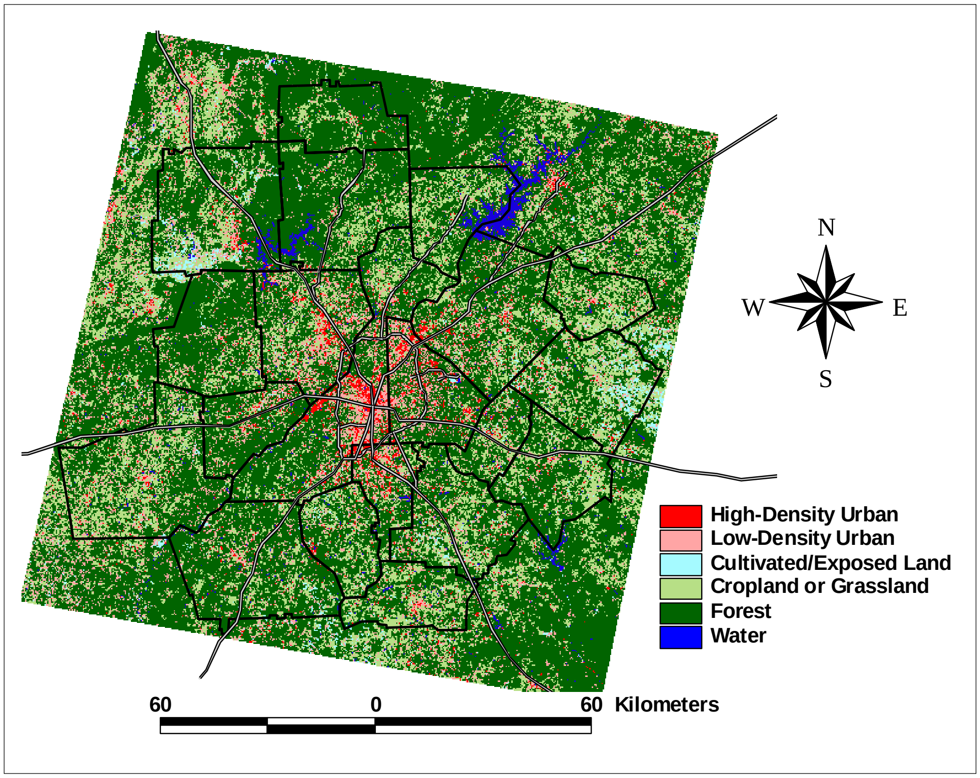

Figure 1.2: Land use/cover image of Atlanta MSA based on analysis of Landsat Multispectral Scanner (MSS) imagery taken on 13 April 1973 (Yang and Lo 2002).

The first person known to document a temperature difference between urban and rural environments was Howard (1833) during his climatological research of London, England (Hafner and Kidder 1999). According to Howard (1833), increased temperature is one of the most noticeable products of human–induced micro–climates in cities and has been documented for nearly two centuries (Delage and Taylor 1970). In addition, much research during the second half of the 20th century concludes that a significant UHI can have a considerable impact on the hydroclimate (i.e., rainfall, runoff, evapotranspiration) of a city and its surrounding area (e.g., Bornstein 1968; Huff and Changnon 1972; Changnon 1981).

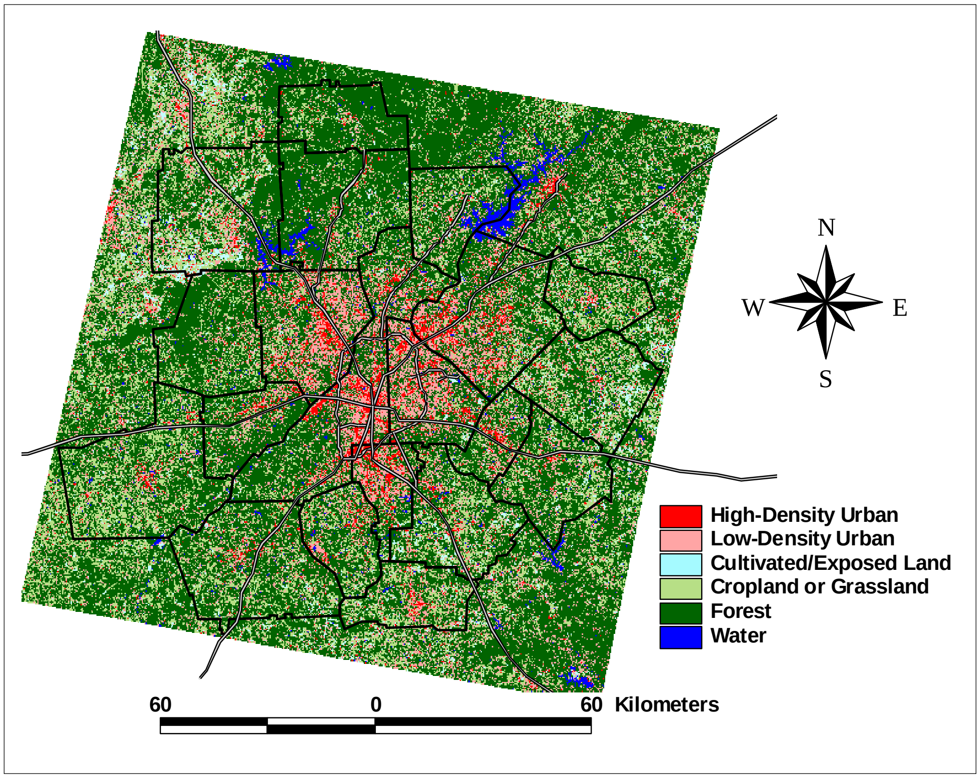

Figure 1.3: Land use/cover image of Atlanta MSA based on analysis of Landsat Thematic Mapper (TM) imagery taken on 29 June 1987 (Yang and Lo 2002).

Several studies have shown significant UHIs in New York City (Bornstein 1968), Washington, D.C. (Draxler 1986), Phoenix, Arizona (Balling and Cerveny 1987), Huntsville, Alabama (Lo et al. 1997), Atlanta, Georgia (Bornstein and Lin 2000), Melbourne, Australia (Morris et al. 2001) as well as others. In addition, much research has been done to determine how UHIs affect urban precipitation (Changnon et al. 1976; Huff and Changnon 1972; Huff and Changnon 1973; Huff and Vogel 1978; Bornstein and Lin 2000). In particular, Huff and Changnon (1973) studied eight U.S. cities (St. Louis, Missouri; Chicago, Illinois; Indianapolis, Indiana; Cleveland, Ohio; Washington, D.C.; Baltimore, Maryland; Houston, Texas; New Orleans, Louisiana; and Tulsa,

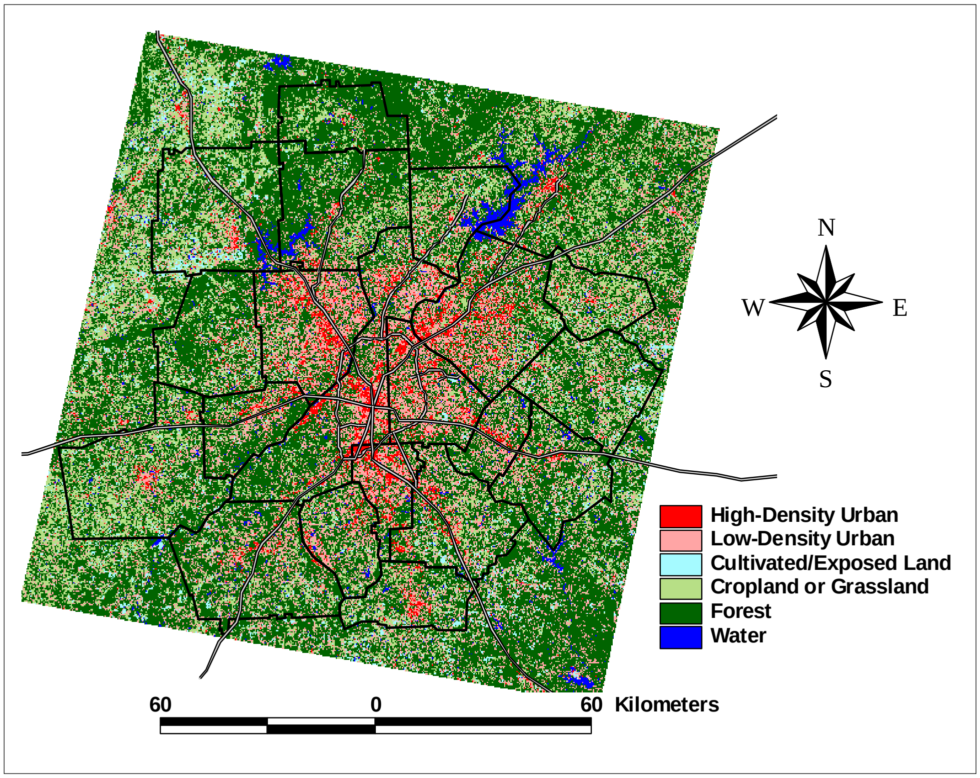

Figure 1.4: Land use/cover image of Atlanta MSA based on analysis of Landsat TM imagery taken on 29 July 1997 and 02 January 1998 (Yang and Lo 2002).

Oklahoma) and observed urban–induced increases in precipitation for all of the cities except Indianapolis and Tulsa. The areas of increased precipitation ranged from directly over the urban center to 80 km downwind of the urban center. More recently, Bornstein and Lin (2000) reported three events of UHI–initiated precipitation during a nine–day period in July and August of 1996. The events listed by Bornstein and Lin (2000) were all slightly downwind of the urban area. That project used data collected during the 1996 Summer Olympics in Atlanta and used a mesoscale (ranging from a couple kilometers to a few hundred kilometers) network (mesonet) of 40 surface weather stations to document the higher temperatures of urban Atlanta. In addition, this mesonet recorded precipitation from predawn thunderstorms (using surface rain gages) that were shown to have initiated during strong UHI conditions and relatively weak, converging surface winds (< 4 ms^{-1}) likely created along UHI–induced surface temperature gradients. Since that time, Atlanta has been widely publicized as “creating its own weather” (Mullen 1999; Chang 2000; Daly 2000) and much work is being done to reduce the thermal gradient between the growing urban center and the surrounding rural areas. For example, the Georgia state government has eased insulation requirements for buildings constructed with roofing material that is at least 60 percent reflective (Mullen 1999; Daly 2000).

Since it has already been shown that the UHI of Atlanta may be able to initiate thunderstorms, this project seeks further evidence of if, when, and where such events occur. Further, this project attempts to study the frequency, temporal, and spatial patterns of UHI–initiated precipitation in Atlanta in order to understand more about the causes and environments associated with these events. Specifically, the typical air mass types and UHI intensities associated with these events are determined. This research is based on examination of radar reflectivity data, surface weather station data, upper–air sounding data, and air mass classification data from the summers of 1996–2000. It attempts to determine whether or not Atlanta’s UHI initiates anomalous thunderstorms regularly, if temporal and spatial patterns are exhibited by the UHI–initiated storms, and if any suggestions can be made as to why the events in question occur when and where they do. The results presented in this thesis should aid a better understanding of the local hydroclimate of Atlanta due to its UHI, as well as support further investigation into the subject of UHI–induced precipitation.

CHAPTER 2

BACKGROUND

This chapter provides an explanation and history of the UHI phenomenon and a review of relevant research on the topic. A brief description of the causes and effects of an UHI will be followed by a thorough review of previous research — hydroclimatology studies specifically. Particular attention will be given to project ATLANTA (Atlanta Land–use Analysis: Temperature and Air–quality), a National Aeronautics and Space Administration (NASA) Earth Observing System (EOS) Interdisciplinary Science project that seeks to observe, measure, model, and analyze how the rapid growth of the Atlanta, Georgia metropolitan area since the early 1970s has affected the region's climate and air quality. It will be discussed in detail in order to understand recent findings about Atlanta's rapid urbanization and its possible effects on the surrounding region's climate.

2.1 The Urban Microclimate

Anthropogenic alteration of the urban climate has been documented for nearly two centuries (Howard 1833).   The term urban heat island was first used in English–language literature by Manley (1958), but it may have been used previously elsewhere (Landsberg 1981). An UHI occurs when the urbanized area of a city exhibits higher temperatures than the surrounding rural areas (Figure 2.1). Myrup (1969) found the primary causes of the UHI to be the larger heat capacity of urban materials (concrete, asphalt, etc.) and the lack of evapotranspiration (the combined processes of evaporation

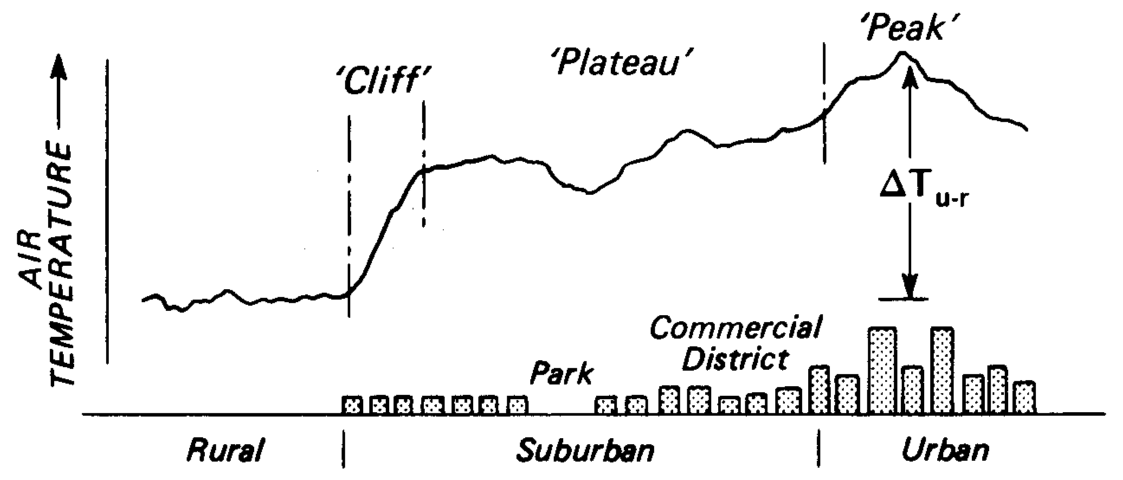

Figure 2.1: Generalized cross–section of a typical urban heat island (Oke 1987).

of water from the surface and transpiration of water from plants to the air as water vapor) in urban areas. Rural areas normally contain larger amounts of moisture than urban areas that are engineered to transport water away from the city. As a result, solar radiation in rural areas must evaporate excess surface water before directly heating the earth's surface. However, this is not necessarily the entire reason for higher urban temperatures. Bornstein (1968) illustrates that daytime urban high temperatures may actually remain lower than rural high temperatures due to the large heat capacity and high heat conductivity of urban building materials. Oke (1987) states that the most notable feature of an urban heat island is the reduced cooling during late afternoon and evening hours under relatively constant weather conditions. The reason given for this moderated cooling is the reduced sky view factor of urban buildings. Essentially, when compared to open, horizontal surfaces (such as most rural areas), urban buildings have much less of their surface area exposed to open air and more area facing other warm, building surfaces. Therefore, radiative loss of heat is reduced, and this results in higher nocturnal minimum temperatures compared to rural areas. Likewise, the urban area is also slower to warm up after sunrise due to many building–shaded parts of the city. Therefore, urban–rural temperature differences grow quickly just after sunset and tend to be most pronounced a few hours (3 to 5 hours according to Oke (1987)) after sunset (Figure 2.2). Figure 2.2 shows the typical temporal variation of surface temperatures associated with an UHI. These warmer nocturnal urban temperatures tend to decrease the frequency of temperature inversions near urban surfaces, which allows for better dispersion of pollutants and decreased chances of fog during the night. The urban–rural temperature difference decreases from its peak through sunrise and may even be inverted during the

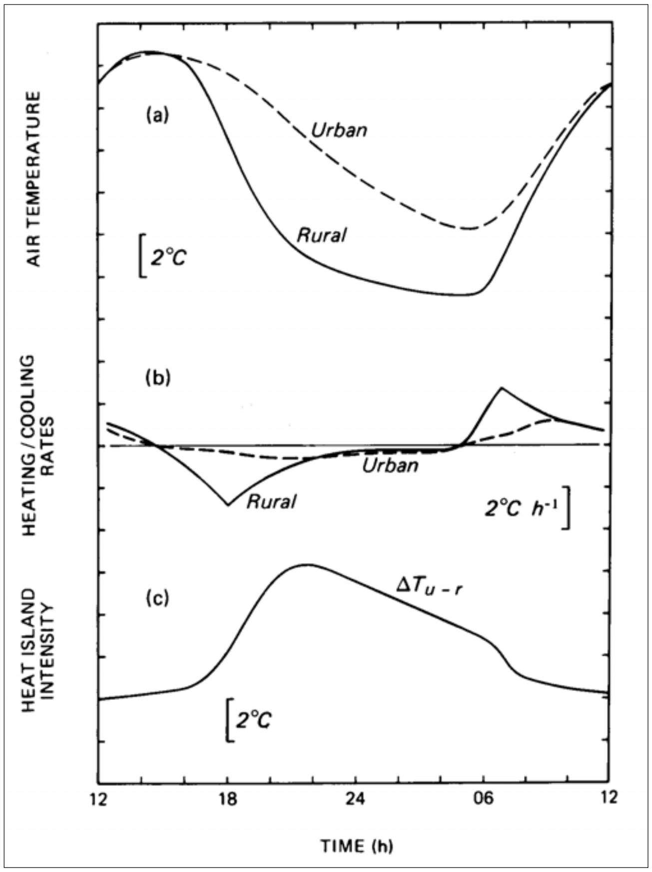

Figure 2.2: Typical temporal variation of urban and rural (a) air temperature, (b) cooling/warming rates, and (c) the resulting heat island intensity under “ideal” weather conditions (Oke 1987).

day as stated above (Bornstein 1968; Oke 1987). On a seasonal scale, Gallo and Owen (1999) found the greatest urban–rural temperature difference (with regard to monthly maximum temperature, minimum temperature, and average temperature) to occur during the summer months of July and August.

Wind speed plays a vital role in the development of the UHI. Many studies have shown wind speed, along with cloud cover, to be the most important meteorological parameters affecting the development and intensity of the UHI (Ackerman 1985; Moreno–Garcia 1994; Kidder and Essenwanger 1995; Figuerola and Mazzeo 1998). The wind speed and cloud cover may partially dictate the stability and radiation budget of a city. Typically, wind speeds within an urban area are lower than in surrounding rural areas due to greater surface roughness created by buildings. However, if the buildings cause strong winds at higher levels to be deflected down into the city, winds may be stronger within the city. Also, urban streets oriented parallel with the wind flow may channel winds through the city at a faster rate than in rural areas (Oke 1987). Under cloudless skies, Oke (1973) suggests that UHI intensity is related to the inverse of the regional wind speed and the geometry (urban density, sky view factor, etc.) of the city. On calm nights, UHI intensity should be inversely related to cloud cover due to increased radiational cooling of rural areas; thick cloud cover may act to minimize radiational cooling in rural areas. Further, wind speeds within the urban canopy may be stronger than in rural areas on relatively calm nights due to the horizontal surface temperature (and therefore pressure) gradients between the urban and rural areas. Much like a sea breeze, the anomalously warm urban center creates relatively low air pressure that causes cooler, rural air to converge on the urban center (Oke 1987). Findlay and Hirt (1969) showed that UHI–induced low pressure (due to anomalous heat) within urban areas resulted in light flow of air from the rural areas toward the urban center during weak synoptic flow. The caveat, *during weak synoptic flow*, proves to be quite important. As surface winds encounter the increased roughness of urban areas, horizontal speeds tend to notably decrease (Landsberg 1981; Oke 1987). Therefore, it becomes clear that urban areas should cause surface winds to decrease under significant synoptic flow and increase under weak synoptic flow.

There are many possible causes and contributing factors to an UHI. Oke (1987) addresses seven different possible features of urban areas that may affect the energy balance of cities (Table 2.1). A few possible causes that have yet to be discussed in this chapter are: increased absorption of solar radiation due to increased surface area and multiple reflection of urban buildings; increased long–wave radiation from air pollution particles in the sky; and anthropogenic heat from buildings and traffic. Increased

Table 2.1: Hypothesized causes of the urban heat island (Oke 1987).

Altered energy balance terms leading to positive thermal anomaly		Features of urbanization underlying energy balance changes
1	Increased absorption of solar radiation	Canyon geometry: increased surface area, and multiple reflection
2	Increased long–wave radiation from the sky	Air pollution: greater absorption and re–emission
3	Decreased long–wave radiation loss	Canyon geometry: reduction of sky view factor
4	Anthropogenic heat source	Building and traffic heat losses
5	Increased sensible heat storage	Construction materials: increased thermal admittance
6	Decreased evapotranspiration	Construction materials: increased ‘water–proofing’
7	Decreased total turbulent heat transport	Canyon geometry: reduction of wind speed

absorption of solar radiation due to multiple reflection is likely negligible given that the typical UHI is most pronounced during the night with a minimum during midday (Oke 1987) and some cities exhibiting temperatures less than rural areas during the day (Bornstein 1968). According to Olfe and Lee (1971), radiative warming from pollutants will probably be important only under stagnant conditions. They calculated that an urban pollutant would not remain over the city for much longer than one hour given a mean wind speed of only 3 m $\sec^{-1}$ (measured by Bornstein (1968)) and that would not be enough time to allow for significant cooling according to calculations of pollutant cooling times by Atwater (1971). Therefore, any effects of pollutants absorbing and emitting longwave radiation would normally be negligible. Also, Bornstein (1968) found that combustion in Manhattan during the winter released 250% more heat than that which had been calculated as reaching the surface from the sun. Conversely, during the summer, heat from combustion decreased to one–fifth of the winter value, while insolation increased by a factor of three.

2.2 Urban Hydroclimatology

Atmospheric moisture is usually reduced over urban areas compared to rural areas. Sisterson and Dirks (1978) explain this dry anomaly over urban areas as being caused by two factors. First, urban surface materials are generally impervious and designed to transport moisture away from the city, so the surface is initially drier than rural areas resulting in less evapotranspiration. Secondly, higher surface temperatures (due to lower moisture) lead to greater vertical mixing and a much deeper mixing layer to transport the small amounts of moisture higher into the atmosphere. The strong mixing layer over the urban area may also entrain much drier air from above which acts to dilute the moisture content of the column (Sisterson and Dirks 1978). While this urban dry island may not seem conducive to precipitation, it can be quite accommodating to vertical motion. If surface moisture were advected into the urban area, the instability created by dry air over moist air may result in convection. Such a situation may not be uncommon. Duckworth and Sandberg (1954) showed that strong radiation inversions often occur adjacent to the ground in rural areas, but they rarely occur over urban areas based on a study in San Francisco. However, at higher altitudes (between 30 and 300 m depending on city size), urban temperatures sometimes become cooler than rural temperatures at the same heights. Bornstein (1968) showed similar results for New York City. He also illustrated that such weak, elevated inversions over urban areas were more likely with very light winds and strong rural surface inversions. Duckworth and Sandberg (1954) suggested the following possible causes of this cross–over effect: vertical mixing over the urban area, an urban convection cell, radiative loss by the smoke pall, and variations in the wind field between 30 and 300 m. The last explanation is generally believed to be most probable (Duckworth and Sandberg 1954; Bornstein 1968). However, Clarke (1969) suggests that the cross–over effect occurs when urban heating is not sufficiently large enough to penetrate the entire surface inversion; therefore, the elevated urban inversion represents the upper extent of the rural surface inversion (Bornstein 1968). Regardless of the causal mechanism of the cross–over effect, it may be a significant factor in urban–induced precipitation. If rural surface inversions suppress weak updrafts or at least prevent mixing of a moist surface layer, convection (and possibly precipitation) may be likely upon entering the less stable urban air column.

2.3 Urban Impacts on Precipitation

The first documented case of urban–induced changes in precipitation was by Landsberg (1956) in Tulsa, Oklahoma. He noted indications that the city was causing increased precipitation. Urban–induced changes in rainfall tend to be subtle and less detectable than changes in visibility, winds, and temperature. However, Huff and Changnon (1973) found measurable precipitation enhancements in six of eight cities studied. The results of their study show that even though all intensities of daily rainfall appeared to be increased by the effects of urban areas, the most pronounced modifications tended to be on days with moderate to heavy natural rainfall. Therefore, it seems that the UHI acts primarily to enhance rainfall rather than initiate it. Likewise, results from project METROMEX (Metropolitan Meteorological Experiment) indicate that the urban area of St. Louis, Missouri did not necessarily increase the number of precipitation events, but instead stimulated events that were already occurring. According to that study, urban convective clouds, on average, reached greater maximum heights, lasted longer, and were more likely to merge with other clouds. Therefore, the increases in urban precipitation totals for St. Louis were due more to urban–enhanced raincells rather than urban–initiated raincells. Nevertheless, observations from METROMEX show that, during forenoon hours, the urban area experienced earlier cloud build–up and enhanced frequencies of radar first echoes due to rapid deepening of the boundary layer (Changnon 1981). As a precursor to METROMEX, Huff and Changnon (1972) performed a climatic study of St. Louis and found summer increases in the immediate downwind area of the city for the following categories: rainfall (10–20%), moderate rain days (10–25%), heavy rainstorms (80%), thunderstorms (20%), and hailstorms (30%). Possible causes of the increased precipitation were suggested as: increased condensation nuclei over the city, increased roughness causing surface convergence, and instability due to urban heating.

Increased surface temperatures in urban areas create a less stable atmosphere over the city by preventing nocturnal surface inversions (Duckworth and Sandberg 1954; Bornstein 1968) that are common in rural areas (Duckworth and Sandberg 1954). Therefore, the warmer urban air tends to rise, and this convection may initiate thunderstorms if sufficient moisture exists. Bornstein and LeRoy (1990) found the urban heat island of New York City (NYC) affected both formation and movement of summer daytime thunderstorms. Under calm regional winds, the NYC UHI initiated convective cloud formation and produced a radar echo maximum directly over the urban area. However, the study also showed that preexisting thunderstorms that moved toward the city tended to bifurcate and move around the urban area due to a building–barrier–induced divergence effect. This resulted in radar echo maximums along the edges and downwind of the city with a minimum directly over the urban area (Bornstein and LeRoy 1990).

The UHI may also affect precipitation patterns due to increased condensation nuclei and surface convergence associated with increased roughness. Previously, it was thought that increased condensation nuclei would lead to increased condensation, and therefore, increased precipitation downwind of the urban area (Landsberg 1956; Changnon 1981; Mather 1991). However, numerical cloud model results by Reuter and Guan (1995) show even the heaviest pollution (primarily sulfur dioxide) from a major petroleum refinery in Wood River, Illinois, increased the accumulated rainfall by only

1.8%. Therefore, Reuter and Guan (1995) concluded that pollution could hardly be responsible for the large increases in rainfall observed in some industrial areas. Rather the increases are likely the result of excess heat and moisture emitted from industrial plants. Conversely, Reisin et al. (1996) concludes that rain efficiency decreases with increasing cloud condensation nuclei concentration, and Rosenfeld (2000) found that urban and industrial air pollution completely inhibits precipitation from some clouds. Based on observations by Advanced Very High Resolution Radiometer (AVHRR) sensors on board the National Oceanic and Atmospheric Administration (NOAA) weather satellites and the Tropical Rainfall Measuring Mission (TRMM) satellite using the visible and infrared sensor (VIRS), the precipitation radar (PR), and the TRMM passive microwave sensor (TMI), Rosenfeld (2000) suggests that increased condensation nuclei, due to pollution, creates a greater number of small droplets, but much less coalescence and drop formation. Therefore, condensation nuclei created by urban pollution may create droplets that do not become large enough to fall as precipitation and ultimately create regions of suppressed precipitation downwind of the source.

In a more recent example of how an UHI can affect precipitation, Craig and Bornstein (2002) used the Fifth–Generation NCAR / Penn State Mesoscale Model (MM5) to simulate urban–induced convective precipitation over Atlanta. The initial simulation, using the configuration shown in Table 2.2, yielded an area of urban–induced precipitation on the edge of the city that disappeared when Atlanta roughness lengths, thermal properties, and building barriers were removed. However, the model also yielded a band of precipitation associated with a stationary front near the city in both simulations. These results were relatively similar to actual observations, but the model

Table 2.2: MM5 parameters used by Craig and Bornstein (2002).

Parameter	Specification
Nested grids	81, 27, 9, and 3 km resolutions
Vertical layers	30 (10 below 1 km)
Minumum full sigma level	46 m
Land–use classes	25 (USGS)
Topographic heights	USGS 30 s data
Sea–surface temperatures	Global Data Assimilation System
Model analysis boundary conditions	NCEP / NCAR
Ice scheme	Dudhia
Convective parameterization	Kain–Fritsch (domains 1 and 2)
Surface temperature	Force–restore
TKE scheme	Gayno–Seaman 1.5

showed the UHI–induced precipitation slightly northeast and about 3 hours earlier than the observed event. Nevertheless, it is evident that Atlanta can, and does, initiate convective storms due to its anomalous urban heat, and these events may be predicted through the use of numerical weather simulations.

2.4 Remote Sensing

Rao (1972) was the first to demonstrate that urban areas could be identified from analyses of thermal data acquired by satellite. Matson et al. (1978) utilized nocturnal Very High Resolution Radiometer (VHRR) thermal data (10.5–12.5 μm) to compare urban and rural surface temperature differences. Price (1979) applied Heat Capacity Mapping Mission (HCMM) data (10.5–12.5 μm) to assess the extent and intensity of urban surface heating in the northeastern United States. Roth et al. (1989) used AVHRR thermal data (10.5–11.5 μm) and found that the greatest differences in surface radiant temperatures were observed during midday even though the greatest difference between urban and rural air temperatures occurred at night. The nighttime observations of Roth et al. (1989) showed little difference in surface temperatures of urban and rural areas, which suggests that the sides of buildings and their configurations may contribute more to higher urban temperatures than the roofs. Therefore, sky view factor appears to be more of a causing factor of the UHI than urban building materials. However, Gallo et al. (1993) successfully used NOAA AVHRR data to assess the UHI over several U. S. cities based on a derived normalized difference vegetation–index (NDVI). Urban and rural differences in the NDVI explained a greater amount of the variance observed in urban–rural temperature difference than past analyses that used urban population data. Similar to the study by Roth et al. (1989), Gallo et al. (1993) found that satellite–derived surface temperatures were minimally related to observed urban–rural temperature differences. Hence, it seems that while urban building materials (at least urban roof–building materials) may not account for much of the UHI, the lack of vegetation in urban areas does.

Lo et al. (1997) noted that because of the relatively low spatial resolution of AVHRR data, Landsat Thematic Mapper (TM) and the airborne Advanced Thermal and Land Applications Sensor (ATLAS) provide better analysis and assessment of the UHI based on comparison of NDVI and thermal infrared data. Lo et al. (1997) found results in agreement with Gallo et al. (1993) — there is a strong negative correlation between NDVI and irradiance of residential, agricultural, and vacant / transitional land cover types. Thus, biomass is likely to be an essential factor in moderating the UHI and its effects. Further, in a study comparing monthly variation in urban–rural differences for maximum, minimum, and average temperatures with monthly NDVI variation, Gallo and

Owen (1999) found statistically significant, although rather small, correlations of 20%, 30%, and 35%, respectively.

Voogt and Oke (1997) recognized that urban surface temperature measurement is difficult because of the complexity of the three–dimensional urban–atmosphere interface. Remotely sensed urban surface temperatures tend to yield strong variations due to viewing restrictions of all urban surfaces by the sensor as well as differential heating due to the urban geometry. Therefore, they made the first attempt to calculate a complete surface temperature that takes into account both the horizontal and vertical surfaces in urban areas by combining surface temperature observations from infrared radiometry sensors and urban surface structural information. The complete urban surface temperature is an area–weighted measure that combines component (roof, walls, ground, vegetation, etc.) surface temperatures in proportion to their areal fraction of the total surface. Results showed that complete surface temperature calculations generally differed from remotely sensed estimates of urban surface temperatures whether they viewed the city from nadir or off–nadir, and the results were consistent for a light industrial site comprised of warehouses and workshops, a downtown office / commercial zone with massive tall buildings, and a suburban residential neighborhood within Vancouver, British Columbia, Canada. Therefore, Voogt and Oke (1997) suggested that most remotely sensed estimates of urban surface temperatures are not as accurate as they seem.

2.5 Project ATLANTA

Project ATLANTA (Atlanta Land–use Analysis: Temperature and Air–quality) was a study funded by NASA EOS that began in 1996. The purpose was to determine Atlanta's effects on local climate and air quality. The project incorporated assessment of land cover / land use change as determined from remote sensing data with temporal numerical model simulations in order to better understand the effects of Atlanta's growth on local and regional climate and air–quality. Data sources include: Landsat Multispectral Scanner (MSS) and Thematic Mapper (TM) for assessment of land cover change; Landsat TM thermal, AVHRR and Geostationary Operational Environmental Satellite (GOES) for land surface thermal characteristics; and ATLAS high spatial resolution multispectral thermal infrared for detailed measurements of thermal energy fluxes that occur for specific surfaces (Quattrochi and Luvall 1997).

Based on data collected during project ATLANTA, the Atlanta UHI produces temperatures up to 5°C greater than the surrounding areas (Bruce 1999). In addition to remotely sensed data, Bornstein and Lin (2000) used data from weather stations set up by the National Weather Service (NWS) and the Georgia Automated Environmental Monitoring Network (GAEMN) (Hoogenboom 1996). Bornstein and Lin (2000) found that Atlanta's UHI tends to initiate convection during nearly calm regional flow conditions while causing moving thunderstorms to bifurcate and move around the urban area. These results coincide with data collected over New York City (Bornstein and Leroy 1990), but they tend to disagree with findings from project METROMEX which showed enhanced storms that moved across the urban center of St. Louis, Missouri. Under nearly calm regional flow, a relative low pressure may be created over the city due to the anomalous high temperatures of the UHI, and cooler air rushes into the urban area causing warm air to rise. This vertical motion can create convective thunderstorms that produce precipitation maximums over the city, and it is most pronounced at night when the UHI is strongest (Bornstein and Lin 2000). However, Bornstein and Lin (2000) note that previous studies have shown that daytime UHIs are more effective in producing vertical motions than those during stable nocturnal conditions. Conversely, when regional flow is significant, winds tend to diverge around the city due to increased surface roughness. This phenomenon creates precipitation maximums on the lateral and downwind edges of the city with a minimum located directly over the urban area.

2.6 Summary

Obviously, much work has been done in attempts to better understand the causing factors of an UHI and its effects. Unfortunately, there is still much to be determined about the primary cause (if it can be narrowed down to one) of an UHI, and it likely varies among cities. Some studies have stressed the importance of vegetation (Gallo et al. 1993; Lo et al. 1997; Gallo and Owen 1999) while others suggested that urban building materials (Myrup 1969) and building geometry (Oke 1987) are the main contributors to an UHI. Likewise, determining how an UHI increases urban precipitation has yielded mixed results that have suggested increased condensation nuclei due to urban pollutants (Landsberg 1956; Changnon 1981; Mather 1991), surface convergence caused by increased surface roughness (Changnon 1981), and instability due to urban heating (Changnon 1981; Bornstein and LeRoy 1990; Bornstein and Lin 2000). Nevertheless, it is likely that most of these causes are valid, but some apply more to certain cities since they vary in their building shapes, sizes, locations, geometries, etc.

Atlanta is a sprawling metropolis (Sierra Club 1998), and this project seeks to determine if, when, and where precipitation is initiated by its UHI. It is imperative that patterns of actual UHI–induced precipitation events be established before confident claims can be made about the causes of such events. Since several possible causes have been proposed for various cities by past studies (Landsberg 1956; Changnon 1981; Bornstein and LeRoy 1990; Bornstein and Lin 2000), a better understanding of when and where these events occur should contribute to the accurate diagnosis of the causes. Therefore, this study constructs a climatology of UHI–initiated precipitation during the period 1996–2000, in order to determine spatial and temporal patterns associated with such events. In addition, possible causes of UHI–induced precipitation in and around Atlanta are discussed.

CHAPTER 3

METHODOLOGY

This project seeks to determine whether precipitation initiated by Atlanta’s UHI occurs regularly, as well as when and where it occurs. Learning more about the patterns of UHI–initiated precipitation should lead to a better understanding of the causes of such events. Therefore, this project also analyzes the air mass types and urban–rural temperature differences of each event in order to learn more about the causes of such events.

In order to document possible cases of UHI–induced precipitation, national radar mosaics based on WSR–88D data were analyzed in order to identify possible UHI–initiated precipitation over the Atlanta area during periods of weak synoptic flow. Radar reflectivity was used since it is able to display data from the entire study area at 15–min intervals. Hourly data from surface weather stations in the Atlanta area, surface meteorological maps, and upper–level meteorological charts were used to help determine periods of weak flow. The surface station data were also used to understand the surface environment in which these events occurred. Radiosonde observations from the National Weather Service (NWS) Forecast Office in Peachtree City, Georgia (KFFC) were used to determine upper–level wind speeds as well as a vertical temperature profile in order to illustrate the stability and moisture content of the lower atmosphere during these events. Finally, data from an air mass classification technique based on typical characteristics of each air mass were used to determine what types of air masses are associated with initiation of convective precipitation due to Atlanta's UHI.

3.1 Reflectivity Data

The 2–km 15–min radar mosaics for this project were provided by the Global Hydrology Resource Center (GHRC) at the Global Hydrology and Climate Center, Huntsville, Alabama. The GHRC generates composite products in hierarchical data format (HDF) for the continental United States (CONUS) based upon composites of radar reflectivity data received from Weather Services International Corporation (WSI) every 15 minutes (Figure 3.1). The 2–km pixels within the CONUS mosaics are assigned one of 16 categories based on the original reflectivity value (Table 3.1). The HDF files were viewed using software written in Research Systems, Inc. Interactive Data Language (IDL) version 5.5.

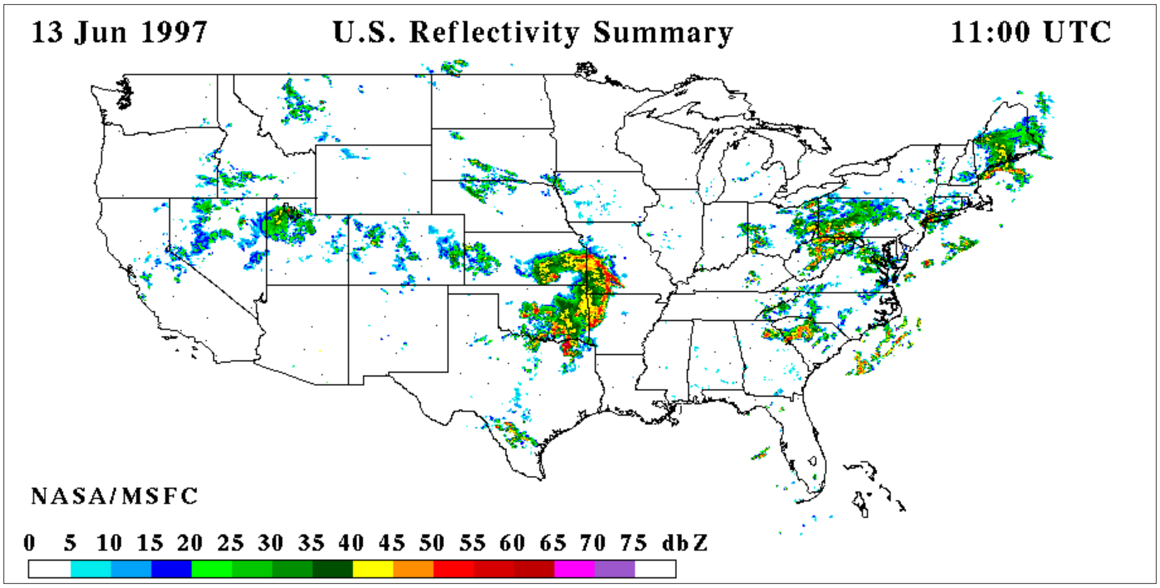

Figure 3.1: An example of a composite radar reflectivity image produced by GHRC for 1100 UTC 13 June 1997.

Table 3.1: GHRC 2–km 15–min reflectivity categories.

Level	Reflectivity (dbZ) Range
0	0 <= < 5
1	5 <= < 10
2	10 <= < 15
3	15 <= < 20
4	20 <= < 25
5	25 <= < 30
6	30 <= < 35
7	35 <= < 40
8	40 <= < 45
9	45 <= < 50
10	50 <= < 55
11	55 <= < 60
12	60 <= < 65
13	65 <= < 70
14	70 <= < 75
15	75 <=

3.2 Surface Station Data

This project makes use of 10 different surface meteorological stations in and around Atlanta (Figure 3.2 and Table 3.2). Five of these stations are part of the Automated Surface Observing System (ASOS) sponsored by the Federal Aviation Administration (FAA), NWS, and Department of Defense (DoD). Data from these stations were obtained from the National Climatic Data Center (NCDC) in Asheville, North Carolina and the Southeast Regional Climate Center in Columbia, South Carolina. These stations report observations at least once every hour for the following meteorological variables: wind direction (true), wind speed (kts), wind gust (kts), wind variability (true), surface visibility (statute miles), sky conditions, air temperature (ºC), dewpoint temperature (ºC), altimeter setting (in. of mercury), precipitation occurrence, precipitation amounts (hundredths of in.), and supplemental remarks in addition to the time of observation. This study only used the wind, temperature, dewpoint temperature,

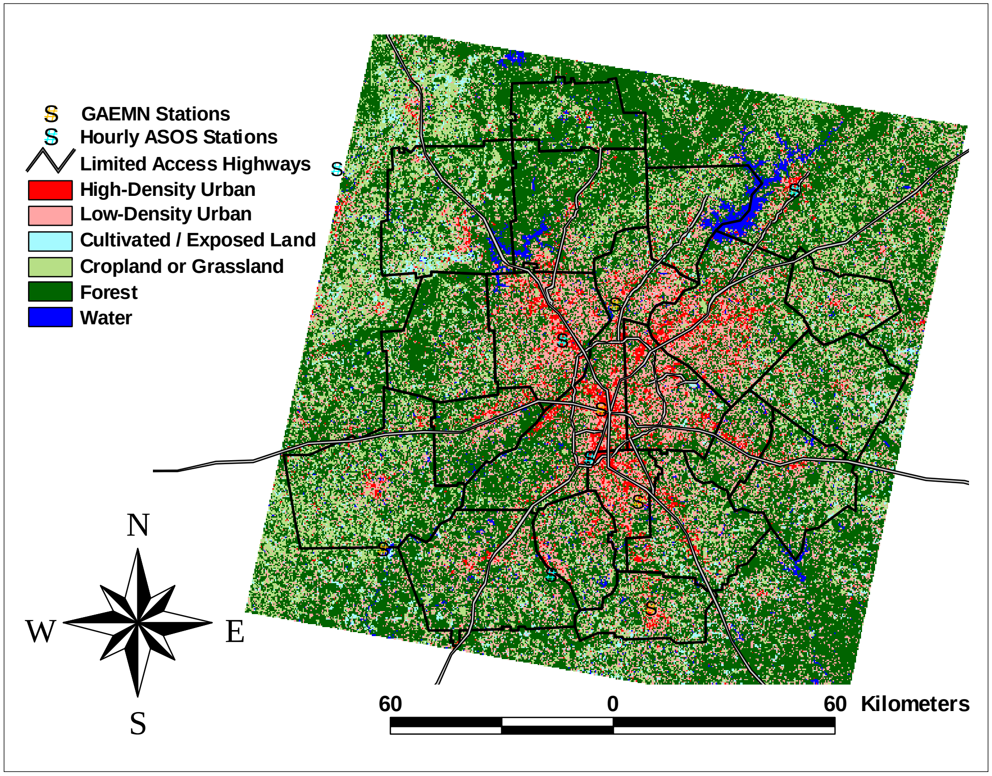

Figure 3.2: Surface weather stations overlaid on 1997–1998 land use /cover.

and air pressure / altimeter data. The Office of the Federal Coordinator of Meteorology (OFCM) determines the siting specifications for all federally approved weather observing stations. According to the OFCM (1994), the pressure sensor is not less than 3 ft (1 m) above ground level. Wind sensors (wind direction and wind speed) are oriented with respect to true north, and they are mounted 30 to 33 ft (9 to 10 m) above the average ground height within a radius of 500 ft (150 m). The temperature and dew point sensors are mounted so that the aspirator intake is 5 ± 1 ft (1.5 ± 0.3 m) above ground. Five ft (1.5 m) above ground is the preferred height (OFCM 1994). Much more detail regarding the siting of federally approved weather stations can be found in *Federal Standard for Siting Meteorological Sensors at Airports* (OFCM 1994).

Table 3.2: List of surface weather stations used in this study.

Station ID	Station Name	County	Latitude (°North)	Longitude (°West)	Elevation (meters)	Network
ATA	Clark Atlanta University	Fulton	33.74	84.41	312.4	GAEMN
ATL	Atlanta Hartsfield Int. Airport	Fulton	33.63	84.45	307.8	ASOS
DWY	Cherokee Town and Country Club	Fulton	34.00	84.36	276.1	GAEMN
FFC	Peachtree City Falcon Field	Fayette	33.35	84.57	243.2	ASOS
GFN	UGA Experiment Station Griffen	Spalding	33.26	84.28	283.1	GAEMN
GVL	Gainesville Lee Gilmer Airport	Hall	34.27	83.83	388.6	ASOS
JBO	Clayton County International Park	Clayton	33.52	84.31	246.8	GAEMN
MGE	Marietta Dobbins Air Force Base	Cobb	33.92	84.52	330.1	ASOS
RMG	Rome R. B. Russell Airport	Floyd	34.35	85.17	194.8	ASOS
ROP	Roopville Plant Wansley	Carroll	33.42	85.05	266.0	GAEMN

The remaining surface station data used in this project were obtained from Dr. Gerritt Hoogenboom, director of the Georgia Automated Environmental Monitoring Network (GAEMN) at the University of Georgia campus in Griffin, Georgia. GAEMN data are summarized at 15–minute intervals for agricultural and environmental purposes, and each station is designed to report the following meteorological variables: air temperature (°C), relative humidity, wind speed (m s^{-1}), wind direction (true), rainfall (mm), barometric pressure (kPa), as well as observation time. Temperature and moisture are recorded at a height of 2 m above ground and wind sensors are mounted at a height of

3.5 m. Most of the stations are also equipped to record as many as 20 other meteorological and agricultural–related variables. This project uses temperature, humidity, wind, and pressure observations only.

Surface meteorological charts corresponding with each UHI precipitation event were used to help determine the existence and location of any surface fronts, boundaries, or other forcing mechanisms. These charts were accessed from Unisys Weather Image and Map Archive (http://weather.unisys.com/archive) and an example can be shown in Figure 3.3.

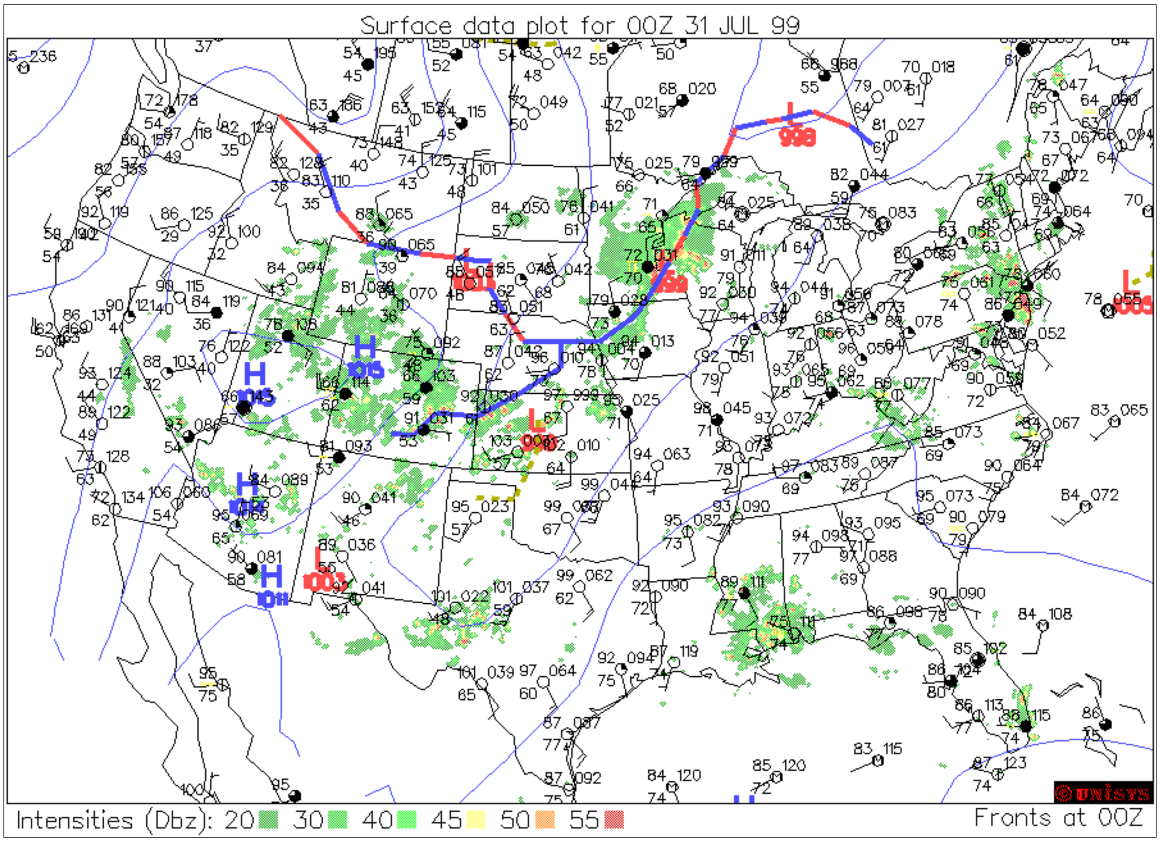

Figure 3.3: Surface map obtained from Unisys Weather Image and Map Archive.

3.3 Upper–Air Data

Upper–air observations for the Atlanta area were based on radiosonde data taken at KFFC. This project makes use of KFFC radiosonde data (usually recorded at 0000 and 1200 UTC) for each event day in order to identify possible anomalies in the temperature and moisture profiles due to the UHI. Upper–air data for this study were provided jointly by the Forecast Systems Laboratory (FSL) in Boulder, Colorado and NCDC.

3.4 Synoptic Classification Data

In order to determine the type of air masses that were most commonly associated with UHI–induced precipitation, air mass types, determined by the Spatial Synoptic Classification (SSC) method, were identified for each event (Sheridan 2002). The SSC requires initial identification of the distinctions between the major air masses that traverse the region as well as their typical meteorological characteristics. Source region delineation is less important for this method since air masses tend to be modified as they traverse far from their source region, although SSC categories are relatively synonymous with traditional air mass classification categories (e.g, dry polar (DP) is synonymous with continental polar (cP)). Therefore, this method of classification identifies resident air masses at hundreds of individual weather stations on a national scale based on numerous *seed days.* A seed day is a day that exhibits typical characteristics for each air mass at a particular station based on 30 years (1961–1990) of data (except wind data which is based on the entire period of record).

The SSC categorizes days into one of the following six air mass types: dry polar (DP), dry temperate (DM), dry tropical (DT), moist polar (MP), moist temperate (MM), and moist tropical (MT). DP is the coldest, and often the driest, air mass in a region. DM air is typically associated with mild, dry conditions and it is most frequent during strong zonal flow aloft. DT is very hot and dry air, and MP is cooler, more humid, and cloudy. MM is similar to MP, but with much higher temperatures and dew points. MT represents warm, humid conditions similar to the traditional maritime tropical (mT) air mass type. Atmospheric instability and convective activity are common within the MT air mass (Sheridan 2002). A seventh category, transitional (TR), is applied to days during a period of transition between two air masses. Table 3.3 shows typical characteristics of each air mass type for Atlanta during the month of July, and Table 3.4 lists air mass frequency by month for Atlanta.

SSC data for 1996–1999 were obtained from Scott Sheridan at Kent State University (http://sheridan.geog.kent.edu/ssc.html). Unfortunately, there were no available SSC data for the first recorded event day (09 May 1996), so neither that day nor the second event day (11 May 1996) were included in the SSC analysis since three days of SSC type data were required for analysis.

Table 3.3: Mean characteristics of each air mass type for July in Atlanta.

July	DM	DP	DT	MM	MP	MT	TR
Frequency (%)	19.8	2.5	2.5	31.2	2.0	35.9	6.1
2000 UTC Temperature (ºC)	31.7	26.7	36.2	26.3	21.4	31.2	29.7
0800 UTC Temperature (ºC)	21.2	17.1	25.1	21.2	19.5	22.5	21.3
2000 UTC Dewpoint (ºC)	17.6	15.1	18.2	20.7	18.9	20.8	18.9
Wind Direction	NW	W	NW	SW	E	W	W
Wind Speed (m s^{-1})	3.2	3.2	3.6	3.5	4.6	3.3	3.8
Cloud Cover (tenths)	2.8	4.1	2.5	8.0	9.7	5.3	5.9

Table 3.4: Air mass frequency (% of total) by month for Atlanta.

Month	DM	DP	DT	MM	MP	MT	TR
Jan	23.2	23.2	3.4	10.8	20.6	8.2	10.5
Feb	28.0	22.0	5.1	8.3	17.4	9.1	10.3
Mar	31.9	14.7	7.6	11.8	11.2	12.8	9.9
Apr	34.7	14.4	9.2	12.1	5.1	15.6	8.9
May	34.4	10.9	1.5	18.2	3.0	25.9	6.1
Jun	31.0	5.7	2.1	19.3	2.6	33.3	6.0
Jul	19.8	2.5	2.5	31.2	2.0	35.9	6.1
Aug	22.9	1.2	2.0	24.6	1.7	42.5	5.1
Sep	29.8	5.1	1.4	18.1	5.1	35.8	4.7
Oct	43.4	14.9	2.7	14.1	5.4	12.7	6.8
Nov	34.5	16.8	3.8	12.5	8.8	13.0	10.7
Dec	26.5	23.8	2.4	10.3	16.6	11.5	9.0

3.5 Land Use / Land Cover Data

As part of Project ATLANTA, much research has focused on learning more about the rapid growth and evolution in land use and land cover of Atlanta. This study utilizes land use imagery from 1997 (Yang and Lo 2002) in order to better understand where UHI–initiated precipitation events begin in relation to the urban areas of Atlanta. The 1997 land use image (Figure 1.4) is based on Landsat TM imagery from 29 July 1997. However, due to clouds in the initial image, another image taken on 2 January 1998 was used to supplement the 1997 image (Yang and Lo 2002).

3.6 Research Methodology

Due to past research that suggested the summer months have the most pronounced UHI, the number of days included in this study was reduced to the warm season months of May through September, since that is when the UHI should be significant (Huff and Changnon 1972; Gallo and Owen 1999). Days that were not considered to have weak synoptic flow were removed from the analysis in order to avoid precipitation events that were significantly influenced by features other than the UHI. This study partially adopts the approach of Brown and Arnold (1998) to determine weak synoptic flow. In their study of non–classical mesoscale circulations and convection initiated by land–cover boundaries, weak synoptic flow was defined as: (1) no synoptic–surface forcing mechanism identifiable within 500 km; (2) 500 mb wind speeds within the region of less than 15 kts; and (3) surface wind speeds of less than 10 kts. However, Vukovich (1974) points out that while increased vertical wind shear may reduce the intensity of the UHI under synoptic high pressure systems, clear nocturnal skies should allow the differential heating processes of a typical UHI to prevail. Therefore, this study does not remove days with stronger upper–level winds since the UHI, while perhaps weakened, should remain the dominant factor under synoptic high pressure (Vukovich 1974). Further, past studies of UHI–altered precipitation (Changnon 1981; Bornstein and LeRoy 1990; Bornstein and Lin 2000) did not remove days from analysis based on upper–level flow. The purpose of these selection criteria is to avoid precipitation events caused by forcing mechanisms other than those associated with the UHI.

The first step in selecting days for the study was to remove days when there was a synoptic–surface forcing mechanism (e.g., front) within 500 km of the study area. This was accomplished by examining the Unisys national surface meteorological charts (Appendix A). Days that had a synoptic–surface forcing feature within 500 km of Atlanta during all observations were removed from further study. Observations were available for only 0000 UTC and 1200 UTC on most days.

Radar reflectivity data from summer days with weak synoptic flow were analyzed in order to find precipitation cells that initiated around Atlanta. Events were sought based primarily on their reflectivity appearance (size and shape) and location (proximity to Atlanta and other cells) at initiation in order to identify precipitation events that were likely induced (not simply enhanced) by the urban area. Moreover, events were selected so it could not easily be argued that they were initiated by any means other than the UHI. Therefore, due to the strict criteria required for events to be included as UHI–initiated precipitation, any errors in selection likely underestimate the actual number of events.

The reflectivity data were displayed in a 24–hour loop at 15–minute intervals using software written in Research Systems, Inc. Interactive Data Language (IDL) version 5.5 (Appendix B). This visual analysis is subjective; events were sought based on the location of each cell as well as its proximity to other cells (Figure 3.4). For example, even if a cell initiated directly over downtown Atlanta, it was not included in the study if it occurred during a warm afternoon and there were other cells across the region. Most likely, such a precipitation cell (Figures 3.4a) is due to daytime heating and instability, and is not limited to urban areas. Further, even if a study day had no major surface forcing mechanisms identified on the synoptic chart but there was some influence of an atmospheric boundary (Figure 3.4b), that event was not included. This study contains only precipitation events that were relatively isolated and clearly located over the Atlanta area (Figures 3.4c and 3.4d). Both Figure 3.4c and 3.4d show isolated cells over Cobb County. Large (i.e., supercells), multi–cell, and stratiform precipitation events were not included in the study.

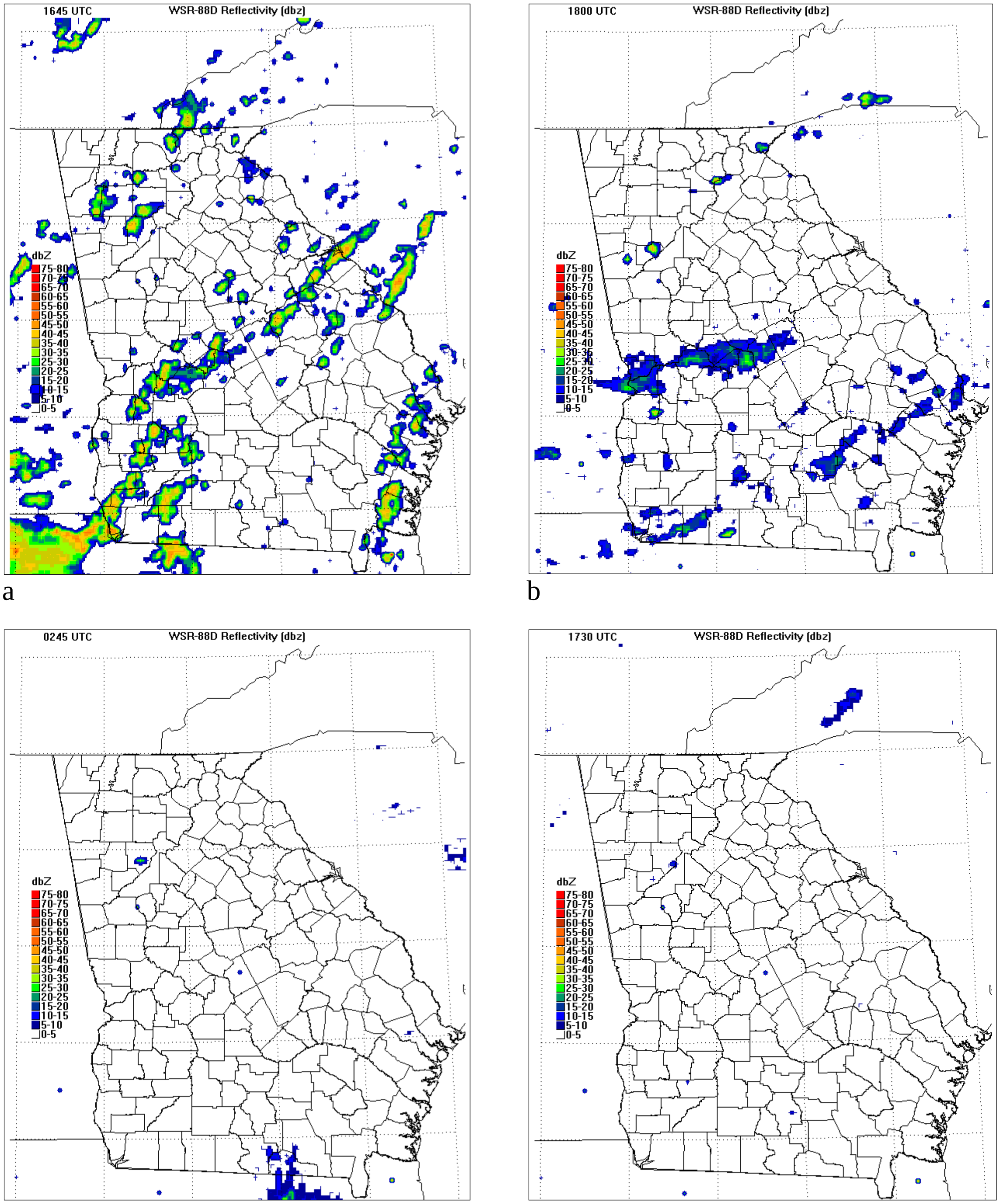

Figure 3.4: GHRC radar reflectivity data displayed using software written in IDL 5.5. (a) 1645 UTC 01 August 2000, scattered afternoon showers (b) 1800 UTC 26 July 1996, obvious influence of a boundary as at least 10 cells are seen stretching along a line from eastern Alabama up to southern North Carolina (c, d) 0245 UTC and 1730 UTC 06 August 2000, good examples of probable UHI–induced precipitation with single cells over Atlanta and no other nearby cells.

Examination of surface wind data from the network of surface stations used in this study was performed after potential UHI–induced precipitation events were identified with radar imagery. Any potential events with surface wind speeds greater than 5.1 m s^{-1} (10 kts) within Atlanta, at the event's initiation time, were removed from the study.

Once UHI–initiated storms were identified, each cell was recorded based on its initiation time, termination time, approximate initiation latitude, approximate initiation longitude, and initiation county or counties. Latitude and longitude values were taken from the approximate center of the first radar echo associated with the storm, but occasionally the cells overlapped multiple counties. Termination location is of little relevance to this study since the primary objective is to seek if, when, and where precipitation cells are initiated by UHI.

Each event was plotted according to its initiation location in ESRI ArcView GIS version 3.2 (ArcView) in order to illustrate the spatial distribution of these events. The events were also overlaid on the 1997 Landsat image of Atlanta as well as county boundaries and interstate highways. ArcView was then used to illustrate the number of UHI–induced precipitation events per county during the five–year study period.

Temporal patterns were examined by creating graphs of the number of UHI–induced precipitation events and event days by year and month. An UHI precipitation *day* is defined by this study as any day where at least one UHI precipitation event occurred. An UHI precipitation day may experience multiple UHI precipitation events. Also, the initiation times of all events were graphed in order to illustrate diurnal patterns. However, because this study attempts to filter out those times of day when convective precipitation is widespread, there may be a bias towards nocturnal events. This point is discussed in more detail in Chapter 4.

Hourly data (temperature, dewpoint, wind direction, wind speed, and atmospheric pressure) from the surface meteorological stations around Atlanta were imported into the Unidata version of the General Meteorology Package version 5.6 (GEMPAK) in order to create local surface maps based solely on local station observations for each UHI precipitation event. These maps display any differences in temperature and wind across the Atlanta area that might lead to UHI precipitation as well as illustrating the local surface conditions required to be considered weak synoptic flow. The surface charts were created for each hour associated with an UHI precipitation event (Appendix C) in order to display possible temperature boundaries around the edge of the UHI and wind convergence boundaries induced by the UHI. Unfortunately, these charts were of limited utility due to the sparse network of weather stations around Atlanta. Therefore, graphs of urban–rural temperature differences were plotted in order to show, in greater detail, the strength of the UHI on days of UHI–initiated precipitation as compared to UHI intensity on average summer days.

Two stations were chosen to represent the urban and rural environments. Based primarily on the 1997–1998 land use image (Figure 1.4), the Clark Atlanta University (ATA) station is in the most urban location and the Roopville Georgia Power Plant in Wansley, Georgia (ROP) is located in the most rural location. Both stations are part of the GAEMN network, so their instrumentation is identical. The 15–minute temperature values for both stations were graphed according to their time of observation for the 24–

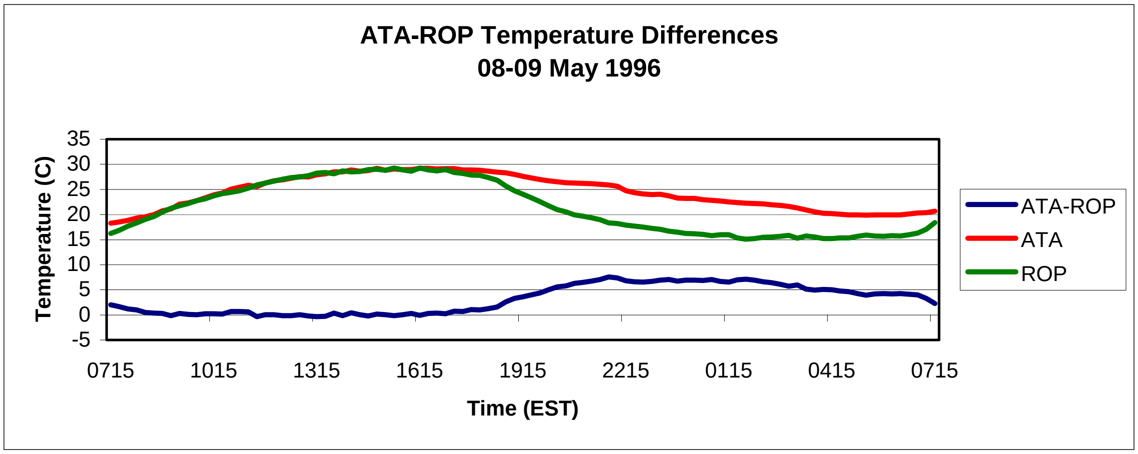

Figure 3.5: Example graph of 24–hour urban–rural temperature differences associated with an UHI–induced precipitation event; graphs for each event are listed in Appendix D.

hour period leading up to each UHI–induced precipitation event (Figure 3.5). Next, average temperatures for both stations were calculated at 15–minute intervals based on all of the 24–hour periods associated with the UHI–initiated precipitation events. This yielded average temperature values for both stations over a 24–hour period before an event. These averages were also graphed and will be discussed in Chapter 4. For comparison, average temperature values for both stations were calculated at 15–minute intervals for the entire study period as well as 20 convective precipitation days that were not associated with Atlanta’s UHI, and these are also discussed in Chapter 4. A difference of means test was conducted to determine whether there was a statistically significant difference (α = 0.05) in the intensity of the UHI for an average UHI–initiated precipitation day and an average study period day. Since both the mean temperature and standard deviation could be calculated for each event, the standard normal distribution (Z–score) method was used to compare the event days and average days UHI–intensity. In addition, monthly average temperatures for both ATA and ROP were calculated for the 24–hour periods leading up to each UHI–induced precipitation event as well as for the entire study period. Also, the average monthly urban–rural temperature differences (based on ATA–ROP) were calculated for each event and the total study period.

GEMPAK was also used to display radiosonde data for each UHI precipitation day in the form of Skew–T/Log–P diagrams (Appendix E). This data is generally available only at 0000 UTC and 1200 UTC each day. Therefore, Skew–T/Log–P diagrams were created for the observation times immediately before and after each UHI precipitation event. Nine stability indices were calculated for each sounding in order to determine whether convective precipitation was expected for each event day as well as whether any of the indices were able to consistently predict UHI–initiated precipitation. The stability indices used in this study are: Showalter Index, Lifted Index (LI), Severe Weather Threat (SWEAT) Index, K Index, Cross Totals (Ctot), Vertical Totals (Vtot), Total Totals (Ttot), Convective Available Potential Energy (CAPE), and Convective Inhibition (CIN). In addition, average soundings were calculated based on all UHI–induced precipitation days (average UHI sounding) as well as all days included in the study (average total period sounding) and 20 days that experienced convective precipitation but were not counted as UHI–induced precipitation events. Each average sounding was determined by calculating the mean temperature (ºC) and dewpoint (ºC) at every observed pressure level for all days. The pressure values (mb), and their associated temperature and dewpoint values, were then aggregated into groups of 20 mb (100–119, 120–139,…961–980, 981–1000), and each group was given a label based on the median pressure within that group. For example, the group ranging from 100–119 mb was labeled *Group 110*. For the purposes of plotting a skew–T / log–P, a mean pressure value was calculated for each group based on the pressure levels included within that group.

Each group’s temperature and dewpoint values were determined by calculating the mean of all available observations within the 20 mb range of that group. After the two average soundings were completed, the two files were merged based on like pressure groups. Finally, mean group temperature and dewpoint values for the average total period sounding were subtracted from the average UHI sounding in order to find the temperature and dewpoint differences between the two soundings at each level. A difference of means test was conducted to determine whether there was a statistically significant difference between the temperatures and dewpoints of the average UHI sounding and the average total period sounding at each level. Also, the mean 1000–550 mb layer temperature and dewpoint for each event sounding was compared to the mean values for an average day in order to determine if most of the events illustrated higher temperature and dewpoints through that layer. As seen in Chapter 4, that particular layer showed a higher moisture content for the average event sounding, and comparing each event’s layer to the average shows whether this was the result of certain influential observations or actually a representative average. The 850–700 mb lapse rate was also calculated for each event as well as the total period average since that layer appeared to have a greater lapse rate on UHI–induced precipitation days.

Finally, air mass types, according to the SSC, that were present during the day of and the two days prior to each UHI–initiated precipitation event were analyzed in order to determine whether these events occurred under warmer, more humid air masses and/or if the events were preceded by warmer/cooler and moister/drier air. First, graphs were produced based on the frequency (percentage of total) of each air mass type during UHI–induced precipitation days.

Likewise, graphs depicting the frequency, based on the SSC, of each air mass type during the entire study period were also produced. Then a third graph was made to depict the frequency of each air mass type during a two–day period prior to each event. The purpose of the third graph is to determine if UHI–induced precipitation occurred due to the transition of air masses over the area. A two–day period was analyzed in case there was an air mass transition at the end of a day or an UHI–induced precipitation event at the beginning of a day.

It was hypothesized that a warm, relatively dry air mass (such as air mass type DT) might create a stronger UHI due to the lower specific heat value of drier air, and that may, in turn, enhance the likelihood of precipitation initiated by the UHI. Therefore, the mean urban–rural (ATA–ROP) temperature difference was calculated for each air mass type based on the 24–hour mean temperature differences between ATA and ROP for every day of the study period. The mean urban–rural temperature difference was also calculated for each air mass type based on the nocturnal (21–13 UTC; 17–09 EDT) mean temperature difference between ATA and ROP for every day of the study period and is discussed in Chapter 4.

3.7. Summary

Using radar reflectivity data from the GHRC, surface meteorological data from ASOS and GAEMN sites, archived synoptic surface charts from Unisys, upper–air sounding data from KFFC, and air mass types for Atlanta, this project applied a methodology that was focused primarily on determining whether the UHI of Atlanta initiated thunderstorms due to the urban–rural temperature difference and/or other conditions related to this difference (e.g., lapse rate, moisture content, surface wind convergence). Possible events were identified using the radar reflectivity data and suitable conditions were verified using the surface data. Further, temporal and spatial patterns of the UHI–induced precipitation events were determined based on five years of data. Urban–rural temperature differences for each event were calculated based on data from an urban station (ATA) and a rural station (ROP); differences were calculated based all event days, the total study period, and 20 non–UHI convective precipitation events. Likewise, the differences between the average temperature and dewpoint of the mean UHI–induced precipitation sounding, the mean sounding for the entire study period, and the mean sounding for the 20 non–UHI convective precipitation events were calculated at 45 vertical levels. Statistical tests were performed to determine if there were significant differences between UHI intensity on UHI–induced precipitation days and average days as well as the average event day sounding and the average sounding for the entire study period. Average urban–rural temperature differences were also calculated for each air mass type. All of these findings are discussed in the next chapter, where they are placed in the context of the existing literature on UHIs and are used to better understand the role of Atlanta’s UHI in producing convective precipitation.

CHAPTER 4

RESULTS

This project seeks a better understanding of precipitation initiated by the UHI of Atlanta, Georgia during the warm season (May – September) of 1996–2000 in order to determine if, when, and where the UHI of Atlanta induces precipitation. By learning more about the spatial and temporal patterns as well as the typical air mass types and UHI–intensities associated with Atlanta's UHI–induced precipitation events, this study attempts to further the understanding of the conditions necessary for UHI–initiated precipitation.

Bornstein and Lin (2000) showed three precipitation events that were likely initiated by Atlanta's UHI, but their study only covered a nine–day period, and it did not systematically filter out cases that may have been initiated by features other than the UHI. Because this study only includes days with weak synoptic forcing, only precipitation events initiated due to the characteristics of Atlanta's UHI should be identified.

This study included 765 days, but 569 days were deemed to have synoptic flow weak enough to be included in the study based on the proximity of no surface fronts, strong boundaries, or tropical systems near the Atlanta area. Based on research by Bornstein and Lin (2000), this author expected to identify many events over the five–year period. Surprisingly, only 20 days (3.5% of study days) were identified as UHI–induced precipitation days. Based on this rather small sample, there were some significant patterns in surface and upper–air data associated with these days that differ when compared to average days throughout the study period. However, the analysis of synoptic air mass types associated with UHI–induced precipitation days yielded rather inconclusive results that should be researched over a longer study period.

4.1 UHI–Initiated Precipitation Events

During the warm season of the years 1996–2000, 37 events of UHI–initiated precipitation were identified in the Atlanta area based on radar reflectivity (Table 4.1). These events occurred during 20 separate days. It can be seen that most of the events did occur near high–density urban areas of Atlanta (Figure 4.1). While low–density urban areas are widespread across Atlanta, much of the high–density urban locations are situated near or along major limited access highways (i.e., interstate highways). It is evident that most events were also located near these limited access highways. When the events were tabulated by individual counties, it is obvious that counties nearer the urban center experienced more events while those counties on the edge of metropolitan Atlanta experienced fewer events. Figures 4.1 and 4.2 show the location of each event based on the latitude and longitude of the storm center. However, many storms were large enough to cover portions of multiple counties, therefore an event is considered to have begun in a county if the first echo was in any part of that county. If the first echo of an event was located in multiple counties, then each of those counties were counted.

Table 4.1: UHI–initiated precipitation events listed by event number, date, initiation and end times (UTC), and initiation county.

EVENT #	YEAR	MONTH	DAY	DOY	INIT–END TIMES (UTC)	INITIATION COUNTY
1	1996	May	09	130	1115–1445	Fulton
2	1996	May	09	130	1115–1445	Cherokee
3	1996	May	11	132	0730–0900	Forsyth
4	1996	June	11	163	0200–0315	Cobb
5	1996	June	18	170	0515–0730	Cobb
6	1996	June	18	170	0515–0800	Henry
7	1996	June	18	170	0515–0815	Douglas
8*	1996	June	18	170	0530–0600	DeKalb
9*	1996	June	20	172	0700–0745	Cobb
10	1996	July	02	184	1730–2100	Fulton
11	1996	July	30	212	1100–1545	Cobb/Fulton
12	1996	August	03	216	1315–2130	DeKalb
13	1996	August	04	217	0800–1630	Henry
14	1996	August	07	220	1100–1200	Cherokee
15	1997	June	12	163	0715–0800	Fulton
16	1997	June	17	168	0700–0815	Paulding
17	1997	July	09	190	0030–0230	DeKalb
18	1997	July	09	190	0115–0445	Fulton
19	1997	July	09	190	0115–0445	Gwinnett
20	1997	July	18	199	0215–0345	Bartow
21	1997	July	18	199	0530–0600	Cherokee
22	1998	July	28	209	0400–1045	Douglas
23	1998	July	28	209	0400–1045	Fulton
24	1999	June	26	177	1000–1114	Cherokee
25	1999	June	26	177	1000–1300	Cobb/Fulton/Gwinnett
26	1999	July	31	212	0445–0515	Gwinnett
27	1999	July	31	212	0615–0645	Gwinnett
28	2000	May	2	123	0300–0330	Forsyth
29	2000	July	31	213	0515–0730	DeKalb
30	2000	July	31	213	0530–0545	Cobb
31	2000	July	31	213	0530–0700	Gwinnett
32	2000	July	31	213	0530–0715	DeKalb/Henry
33	2000	July	31	213	0530–0745	Newton/Henry
34	2000	August	06	219	0245–0300	Cobb
35	2000	August	06	219	0730–0745	Clayton
36	2000	August	06	219	1730–1745	Cobb
37	2000	August	06	219	1900–2000	Gwinnett/Forsyth

* Bornstein and Lin (2000) identified these events as well as one on 26 July 1996 at 1730 UTC, but the 26 July event was excluded from this study due to the apparent influence of a stationary front northwest of Atlanta.

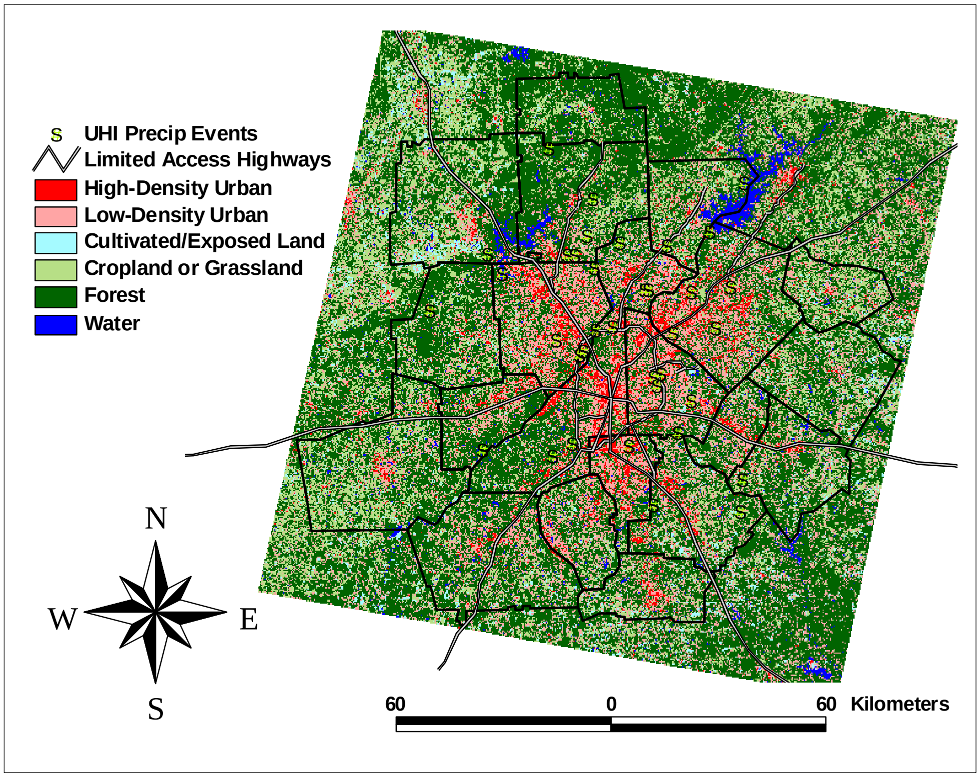

Figure 4.1: UHI–initiated precipitation events plotted by location of storm center overlaid on 1997–1998 land use/cover, county borders, and limited access highways.

Cobb County experienced the most events (eight) while DeKalb, Fulton, and Gwinnett Counties each had five or more events. Eight of the 20 counties saw no events during this study period.

The UHI–induced precipitation events recorded in this project illustrate expected patterns with respect to occurrence times. Most of these events took place during the predawn hours with only three events occurring between the hours of 14 and 00 UTC (09 and 19 EST) (Figure 4.3). This pattern is directly opposite that of typical summertime convective precipitation in Georgia according to Outlaw and Murphy (2000) who analyzed 10 years (1985–1994) of July radar data from Athens and Waycross, Georgia.

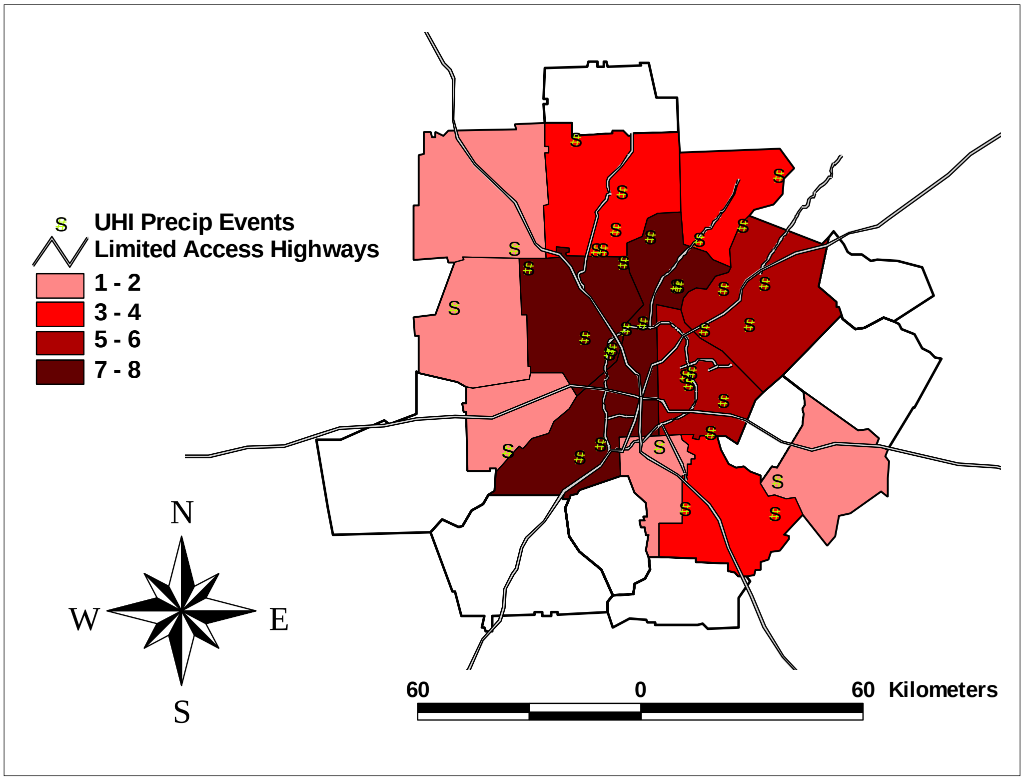

Figure 4.2: Atlanta counties by the number of UHI–initiated precipitation events that began in that county overlaid with event locations and limited access highways.

They found that July convective precipitation across northern Georgia most often began around 16 UTC (11 EST) with only two convective initiations occurring from 01 to 07 UTC (20 to 02 EST). During their 10–year study, 84% of convective precipitation events initiated between 12 and 20 UTC (07 and 15 EST). The difference between typical Georgia summertime convective precipitation and UHI–induced convective precipitation is consistent with previous research (Bornstein 1968; Landsberg 1981) that showed UHIs to be most intense at night. However, events may have occurred during periods of widespread general convection that were left out of the study due to the inability to distinguish between UHI–induced precipitation and general convective precipitation.

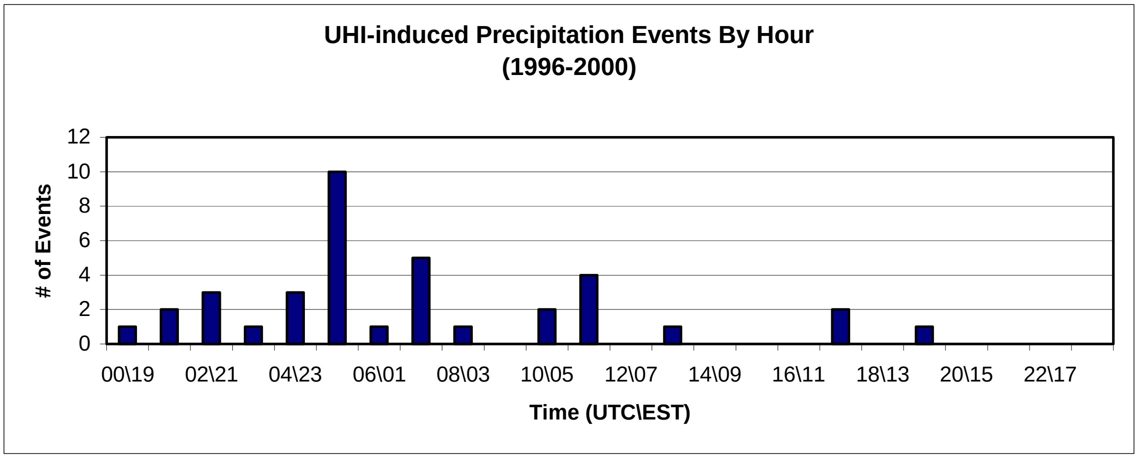

Figure 4.3: Graph of UHI–induced precipitation events by hour.

Therefore, the results of this study may show a larger fraction of nocturnal events than actually occurred.

In addition to illustrating patterns of occurrence during predawn hours, UHI–induced precipitation events documented in this study show a maximum number of events during the month of July (Figure 4.4) with 16 total events (43.2%) during seven different days (Figure 4.5). Every year in the study period experienced events during the month of July. Conversely, September is the only month included in the study without a single documented UHI–initiated precipitation event. May experienced four events (10.8%) across three days, June saw 10 events (27.0%) over six days while seven events (18.9%) during four separate days occurred in August.

Even though this study covers only five years, there is significant annual variation in the number of UHI–initiated precipitation events (Figure 4.6). The most events occurred in 1996 with 14 (37.8%) over 10 days. There were seven events (18.9%) over four days in 1997, two events (5.4%) during the same day in 1998, four events (10.8%)

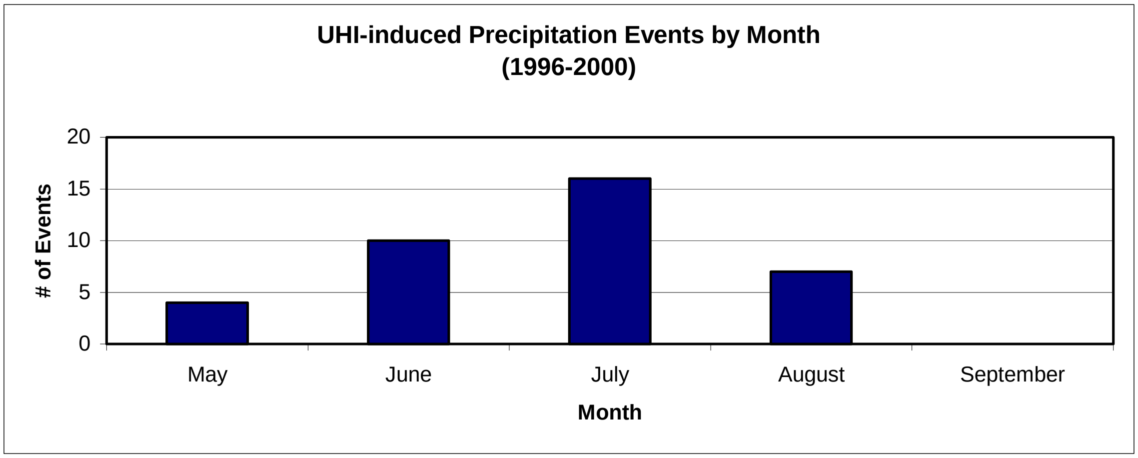

Figure 4.4: Graph of UHI–induced precipitation events by month.

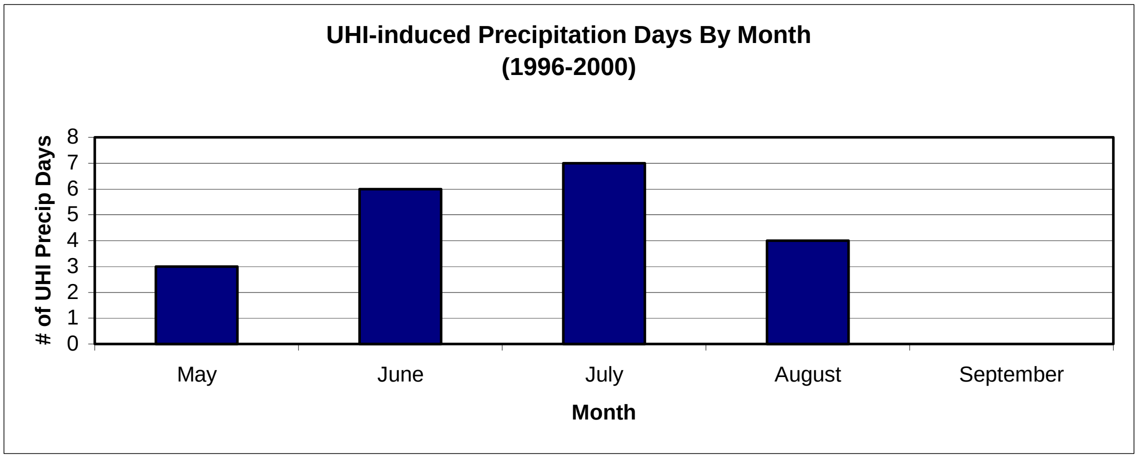

Figure 4.5: Graph of UHI–induced precipitation days by month.

across two days in 1999, and 2000 saw an increase with 10 events (27.0%) over two days. It should also be noted that the last three years of this study each had two or fewer event days (Figure 4.7). The decreased number of event days after 1997 could be explained by the intense drought that Georgia was experiencing during the 1998–2000 period. According to the Georgia Department of Natural Resources (2001), the worst drought in Georgia's history began around May 1998 and continued to worsen through 2000. Sporadic rainfall during the late summer and fall of 2000 provided limited relief to

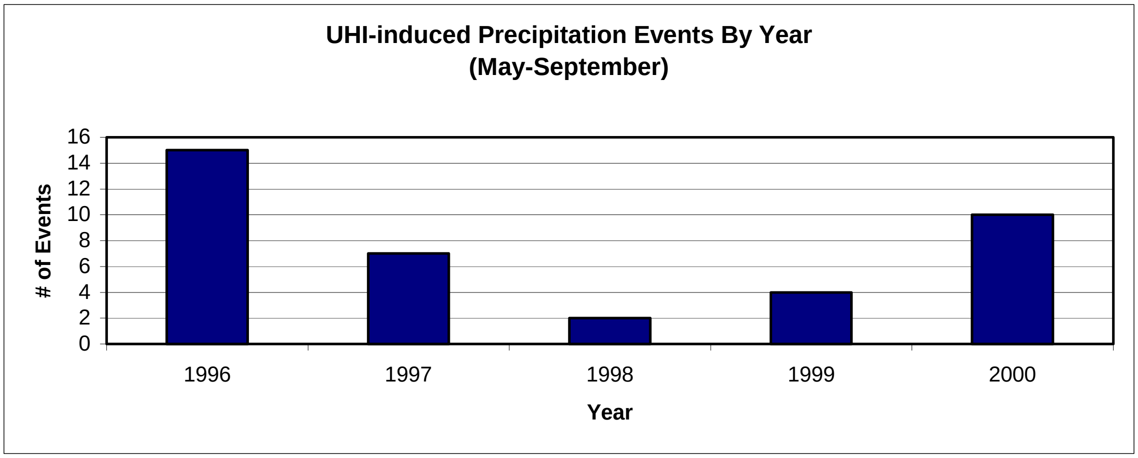

Figure 4.6: Graph of UHI–induced precipitation events by year.

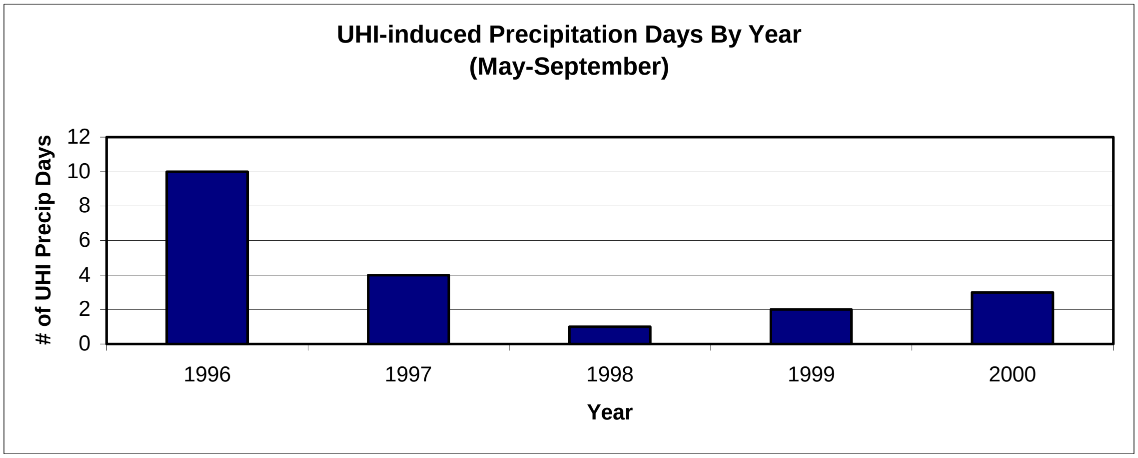

Figure 4.7: Graph of UHI–induced precipitation days by year.

some parts of the state. While there certainly may be other causes for the relatively small number of events and event days during the 1998–2000 period, the severe drought seems like a logical explanation. As will be shown later in the chapter, low–level moisture seems to play a major role in determining whether Atlanta's UHI initiated precipitation. A severe drought would significantly lower moisture content near the surface due to decreased evapotranspiration, so fewer UHI–induced precipitation was likely because of reduced low–level moisture content created by the widespread drought from 1998–2000.

4.2 Surface Analysis

This study makes use of data from 10 surface weather stations (Figure 3.2 and Table 3.2) within the 20–county Atlanta area (five GAEMN stations and five ASOS stations). Two more GAEMN surface stations (Duluth and Dempsey) have data available, but due to their close proximity to other stations, their data were not used in this study. Also, two ASOS stations located outside of metropolitan Atlanta (Gainesville and Rome) were used in this study. Unfortunately, the weather station network is relatively sparse throughout most of the area, especially to the east and west of the city along Interstate Highway 20.

A higher spatial density of hourly surface weather stations would provide more insight into possible patterns of surface temperatures and winds associated with UHI–induced precipitation. It might then be possible to distinguish subtle areas of weak (<5 m s^{-1}) convergence that have been observed with UHIs (Findlay and Hirt 1969; Balling and Cerveny 1987; Bornstein and Lin 2000). The temperature (°F), dewpoint (°F), wind direction (true), wind speed (kts), and altimeter setting (coded in. of mercury) data from the 10 stations available were plotted for the initial hour of each event. Wind speed values were rounded to the nearest 5 kts using the barbs, however, all observations reported in this project are less than 10 kts. The low surface wind speed values are consistent with strong UHIs (Oke 1973; Balling and Cerveny 1986; Morris et al. 2001), however, low surface wind speeds are also a characteristic of weak synoptic flow which was required for days to be included in this study.

Essentially, no significant patterns were illustrated by the plotted surface stations in this study. Some consistencies in the surface data include low wind speeds and higher temperatures near the urban center, but this was expected due to the selection criteria of this study. The network of surface stations is not dense enough nor does it cover enough of the area to perform useful analysis of convergence zones or mesoscale boundaries. Therefore, the surface weather stations in this project act more as justification for inclusion of the study days based on typical weak synoptic flow UHI characteristics rather than revealing tendencies of UHI–induced precipitation events.

In order to determine if UHI–initiated precipitation days experienced greater UHI intensity than normal warm season days and normal convective precipitation days, the average urban–rural temperature difference (based on ATA and ROP) for the three types of days were graphed and compared by hour (Figures 4.8, 4.9, and 4.10). At first glance, Figures 4.8 and 4.9 show little difference from one another. However, a difference of means test ($\alpha = 0.05$) that compared the average urban–rural temperature difference for both types of days yielded some significant differences (Table 4.2). Statistically significant differences between the average UHI–induced precipitation day urban–rural temperature difference and the average study period day urban–rural temperature difference occur in a rather sporadic manner with respect to time of day (Figure 4.11). Figure 4.10 is apparently different from the other two graphs with temperatures approximately 2–3°C greater throughout most of the day. Figure 4.10 also shows a weaker UHI due to the larger rural temperatures.

As with past research (Oke 1987), times of significant difference in Figure 4.8 seem to occur earlier, just after sunset. However the peak frequency of events is just after midnight (Figure 4.3). Nevertheless, Table 4.2 and Figure 4.11 show that, on average, UHI–induced precipitation days tended to experience greater UHI intensity for several

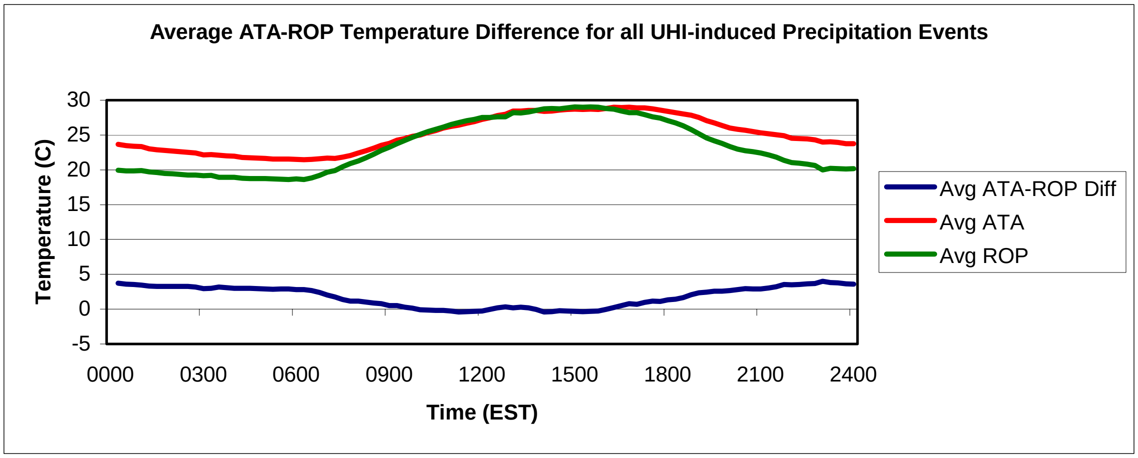

Figure 4.8: Average hourly urban–rural temperature difference for all UHI–induced precipitation events based on 24–hour observation period before each event.

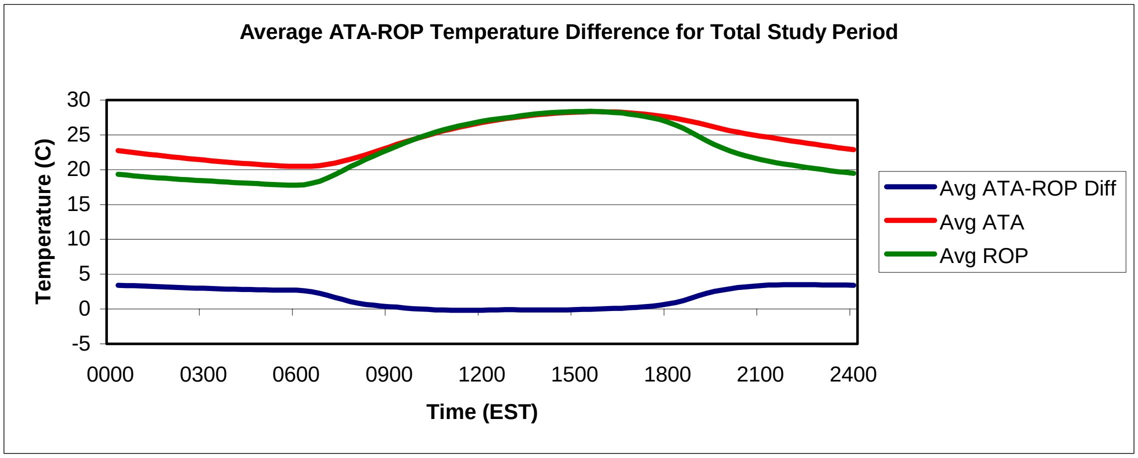

Figure 4.9: Average hourly urban–rural temperature difference for total study period.

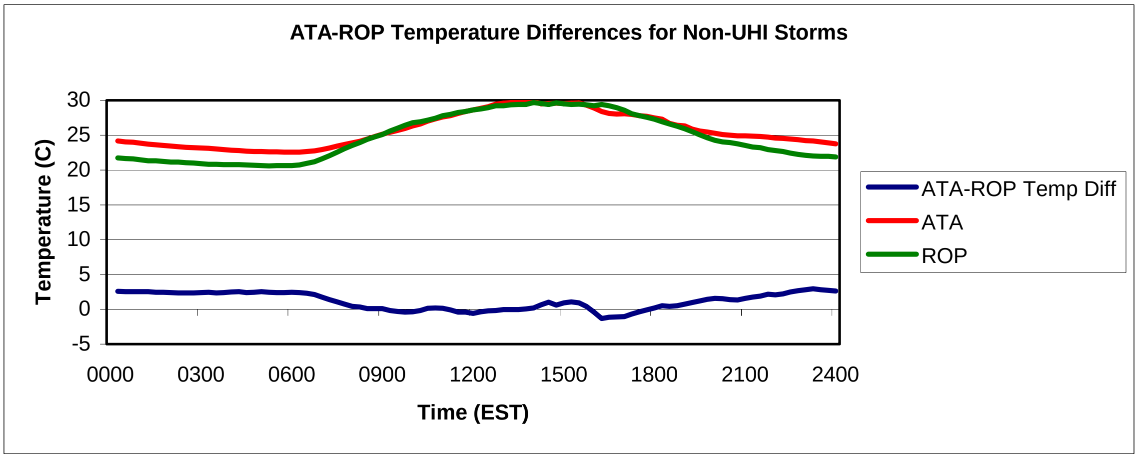

Figure 4.10: Average hourly urban–rural temperature difference for 20 convective precipitation days not selected as UHI–induced precipitation events.

Table 4.2: List of hourly Z–scores (standard normal distribution) calculated when comparing urban–rural temperature difference of average UHI–induced precipitation day (UHI) and average total study period day (average day); Z–scores are the result of a two–tailed test for statistically significant difference between the two types of days.

Hour (UTC)	Z–score ($\alpha = 0.05$)	Significant Difference	Larger Temp Difference
0000	0.71	No	n/a
0100	4.42	Yes	Average Day
0200	1.58	No	n/a
0300	2.86	Yes	UHI
0400	3.21	Yes	UHI
0500	2.39	Yes	UHI
0600	1.10	No	n/a
0700	1.51	No	n/a
0800	2.34	Yes	UHI
0900	2.29	Yes	UHI
1000	2.19	Yes	UHI
1100	2.02	Yes	UHI
1200	2.00	Yes	UHI
1300	6.08	Yes	UHI
1400	2.72	Yes	UHI
1500	1.12	No	n/a
1600	3.23	No	n/a
1700	1.66	No	n/a
1800	1.76	No	n/a
1900	2.74	Yes	UHI
2000	3.28	Yes	UHI
2100	6.34	Yes	UHI
2200	9.99	Yes	UHI
2300	7.03	Yes	UHI

hours during the day. Table 4.2 and Figure 4.10 show the hourly Z–scores calculated when comparing the UHI intensity of average UHI–induced precipitation days and average study period days. The only time of the day when UHI intensity appears to have been significantly greater on average study period days was 2100 EST.

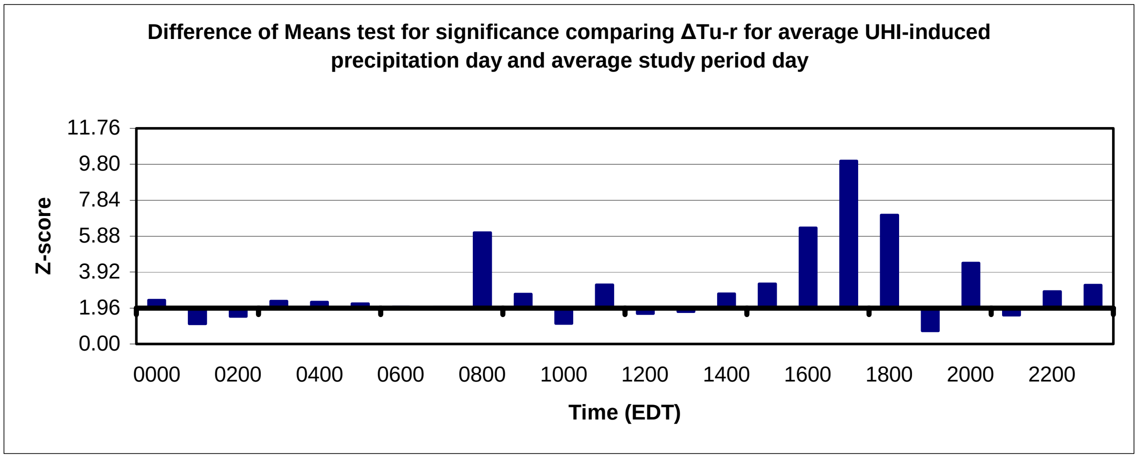

Figure 4.11: Graph showing Z–score values for each hour based on urban–rural temperature difference for average UHI–induced precipitation days and average total study period days; values greater than 1.96 illustrate a statistically significant difference.

Based on the surface station data in this study, no clear difference in UHI intensity can be discerned during hours of peak UHI–induced precipitation. However, it is seen that the daytime hours leading up to the events (urban and rural surface temperatures were analyzed for a 24–hour period prior to each event) show significantly stronger UHI intensities, on average. Perhaps this implies that UHI–induced precipitation is not necessarily more frequent during greater urban–rural temperature differences. More likely, UHI–induced convection does not become strong enough to create precipitation until a few hours after the peak UHI intensity. More research into this specific subject is certainly warranted.

Average urban–rural temperature differences for each month were also calculated based on all UHI–induced precipitation events as well as the total study period. Tables 4.3 and 4.4 show the results of these analyses. While July had the lowest urban–rural temperature difference based on average UHI–induced precipitation events as well as the entire study period, July also saw the greatest temperature values for both the urban and rural locations. Therefore, even though the UHI appears to be weaker during July because of smaller urban–rural temperature values, the urban area was actually warmer during July than any of the other months. However, the rural site was also much warmer during July. Since July experienced more events and event days than any other month, it seems that a greater urban–rural temperature difference does not necessarily yield more UHI–initiated precipitation.

Table 4.3: Average monthly temperature values for ATA, ROP, and the difference between the two based on the 24–hour periods prior to each UHI–initiated precipitation events.

	ATA Average Temperature	ROP Average Temperature	ATA–ROP Average Temperature Difference
May	23.4 ºC	19.9 ºC	3.5 ºC
June	23.6 ºC	22.1 ºC	1.5 ºC
July	26.3 ºC	25.1 ºC	1.2 ºC
August	26.0 ºC	24.3 ºC	1.7 ºC

Table 4.4: Average monthly temperature values for ATA, ROP, and the difference between the two based on the entire study period.

	ATA Average Temperature	ROP Average Temperature	ATA–ROP Average Temperature Difference
May	22.0 ºC	20.1 ºC	1.9 ºC
June	24.7 ºC	23.1 ºC	1.6 ºC
July	26.5 ºC	25.2 ºC	1.3 ºC
August	26.2 ºC	24.3 ºC	1.9 ºC
September	22.8 ºC	21.2 ºC	1.6 ºC

4.3 Upper–Air Analysis

Upper–air data for this project are based primarily on 0000 UTC and 1200 UTC soundings released from KFFC. While KFFC is relatively near some urban land use areas (Figure 3.2), it is essentially removed from the urban center of Atlanta. Therefore, upper–air data from KFFC are not considered to be completely representative of urban Atlanta. Nevertheless, the data are used in this project in order to identify the conditions under which UHI–induced precipitation occurred more often (e.g., drier, moister, warmer, capped, isothermal). The hypothesis is that sounding data would likely illustrate that Atlanta's UHI initiated precipitation when low–level temperature and moisture values were higher than average. Such a situation would have required an intense UHI and a moist air mass; those types of conditions could be the result of a moist tropical (MT) air mass.

To find any differences between the average sounding based on observations immediately before and after each UHI–induced precipitation event (Figure 4.12) and the average sounding based on all available observations during the study period (Figure 4.13), average temperature and dewpoint values at 45 vertical levels were compared for both soundings (Figure 4.14). Also, a difference of means test was conducted to determine whether differences between the two average soundings were significant (Table 4.5). However, it should be noted that the average soundings created for this study include observations from all times of the day into a single average. While it is possible that certain morning or evening soundings could strongly influence the average, it is not likely that low–level temperature and moisture values changed rapidly before or after each UHI–induced precipitation event due to the weak synoptic flow criteria required to include days in this study. Also, the 36 event soundings used in this study were composed of 18 soundings taken at 0000 UTC and 18 soundings taken at 1200 UTC, so the normal differences between morning and evening conditions should balance each other. Figure 4.14 and Table 4.5 show that the two average soundings were quite different from one another throughout most of the atmosphere based on a difference of means test ($\alpha = 0.05$). Figures 4.12 and 4.13 show that UHI–initiated precipitation days tended to have a less pronounced inversion than average days, and the inversion was slightly higher in the atmosphere. This is likely due to the increased surface temperature of stronger UHI days, and it is consistent with past studies that noticed the cross–over effect associated with strong UHIs (Duckworth and Sandberg 1954; Bornstein 1968; Clarke 1969). The weaker inversion should be conducive to convective development. In addition, Figure 4.12 shows much more variability in dewpoint with height than Figure 4.13. Figure 4.14 illustrates that the dewpoint is significantly higher throughout the lower half of the atmosphere for the UHI–initiated precipitation sounding. While the urban–rural temperature differences were significantly different throughout the atmosphere for UHI–induced precipitation days and average days, dewpoint values in the lower atmosphere (below 550 mb) showed a much larger difference. This implies that while a stronger UHI may be somewhat conducive to UHI–induced precipitation, moisture content is probably more important. This would also explain the dramatic decrease in events during drought years.

The average UHI–induced precipitation sounding was also compared to a sounding composed of average values from 20 days (four days selected from each study year listed in Table 4.6) that were under weak synoptic flow and experienced convective precipitation, but were not included as UHI–induced precipitation events. There were 20 non–UHI convective precipitation days selected because there were 20 UHI–induced precipitation days found in this study. Figure 4.15 shows the differences

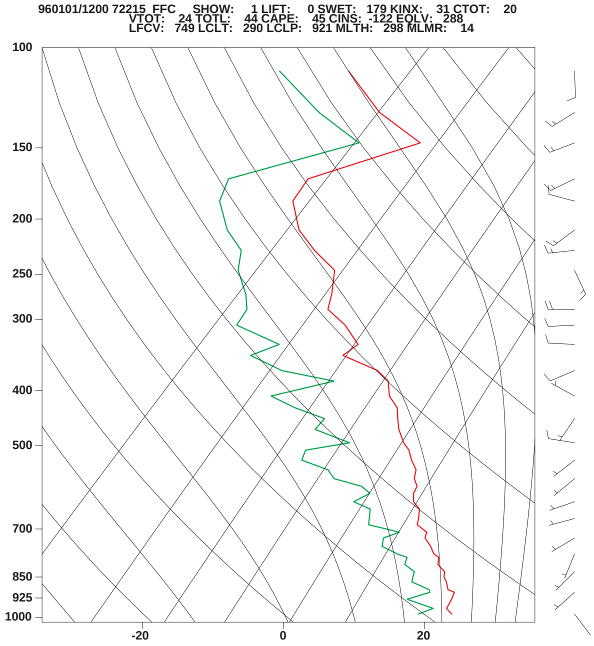

Figure 4.12: Average sounding based on observations immediately before and after each UHI–induced precipitation event.

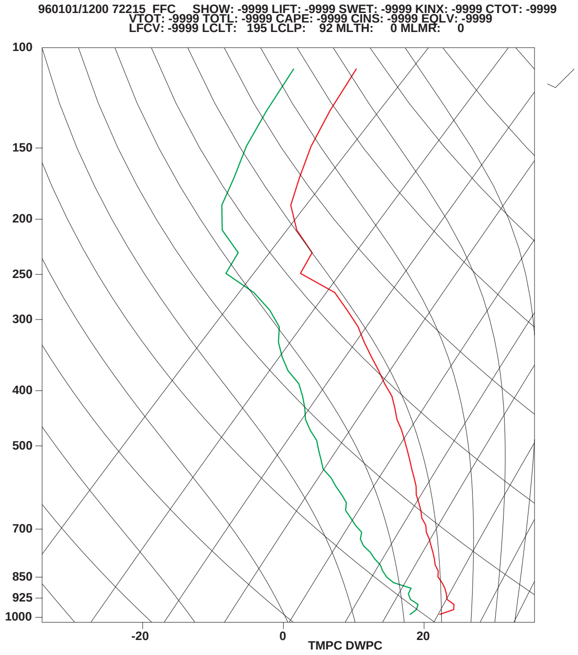

Figure 4.13: Average sounding based on all available observations from the entire study period.

Table 4.5: List of Z–scores calculated when comparing temperature and dewpoint values for average soundings based on UHI–induced precipitation days and the total study period.

Average Pressure	Temperature Z-Score (α = 0.05)	Significant Difference	Dewpoint Z–Score (α = 0.05)	Significant Difference
990	31.41	Yes	40.25	Yes
970	68.90	Yes	123.69	Yes
950	No data	No data	No data	No data
930	11.86	Yes	12.65	Yes
910	37.52	Yes	98.16	Yes
890	31.75	Yes	112.42	Yes
870	29.64	Yes	51.96	Yes
850	22.66	Yes	29.93	Yes
830	69.62	Yes	113.65	Yes
810	21.34	Yes	58.76	Yes
790	19.03	Yes	150.94	Yes
770	22.82	Yes	126.90	Yes
750	0.82	No	85.18	Yes
730	83.01	Yes	130.53	Yes
710	2.54	Yes	126.03	Yes
690	68.06	Yes	32.16	Yes
670	41.13	Yes	98.70	Yes
650	31.63	Yes	81.93	Yes
630	59.40	Yes	28.83	Yes
610	40.62	Yes	117.98	Yes
590	7.19	Yes	90.26	Yes
570	12.35	Yes	12.13	Yes
550	44.42	Yes	28.84	Yes
530	21.22	Yes	68.01	Yes
510	6.43	Yes	42.11	Yes
490	9.07	Yes	102.49	Yes
470	33.15	Yes	15.65	Yes
450	4.35	Yes	97.42	Yes
430	16.25	Yes	42.56	Yes
410	22.11	Yes	115.31	Yes
390	3.20	Yes	86.14	Yes
370	10.49	Yes	24.32	Yes
350	155.06	Yes	125.72	Yes
330	19.90	Yes	10.35	Yes
310	66.70	Yes	85.33	Yes
290	81.38	Yes	53.37	Yes
270	5.55	Yes	22.49	Yes
250	24.70	Yes	7.19	Yes
230	0.00	No	3.28	Yes
210	4.01	Yes	9.25	Yes
190	5.28	Yes	10.14	Yes
170	49.76	Yes	22.25	Yes
150	515.42	Yes	593.32	Yes
130	367.13	Yes	391.20	Yes
110	53.18	Yes	105.32	Yes

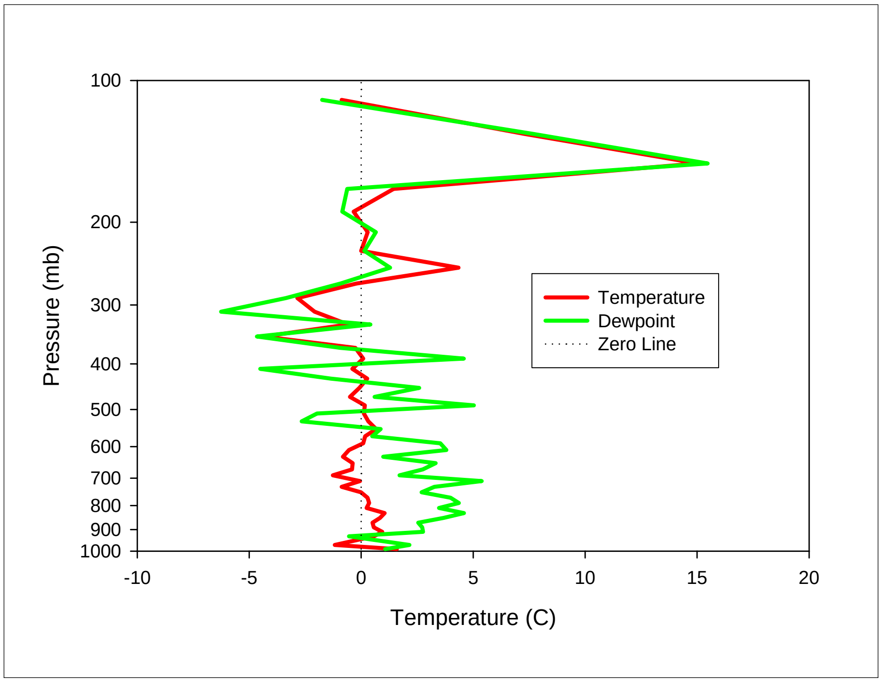

Figure 4.14: Average UHI–induced precipitation sounding temperatures and dewpoints minus average total period sounding temperatures and dewpoints; positive values imply greater temperatures for average UHI sounding.

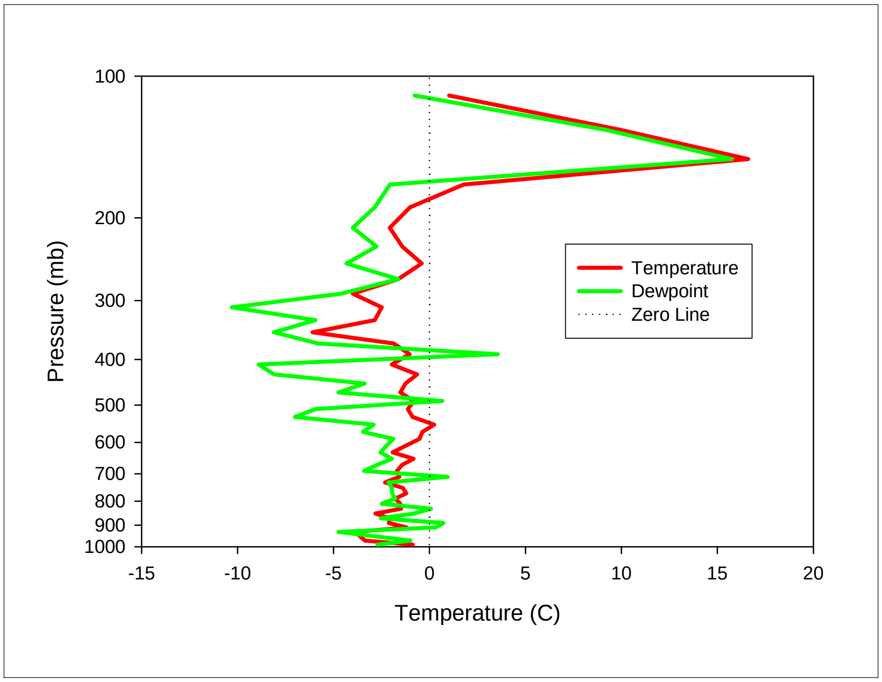

Figure 4.15: Average UHI–induced precipitation sounding temperatures and dewpoints minus the average convective precipitation sounding temperatures and dewpoints; positive values imply greater values for the UHI–induced precipitation soundings.

Table 4.6: Four days from each year in the study period with convective precipitation during weak synoptic flow, but no apparent association with Atlanta's UHI.

1996	1997	1998	1999	2000
25 June	26 June	18 June	27 June	11 July
17 July	01 July	08 July	06 July	29 July
31 July	28 July	25 July	17 July	02 August
01 August	15 August	09 August	13 August	24 August

between the two average soundings, and it is evident that UHI–induced precipitation days experienced relatively cooler, drier, and more stable conditions than those days with widespread convective precipitation. This suggests that UHI–initiated precipitation tends to occur when conditions are more humid and unstable than average, but not humid and unstable enough for widespread convection.

To determine whether low–level (below 550 mb) temperature or dewpoint must be greater than an average day for the UHI to initiate thunderstorms, graphs were made to show how each of the events mean 1000–550 mb temperature and dewpoint values compared to the average values (Figure 4.16 and 4.17). That particular layer was chosen because of its higher moisture content illustrated in Figure 4.14. It is apparent that the 1000–550 mb layer was warmer than average (12ºC) for only two soundings (5.6%); it must be noted that those two sounding were not on the same day. Conversely, the same layer was moister than average (3.1ºC) for 21 of 36 soundings (58.3%). Therefore, while neither temperature nor dewpoint values for event soundings were above average enough to make conclusive statements about low–level conditions required for UHI–induced precipitation, it is evident that a higher low–level moisture content is more closely related to UHI–induced precipitation than higher low–level temperatures. However, higher low–level temperatures would be less conducive to convective formation than a higher low–

level lapse rate, which is present between 850 and 700 mb for the average event sounding (Figure 4.14). The lapse rate between 850 and 700 mb on the average sounding for the entire period is 5.6ºC km^{-1}. Only seven of the UHI–event day soundings yielded lapse rates less than the total period average; the average 850–700 mb lapse rate for UHI–induced precipitation days was 6.3ºC km^{-1} (Figure 4.18). Decreasing temperature with height may initiate convection that could produce precipitation when encountering the increased moisture at the same level. It is likely that the observed increased lapse rate between 850 and 700 mb is just as important for UHI–induced precipitation as is the increased moisture content. Perhaps the above average lapse rate is steep enough to allow the UHI to trigger convection, but not large enough for widespread development. Figure 4.15 shows that UHI–induced precipitation days experienced lesser lapse rates than convective precipitation not associated with the UHI from the surface to near 500 mb.

Also, for the most part, severe weather indices (Lifted, SWEAT, K, Cross Totals, Vertical Totals, Total Totals, and CAPE) calculated based on KFFC sounding data usually suggested little or no chance of thunderstorms (Table 4.7) based on the interpretations of each index by Sturtevant (1995). Therefore, the lack of any stability indices implying thunderstorms on event days suggests that conditions at the relatively rural location of KFFC were not conducive to convective precipitation development. The K Index seems to have been the most consistent predictor based on this study, as 22 of the 39 observations (56.4%) yielded K Index values indicating more than just scattered thunderstorms. However, the K Index increases as mid–level moisture (i.e., 700 mb)

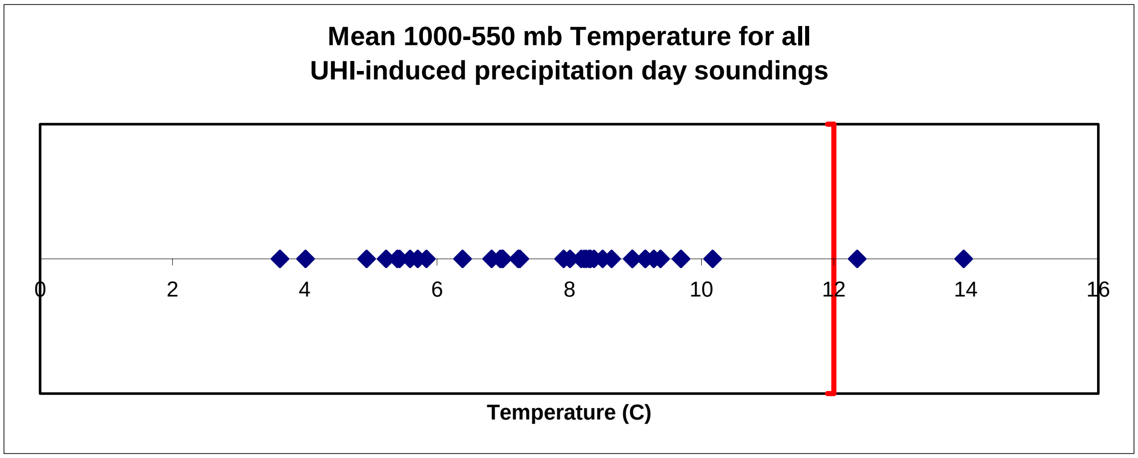

Figure 4.16: Mean 1000–550 mb temperature for each event; the red line represents the mean layer temperature for the entire study period.

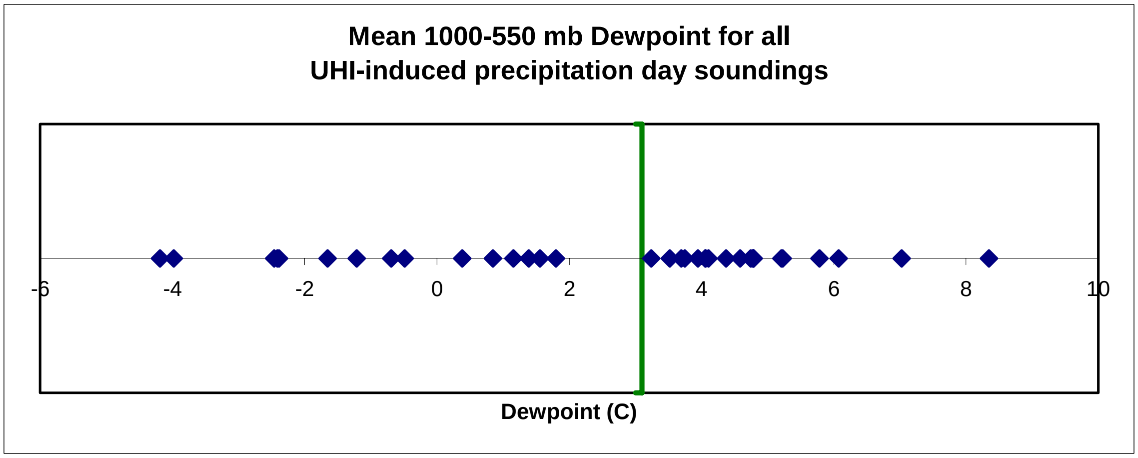

Figure 4.17: Mean 1000–550 mb dewpoint for each event; the green line represents the mean layer dewpoint for the entire study period.

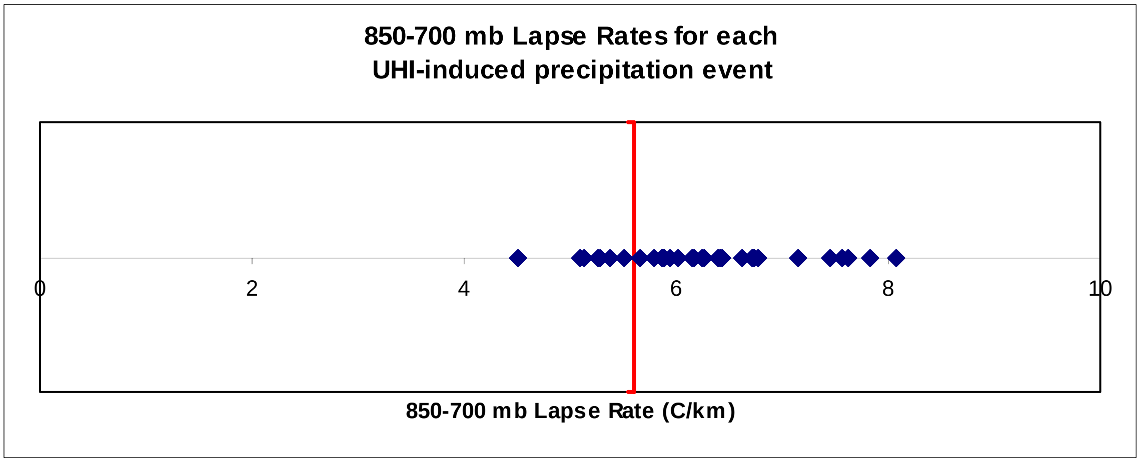

Figure 4.18: Lapse rate for the 850–700 mb layer for each event; the red line represents the average 850–700 mb lapse rate of 5.6ºC km^{-1}.

Table 4.7: List of severe weather indices calculated for each event based on 0000 UTC and 1200 UTC KFFC sounding data; values highlighted based on interpretations by Sturtevant (1995)—green: storms unlikely or weak; yellow: scattered or moderate storms; red: numerous and/or strong storms.

Time (UTC)	Date yymmdd	Showalter	LI	SWEAT	K	Ctot	VTot	Ttot	CAPE (J/Kg)	CIN (J/Kg)
00	960509	2	1	143	15	19	26	45	0	0
00	960511	3	3	114	30	17	26	44	0	0
00	960611	3	1	200	31	19	25	44	0	0
00	960618	2	0	183	32	19	23	41	0	0
00	960620	–1	–3	187	34	21	26	47	0	0
00	960702	2	–3	207	30	17	23	40	0	0
00	960730	–1	–3	237	30	22	24	46	0	0
00	960803	1	–1	176	31	19	25	44	0	0
00	960804	2	0	195	34	18	23	41	0	0
00	960807	1	–2	185	35	20	24	43	924	–40
00	970612	–2	–4	180	35	24	25	49	0	0
00	970617	–3	–5	357	37	24	26	49	0	0
00	970709	1	–1	178	32	20	25	44	1092	–45
00	970718	0	–4	162	34	20	27	47	0	0
00	980728	1	–5	232	29	19	25	44	0	0
00	990731	5	–2	49	13	9	32	41	0	0
00	000502	6	4	68	23	16	26	41	0	0
00	000807	–1	–4	179	31	20	26	47	0	0
00	000820	0	–3	165	14	19	28	46	0	0
12	960509	4	1	123	8	18	25	43	0	0
12	960511	1	–3	193	27	22	26	47	0	0
12	960611	6	3	145	15	16	23	40	0	0
12	960618	1	0	171	32	20	23	43	0	0
12	960620	0	–2	180	35	21	25	46	0	0
12	960702	–1	–2	215	39	21	26	46	0	0
12	960730	7	–3	153	15	10	27	37	0	0
12	960803	2	–1	210	31	19	23	42	0	0
12	960804	1	–3	192	36	20	23	43	0	0
12	960807	1	–2	177	32	20	24	44	0	0
12	970612	0	1	203	36	22	22	44	0	0
12	970617	–2	–3	229	34	23	24	47	0	0
12	970709	1	–3	193	29	20	25	45	1032	–16
12	970718	0	–3	162	32	20	26	46	0	0
12	980728	–2	–3	265	40	23	24	47	0	0
12	990626	0	1	231	36	21	22	43	0	0
12	990731	9	–4	11	8	2	30	32	0	0
12	000501	12	9	32	–29	6	25	30	0	0
12	000806	–1	–3	194	25	22	26	48	0	0
12	000820	–7	–11	–9999	21	28	35	62	0	0

increases, so moist air masses, such as those usually over Atlanta during summer months, should yield higher K Index values.

4.4 Spatial Synoptic Classification

As mentioned before, an UHI tends to be stronger under certain circumstances (clear skies, light winds, high temps), therefore certain air mass types are likely to be more conducive to intense UHIs and UHI–induced precipitation. Using the SSC to separate different air mass types, this study compares various characteristics of each type and correlates them with UHI–initiated precipitation events.

A strong UHI tends to develop when rural areas are able to radiate quickly and cool off more than the urban area. This means that a night that is clear and dry (as well as calm) should yield the strongest UHI, and it is hypothesized that a stronger UHI should increase the chance of UHI–induced precipitation since the urban air column would be more unstable. Therefore, the mean hourly nocturnal (01 – 13 UTC; 20 – 08 EST) temperature difference between an urban site (ATA) and a rural site (ROP) for each SSC type is calculated (Table 4.8). Predictably, air masses that were drier and warmer yielded the highest urban–rural temperature differences. The DT (dry tropical) air mass type showed a mean urban–rural temperature difference of 3.84°C. The lowest mean temperature difference was produced by MP (moist polar) air masses due to the lower temperatures and higher moisture content.

When air mass types of UHI–initiated precipitation days are compared to typical summer days, there are some telling differences (Figure 4.19). While the percentage of MT days is comparable for UHI–initiated precipitation days (40.0%) and the 1996–1999

Table 4.8: Mean hourly nocturnal urban–rural temperature differences for each air mass type.

SSC Type	Mean Temp Difference	Standard Deviation
DM	3.67°C	1.43°C
DP	3.01°C	1.09°C
DT	3.84°C	1.35°C
MM	1.54°C	0.86°C
MP	0.67°C	0.85°C
MT	2.82°C	1.10°C

average (43.6%), there is a notable difference in the percentage of MM, DT, and DM days. The percentage of MM on UHI–induced precipitation days (33.3%) is roughly double the percentage of MM days during the 1996–1999 period (17.2%). DT days also have a higher percentage of UHI–induced precipitation days (13.3%) with over four times the percentage of the average frequency of DT days during the 1996–1999 period (3.3%). However, DM days have approximately half the percentage of the 1996–1999 period (26.4%) with respect to UHI–initiated precipitation days (13.3%). Once again, these results suggest that moist air masses tend to yield UHI–induced precipitation much more often than dry air masses. Also, while warmer temperatures seem more conducive to these events than cooler temperatures, it is the moister air masses, not those with greater urban–rural temperature differences, that produce more UHI–initiated precipitation events. Further, since MM air masses were much more frequent on event days than on average, it appears that events occurred when conditions were moderately unstable (i.e., MM days would provide moist conditions but lower temperatures, so the surface would be cooler than MT days, and the environment would be less stable than an average day, but more stable than a day that reaches convective temperature and allows widespread convection).

The graph of air mass types for two days prior to each event based on percentage of total two–day periods (Figure 4.19) is quite similar to the graph of air mass type percentage of total days for the entire study period. Both show MT to be the most common air mass type followed by MM and DM. Also, unlike the UHI–induced precipitation days, prior days and the total period experienced a small percentage of DT days. This difference in the percentage of DT days seems to be the most significant distinction of UHI–induced precipitation days. It is worth noting that DT days also yield the highest nocturnal urban–rural temperature differences. Event days also show a moderately smaller percentage of DM days with a few more MM days than the total period and prior days. Essentially, it seems that the two–day periods before each event show little difference from the average days of the study period.

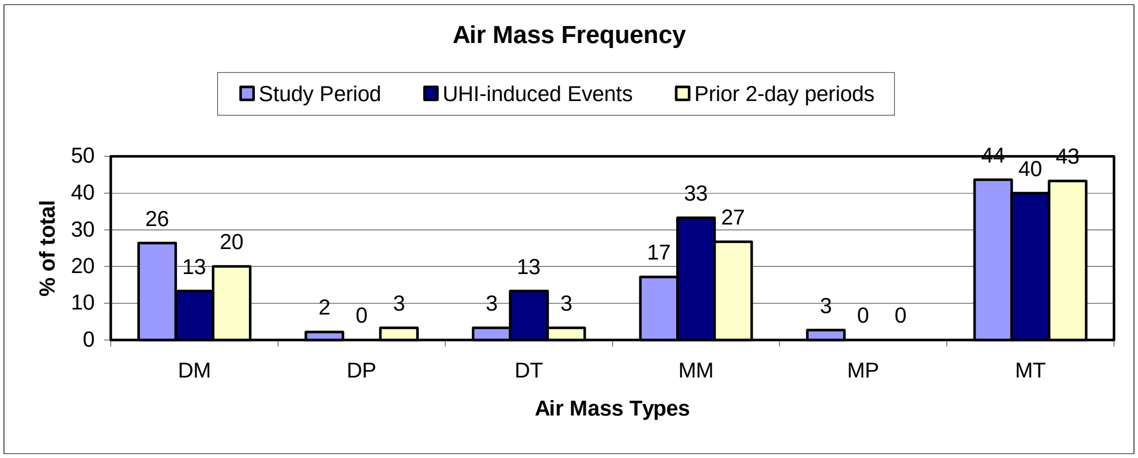

Figure 4.19: Frequency of air mass types for (a) UHI–induced precipitation days, (b) study period days, and (c) two–day periods prior to each event; transitional days (TR) are not listed here.

It was hypothesized that UHI–induced precipitation events might be most common when warm, humid air masses (MM and MT) move into Atlanta right after warm, dry air masses (DM and DT) were present. This would provide a strong UHI due to warm, dry air that would potentially create convection upon the introduction of ample humidity available from MM and MT air masses. Therefore, the transitional air mass types from two days prior to an event day were analyzed (Table 4.9). However, during the period 1996 to 1999 (period of available SSC data), only six (40.0%) of the 15 event days saw a relatively dry air mass followed by a moister air mass. Conversely, five (33.3%) of the 15 days saw a relatively moist air mass followed by a drier air mass. There were also four (26.7%) days with no change in air mass type over the three–day period. This information does not support the hypothesis that transition from warm, dry

Table 4.9: Air mass type of each UHI–induced precipitation event day and the two days prior.

Date (YYYYMMDD)	SSC Type	SSC 1 Day Prior	SSC 2 Days Prior
19960611	DM	TR (transitional)	MM
19960618	MT	DM	DM
19960620	MT	MT	MT
19960702	DT	DT	DM
19960730	DM	DM	MM
19960803	MT	MT	MM
19960804	MT	MT	MT
19960807	MT	MT	MT
19970612	MM	MM	DP
19970617	MM	MM	MT
19970709	MT	MM	DM
19970718	MM	MT	MT
19980728	MM	MT	MT
19990626	MM	MM	MM
19990731	DT	DM	MT

air to warm, humid air is more prone to UHI–induced precipitation. However, the limited number of events recorded in this project, especially due to possible influences of a severe drought, are not sufficient to make conclusive statements about the association between the transition of air mass types and UHI–induced precipitation.

4.5 Summary

The number of UHI–initiated precipitation events during the study period of 1996–2000 is actually rather small. With averages around seven events and four days per year, the contributions of these storms to local water budgets is likely insignificant. However, these events do tend to form near high–density urban areas more often than other parts of Atlanta, so it is probable that particular locations receive precipitation from these storms multiple times each year; this may increase the chances of urban flash–floods. UHI–induced precipitation in Atlanta is most common during predawn hours with a peak around 05 UTC (00 EST), and the month of July is the most likely time of the year for these events.

There is much that can be said about UHI–induced precipitation events based on surface weather station and KFFC sounding data for this study. Statistical tests showed significant differences between UHI–induced precipitation days and typical warm season days with respect to urban–rural temperature differences as well as KFFC sounding data. Based on these differences, it seems that these events may be affected more by low–level moisture and lapse rates than strong urban–rural surface temperature differences. More detailed research that focuses particularly on surface and / or upper–air conditions associated with Atlanta’s UHI–induced precipitation may yield more profound results.

Nevertheless, such a project would require a better network of surface meteorological stations.

Finally, air mass types show some possibly useful patterns associated with Atlanta’s UHI–initiated precipitation. It is evident that UHI–initiated precipitation occurred most often under moist air masses. Based on this study, air masses with greater urban–rural temperature differences did not yield as many events, and this is likely due to their lower moisture content. However, DT days were much more frequent on UHI–induced precipitation days than non–event days, and DT air masses yield the highest nocturnal urban–rural temperature differences among air mass types. Therefore, it may be shown through further research (especially over a longer period of time) that the migration of warm, dry (DT) air masses into Atlanta during the summer may increase the chances of UHI–induced precipitation.

CHAPTER 5

SUMMARY AND CONCLUSIONS

This study analyzed five years (1996–2000) of meteorological data during the warm season months of May, June, July, August, and September in order to find patterns associated with Atlanta's UHI–initiated precipitation. Further, the patterns presented were used to determine what air mass types and UHI–intensities tended to produce UHI–induced precipitation on certain days as opposed to others. Past studies have shown that UHIs commonly enhance precipitation in and around large cities (Huff and Changnon 1972; Huff and Changnon 1973; Changnon 1981) and some studies have even shown UHIs to initiate precipitation (Bornstein and LeRoy 1990; Bornstein and Lin 2000). However, it is still uncertain what particular variables determine whether an UHI will induce precipitation.

The number of UHI–induced precipitation events, based on analysis of 2–km 15–min national radar mosaics, was recorded along with the time and location of each precipitation cell. The strength of the UHI was determined for each event, as well as an average for the total study period and 20 non–UHI convective precipitation days, by comparing the temperature values from a weather station in an urban area (ATA) and a weather station in a rural area (ROP). Also, temperature and dewpoint values from soundings taken at 0000 and 1200 UTC at KFFC on each event day were compared with an average sounding based on the total study period and 20 non–UHI convective precipitation days. Finally, air mass types based on the SSC were compared during days with UHI–initiated precipitation and during average days. Annual variation in the number of events and days was quite large, but that was likely due to the intense drought in Georgia that limited the available moisture in the area during the period 1998–2000. Therefore, the annual patterns exhibited by the results of this project are not likely representative of a larger sample. However the monthly and diurnal patterns found by this project are quite significant. Based both on the frequency of events and event days, July experienced the most UHI–induced precipitation. June was second, followed by August and May. This supports past research (Huff and Changnon 1972; Gallo and Owen 1999) that suggested the UHI is most pronounced during the warmer summer months

Despite the fact that some afternoon events possibly could have been missed due to the exclusion of times with widespread convection caused by daytime heating and the strict criteria used in selecting events, the large number of events that occurred during nocturnal (especially predawn) hours cannot be ignored. This five–year study found 21 events (56.8%) between the times of 0100 UTC and 0700 UTC. Conversely, a 10–year (1985–1994) study by Outlaw and Murphy (2000) analyzed the temporal and spatial patterns of July convective precipitation in Georgia based on radar reflectivity from Athens and Waycross, Georgia, and they found only two events (1.1%) around Athens (approximately 100 km north–northeast of Atlanta) between those hours. It must be noted that Outlaw and Murphy (2000) only looked at the month of July, and their methodology was not identical to this project. Nevertheless, this study found 12 events between the times of 0100 UTC and 0700 UTC in the month of July over a period of five years; that is approximately 12 times as many events as Outlaw and Murphy (2000) found around the less urban Athens area. Further, it is likely that very few, if any, events were left out of this project due to their occurrence during the warm afternoon. While there were many days with widespread, daytime heating–induced precipitation, most of those cells did not have the appearance (relatively small, single–cell, etc.) of the average cell initiated by the UHI. Many of the afternoon precipitation events over Atlanta may have been enhanced by the UHI, but identifying UHI–enhanced events was not the purpose of this study.

The spatial distribution of UHI–initiated precipitation events during this study is relatively consistent. Most events occurred north of Interstate Highway 20, and most events occurred near urban areas (Figure 4.1). However, just because an area occurred within the counties of Atlanta does not necessarily mean it was over an area of urban land cover as shown in Figure 1.4. If an event met the criteria for inclusion outlined in Chapter 3, and the cell was anywhere within the counties of Atlanta MSA, then it was included. Only after plotting events based on their initiation locations were they overlaid on the land use/cover image to determine each event’s proximity to urban areas. A the higher frequency of events in the northern part of Atlanta is likely due to the widespread development north of downtown. Figures 1.2, 1.3, and 1.4 show how much urban land area has increased in the northern half of Atlanta since 1973, particularly near and between Interstate Highways 75 and 85.

Greater urban–rural temperature differences were hypothesized to yield more UHI–initiated precipitation events. Statistical tests performed in this project (see Table 4.2 and Figure 4.10) show that UHI–induced precipitation days did tend to display somewhat larger urban–rural temperature differences than average days. However, the most significant differences in urban–rural temperatures occurred during times of minimum UHI–induced precipitation. Therefore, the intensity of the UHI may not be as important in formation of UHI–induced precipitation as other factors. More likely, UHI–initiated precipitation occurs a few hours after the peak urban–rural temperature even though initial cloud development may occur closer to the time of larger temperature differences.

When sounding data from each UHI–initiated precipitation event (as well as the average of all events) was compared with average sounding data based on the total study period, it was shown that both temperature and dewpoint were significantly different throughout most of the atmosphere, but temperature differences were much smaller than dewpoint differences. The dewpoint temperature for an average UHI–induced precipitation day sounding was greater than for an average study day through nearly the entire lower half of the troposphere (up to 550 mb). In fact, dewpoint temperatures for an average UHI–initiated precipitation day sounding were as much 5º C greater in the lower half of the troposphere. Above 550 mb, dewpoint values for an average UHI–initiated precipitation day became much more variable with height. Nevertheless, it is the lower part of the atmosphere (below 550 mb) that should be more important for initiating precipitation due to the UHI during weak synoptic forcing. Therefore, based on urban–rural surface temperature values as well as average sounding data, it seems that higher moisture content in the lower atmosphere plays a more significant role in determining whether the UHI will initiate precipitation than does temperature. Urban–rural surface dewpoint values were not compared in this study because the urban surface was expected to consistently have much lower moisture content (Myrup 1969; Sisterson and Dirks

1978). The surface maps in Appendix C show that all but one of the observations reported a lower dewpoint for ATA than that for ROP. Also, based on the average soundings for all events and average days, UHI–induced precipitation days appeared to have weaker, more elevated surface inversions. This is consistent with past studies that found the cross–over effect (Duckworth and Sandberg 1954; Bornstein 1968; Clarke 1969) in other large urban areas. Finally, analysis of various stability indices, based on the average UHI–induced precipitation sounding, showed that these events tended to occur during less favorable conditions for strong or widespread convective development. This is supported by the average sounding based on convective precipitation days not associated with Atlanta's UHI. Such days displayed warmer, moister, and less stable conditions than the average UHI–induced precipitation day. Convective precipitation becomes widespread during the afternoon when conditions are quite unstable and the convective temperature is reached due to daytime heating. After an afternoon of convective showers, the environment is more stable and usually cooler due to evaporation of precipitation. However, if the environment is only moderately unstable, the convective temperature may not be reached due to daytime heating and some sort of trigger, or lifting mechanism is required for convective precipitation. Therefore, on these moderately unstable days, no widespread convection occurs before sunset and the environment remains moderately unstable through the night. Once the urban–rural temperature difference becomes significant, the warmer urban area acts as a lifting mechanism and initiates convective precipitation.

Based on air mass types, this project shows that most (73%) UHI–induced precipitation days occur under moist conditions (MM and MT specifically). However, 63% of the total study period experienced moist air masses. Nevertheless, this supports the sounding data with respect to UHI–initiated precipitation occurring on more humid days. In addition, MM and MT days illustrated some of the lowest average urban–rural temperature values (Table 4.7). Therefore, it seems that UHI–induced precipitation may be controlled more by moisture content than urban–rural temperature differences.

Based on this study, as well as Bornstein and Lin (2000), it is apparent that precipitation does occasionally initiate as a result of Atlanta's UHI. This project tries to determine what conditions are most favorable for these UHI–initiated storms, and it seems that low–level moisture plays a major role. A few of the events analyzed here had moisture values lower than average, and many non–event days saw moisture values as high as most event days. Therefore, it is probably not as simple as a single threshold moisture value. However, it does appear that UHI–induced precipitation tended to occur more often when low–level moisture (not necessarily at the surface) was above average and the 850–700 mb lapse rate was between 5ºC km^{-1} and 7ºC km^{-1}.

Overall, this study shows that Atlanta's UHI–induced precipitation tends to occur more often during the warm season with a peak in July. These events are most common at night, especially between midnight and dawn. Urban–rural temperature differences likely play a role in initiation of these storms, but a more intense heat island does not necessarily yield more UHI–induced precipitation. Intense UHIs can occur under dry air masses that do not provide enough moisture for precipitation. Therefore, it appears that higher moisture values and a steeper lapse rate throughout the lower half of the atmosphere, perhaps due to a moister air mass, do increase the chance of UHI–initiated precipitation. It appears that the lower troposphere must be slightly favorable for convection in order for the UHI to initiate development, but it cannot be too favorable or else convective precipitation will be widespread.

REFERENCES

Ackerman, B., 1985: Temporal march of the Chicago heat island. *J.Climate Appl. Meteor.*, **24**, 547–554.

Atwater, M. A., 1971: The radiation budget for polluted layers of the urban environment. *J. Appl. Meteor.*, **10**, 194–204.

Balling, R. C., Jr. and R. S. Cerveny, 1987: Long–term associations between wind speeds and the urban heat island of Phoenix, Arizona. *J. Climate Appl. Meteor.*, **26**, 712–716.

Bornstein, R., 1968: Observations of the urban heat island effect in New York City. *J. Appl. Meteor.*, **7**, 575–582.

Bornstein, R., and M. LeRoy, 1990**:** Urban barrier effects on convective and frontal thunderstorms. Extended Abstracts, *Fourth Conf. On Mesoscale Processes*, Amer. Meteor. Soc., 120–121.

Bornstein, R., and Q. Lin, 2000: Urban heat islands and summertime convective thunderstorms in Atlanta: three case studies. *Atmos. Environ.*, **34**, 507–516.

Brown, M. E., and D. L. Arnold, 1998: Land–surface–atmosphere interactions associated with deep convection in Illinois. *Int. J. Climatol.*, **18**, 1637–1653.

Bruce, V., 1999: Atlanta's urban heat island. EOS Science News Office, NASA Goddard Space Flight Center Scientific Visualization. [Available on–line from http://svs.gsfc.nasa.gov/imagewall/LandSat/atlanta_heat_background.html.]

Chang, K., 2000, August 15: Scientists watch cities make their own weather. *New York Times*, p. F1. [Available on–line from http://query.nytimes.com/search/abstract?res=F60C12F63B5B0C768DDDA10894D8404482.]

Changnon, S. A., 1981: *METROMEX: A review and summary*, Amer. Meteor.Soc., 181 pp.

Changnon, S. A., R. G. Semonin, and F. A. Huff, 1976: A hypothesis for urban rainfall anomalies. *J. Appl. Meteor.*, **15**, 544–559.

Clarke, J. F., 1969: Nocturnal urban boundary layer over Cincinnati, Ohio. *Mon. Wea. Rev.*, **97**, 582–589.

Craig, K. J. and R. D. Bornstein, 2002: MM5 simulations of urban induced convective precipitation over Atlanta. Preprints *Fourth Symposium on the Urban Environment*: Norfolk, Virginia, Amer. Meteor. Soc.

Daly, J. T., 2000: Hot–lanta...lives up to its name. *Res. Reporter*, **29**, 7–12.

Delage, Y., and P. A. Taylor, 1970: Numerical studies of heat island circulations. *Bound. Layer Meteor.*, **1**, 201–226.

Draxler, R. R., 1986: Simulated and observed influence of the nocturnal urban heat island on the local wind field. *J. Clim. Appl. Meteor.*, **25**, 1125–1133.

Duckworth, F. A., and J. S. Sandberg, 1954: The effect of cities upon horizontal and vertical temperature gradients. *Bull. Amer. Meteor. Soc.* **35**, 198–207.

Figuerola, P. I., and N. A. Mazzeo, 1998: Urban–rural temperature differences in Buenos Aires. *Int. J. Climatol.*,**18**, 1709–1723.

Findlay, B. F., and M. S. Hirt, 1969: An urban–induced meso–circulation. *Atmos. Environ.*, **3**, 537–542.

Gallo, K. P. and T. W. Owen, 1999: Satellite–based adjustments for the urban heat island temperature bias. *J. Appl. Meteor.*, **38**, 806–813.

Gallo, K. P., A. L. McNab, T. R. Karl, J. F. Brown, J. J. Hood, J. D. Tarpley, 1993: The Use of NOAA AVHRR Data for Assessment of the Urban Heat Island Effect. *J. Appl. Meteor.*, **32**, 899–908.

Georgia Department of Natural Resources, January 2001: 1998–2000 Georgia Drought Report. Georgia Department of Natural Resources Environmental Protection Division, Atlanta, Georgia, 48 pp. [Available on–line from http://www.state.ga.us/dnr/environ/.]

Hafner, J. and S. Q. Kidder, 1999: Urban heat island modeling in conjunction with satellite–derived surface / soil parameters. *J. Appl. Meteor.*, **38**, 448–465.

Hoogenboom, G., 1996: The Georgia automated environmental monitoring network. Proceedings, *22nd AMS Conference on Agriculture and Forest Meteorology*, Atlanta, GA, pp. 343–346.

Howard, L., 1833: *Climate of London Deduced from Meteorological Observations***,** Harvey and Darton, London.

Huff, F. A., and S. A. Changnon, 1972: Urban effects on daily rainfall distribution. *Preprints 2nd National Conference on Weather Modification*: Santa Barbara, Amer. Meteor. Soc., pp. 215–220.

Huff, F. A., and S. A. Changnon, 1973: Precipitation modification of major urban areas. *Bull. Amer. Meteor. Soc.*, **54**, 1220–1232.

Huff, F. A. and J. L. Vogel, 1978: Urban, topographic and diurnal effects on rainfall in the St. Louis region. *J. Appl. Meteor.*,**17**, 565–577.

Kidder, S. Q., and O. M. Essenwanger, 1995: The effect of clouds and wind on the difference in nocturnal cooling rates between urban and rural areas. *J. Appl. Meteor.*, **34,** 2440–2448.

Landsberg, H. E., 1956: The climate of towns. *Man's Role in Changing the Face of the Earth*, University of Chicago Press, 584–603.

Landsberg, H. E., 1981: *The Urban Climate***.** Academic Press, New York, 275 pp.

Lo, C. P., D. A. Quattrochi, and J. C. Luvall, 1997: Application of high–resolution thermal infrared remote sensing and GIS to assess the urban heat island effect. *Int. J. Remote Sens.*, **18**, 287–304.

Manley, G., 1958: On the frequency of snowfall in metropolitan England. *Quart. J. Roy. Meteor. Soc.*, **84,** 70–72.

Mather, G. K., 1991: Coalescence enhancement in large multicell storms caused by the emissions from a kraft paper mill. *J. Appl. Meteor.*, **30**, 1134–1146.

Matson, M., E. P. McClain, D. F. McGinnis, Jr., and J. A. Pritchard, 1978: Satellite detection of urban heat islands. *Mon. Wea. Rev.*, **106**, 1725–1734.

Moreno–Garcia, M. C., 1994: Intensity and form of the urban heat island in Barcelona. *Int. J. Climatol.*, **14**,705–710.

Morris, C. J. G., I. Simmonds, and N. Plummer, 2001: Quantification of the influences of wind and cloud on the nocturnal urban heat island of a large city, *J. Appl. Meteor.*, **40**, 169–182.

Mullen, L., 1999, April 26: Welcome to the thunder dome: Atlanta's urban heat alters weather patterns. NASA Science News. [Available on–line from http://science.nasa.gov/newhome/headlines/essd26apr99_1.htm.]

Myrup, L. O., 1969: A numerical model of the urban heat island. *J. Appl. Meteor.*, **8**, 908–918.

Office of the Federal Coordinator of Meteorology, August 1994: Federal Standard for siting Meteorological Sensors at Airports. OFCM Publication FCM-S4-1994, Washington, D. C. [Available on–line from http://www.ofcm.gov/siting/text/a-cover.htm.]

Oke, T. R., 1973: City size and the urban heat island. *Atmos. Environ.*, **7**, 769–779.

Oke, T. R., 1987: Boundary Layer Climates 2nd Ed. *Routledge Publishing,* Cambridge University Press, 435 pp.

Olfe, D. B., and R. L. Lee, 1971: Linearized calculations of urban heat island convection effects. *J. Atmos. Sci.*, **28**, 1374–1388.

Outlaw, D. E. and M. P. Murphy, 2000: A radar–based climatology of July convective initiation in Georgia and surrounding area, *NOAA Eastern Region Technical Attachment*, **2000-04**, National Oceanic and Atmospheric Admistration, U. S. Department of Commerce, 15 pp.

Price, J. C., 1979: Assessment of the urban heat island effect through the use of satellite data. *Mon. Wea. Rev.*, **107**, 1554–1557.

Quattrochi, D. A., and J. C. Luvall, 1997: High spatial resolution airborne multispectral thermal infrared data to support anlaysis and modeling tasks in EOS IDS Project ATLANTA. Global Hydrology and Climate Center. [Available on–line from http://wwwghcc.msfc.nasa.gov/atlanta.]

Rao, P. K., 1972: Remote sensing of urban "heat islands" from an environmental satellite. *Bull. Amer. Meteor. Soc.*, **53**, 647–648.

Reisin, T., Z. Levin, and S. Tzivion, 1996: Rain production in convective clouds as simulated in an axisymmetrical model with detailed microphysics 2: Effects of varying drops and ice initiation. *J. Atmos. Sci.*, **53**, 1815–1837.

Research, Atlanta, Inc., 1993: The Dynamics of Change: An analysis of growth in metropolitan Atlanta over the past two decades, Policy Research Center, Georgia State University, Atlanta, GA.

Reuter, G. W., and S. Guan, 1995: Effects of industrial–pollution on cumulus convection and rain showers – a numerical study. *Atmos. Eniviron.,*. **29**, 2467–2474.

Rosenfeld D., 2000: Suppression of Rain and Snow by Urban and Industrial Air Pollution. *Science*, **287**, 1793–1796.

Roth, M., T. R. Oke, and W. J. Emery, 1989: Satellite–derived urban heat islands from three coastal cities and the utilization of such data in urban climatology. *Int. J. Remote Sens.*, **10**, 1699–1720.

Sheridan, S. C., 2002: The redevelopment of a weather–type classification scheme for North America. *Int. J. Climatol.*, **22**, 51–68.

Sierra Club, 1998: 1998 Sierra Club Sprawl Report, Sierra Club, 25 pp. [Available on–line from http://www.sierraclub.org/sprawl/report98/report.asp.]

Sisterson, D. L., and R. A. Dirks, 1978: Structure of the daytime urban moisture field. *Atmos. Environ.*, **12**, 1943–1949.

Sturtevant, J. S., 1995: *The Severe Local Storm Forecasting Primer*. Weather Scratch Meteorological Services, 197 pp.

United States Census Bureau, 2000: Census Bureau Home Page. [Available on–line from http://www.census.gov.]

Voogt, J. A. and T. R. Oke, 1997: Complete urban surface temperatures. *J. Appl. Meteor.*, **36**, 1117–1132.

Vukovich, F.M., 1974: A study of the effect of wind shear on a heat island circulation characteristic of an urban complex. *Mon. Wea. Rev.*, **103**, 27–33.

Yang, X., and C.P. Lo, 2002: Using a time series of satellite imagery to detect land use and land cover changes in the Atlanta, Georgia Metropolitan Area. *Int. J. Remote Sens.*, (in press).

APPENDIX A

SYNOPTIC SURFACE CHARTS

This appendix includes archived national surface maps from Unisys Corporation (http://weather.unisys.com). The observation times for most of these maps are 00 and 12 UTC, but the map for 06 August 2000 was observed at 20 UTC. The observation time nearest each UHI–induced precipitation event is shown in order to illustrate that no surface fronts or forcing mechanisms were present at the time of each event. Figure A.7 shows an event included by Bornstein and Lin (2000) but excluded from this study due to the frontal boundary across Atlanta. The stationary front through the panhandle of Florida in Figure A.12 was excused in this study even though it was not quite 500 km away from Atlanta; any effects of this front on Atlanta were thought to be minimal.

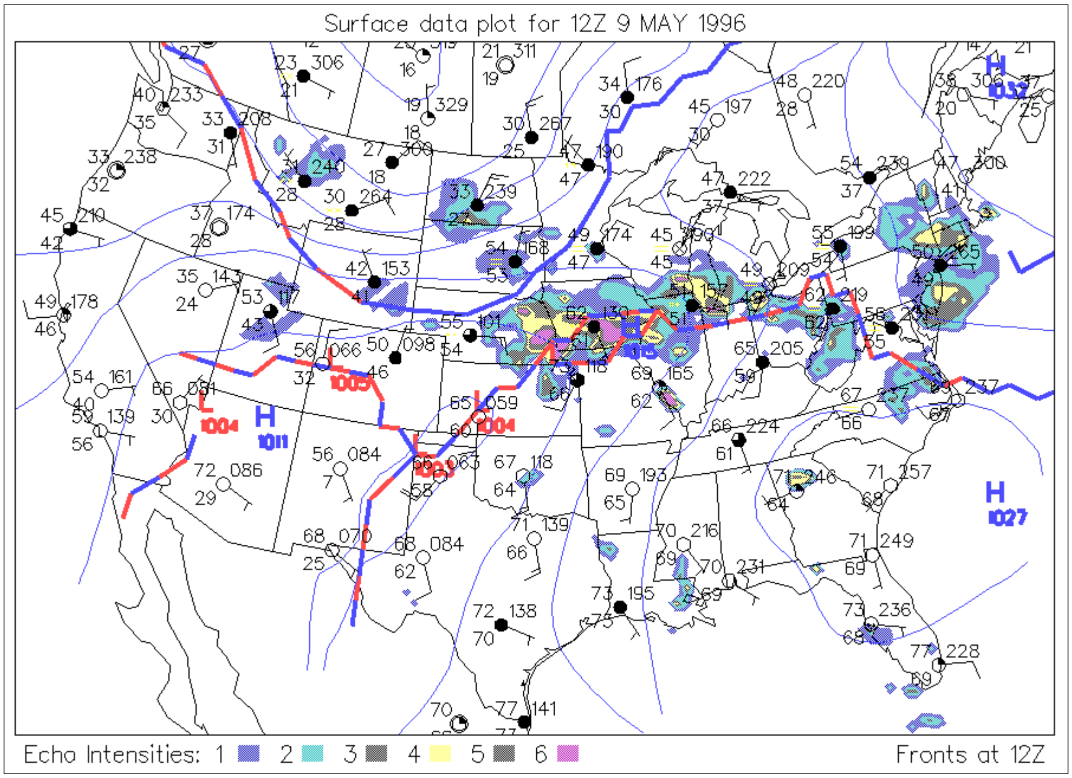

Figure A.1: 1200 UTC 09 May 1996 synoptic surface chart.

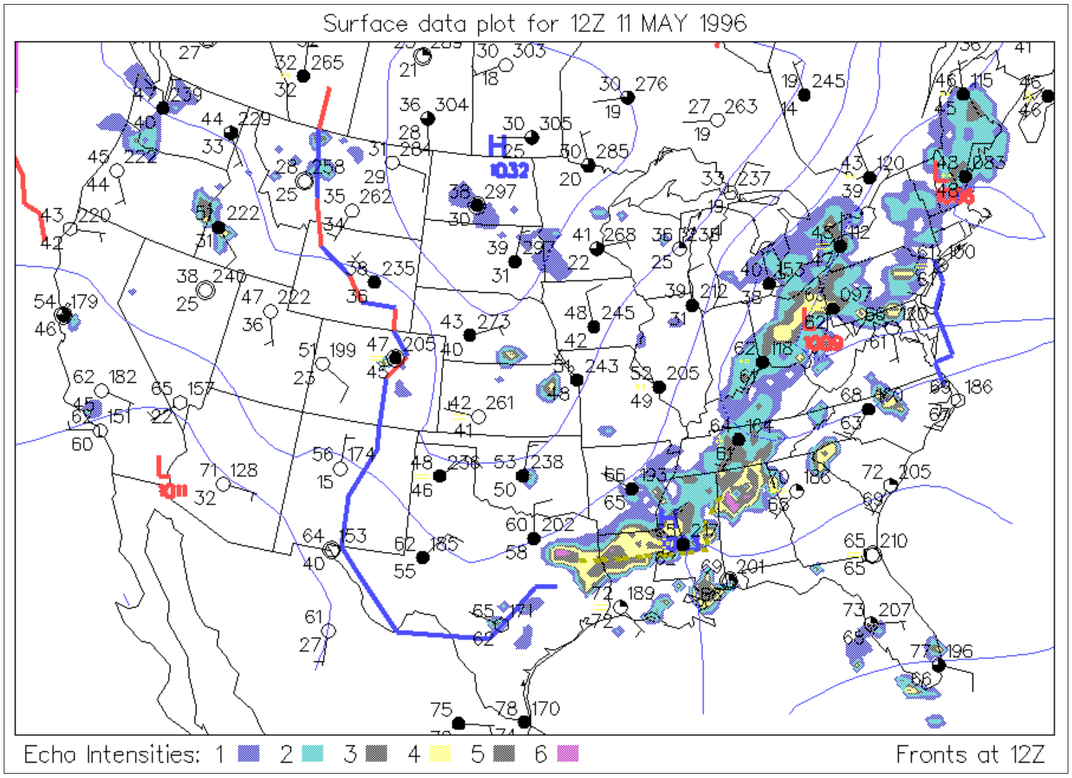

Figure A.2: 1200 UTC 11 May 1996 synoptic surface chart.

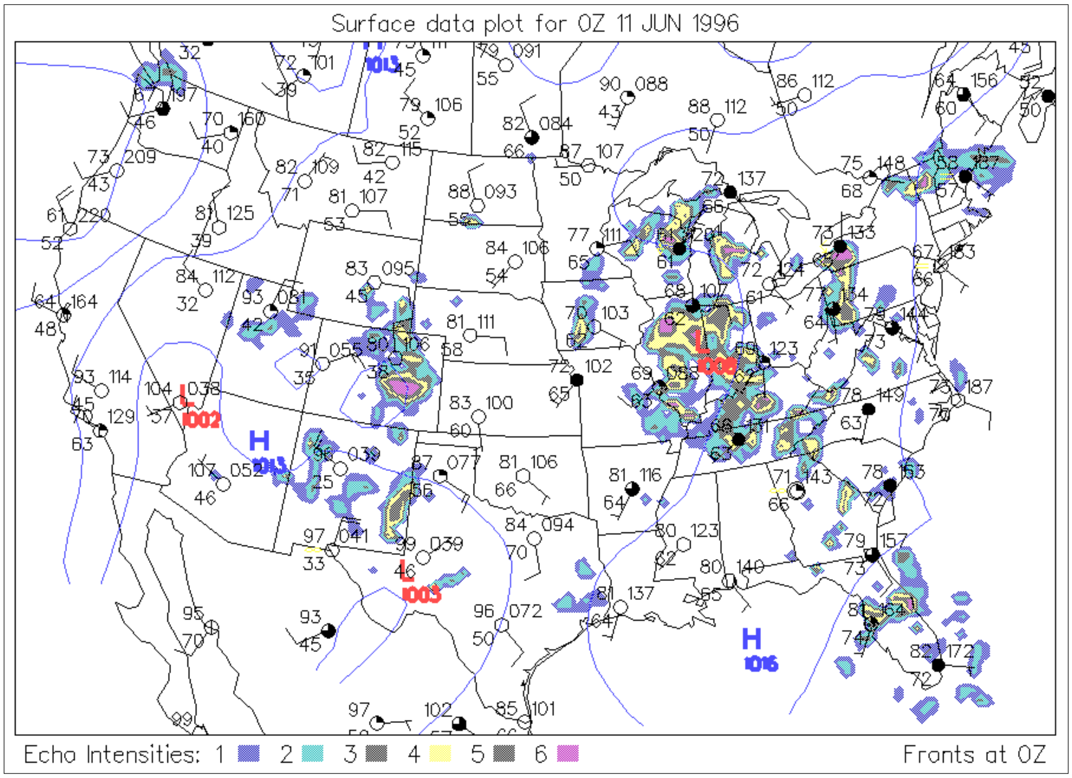

Figure A.3: 0000 UTC 11 June 1996 synoptic surface chart.

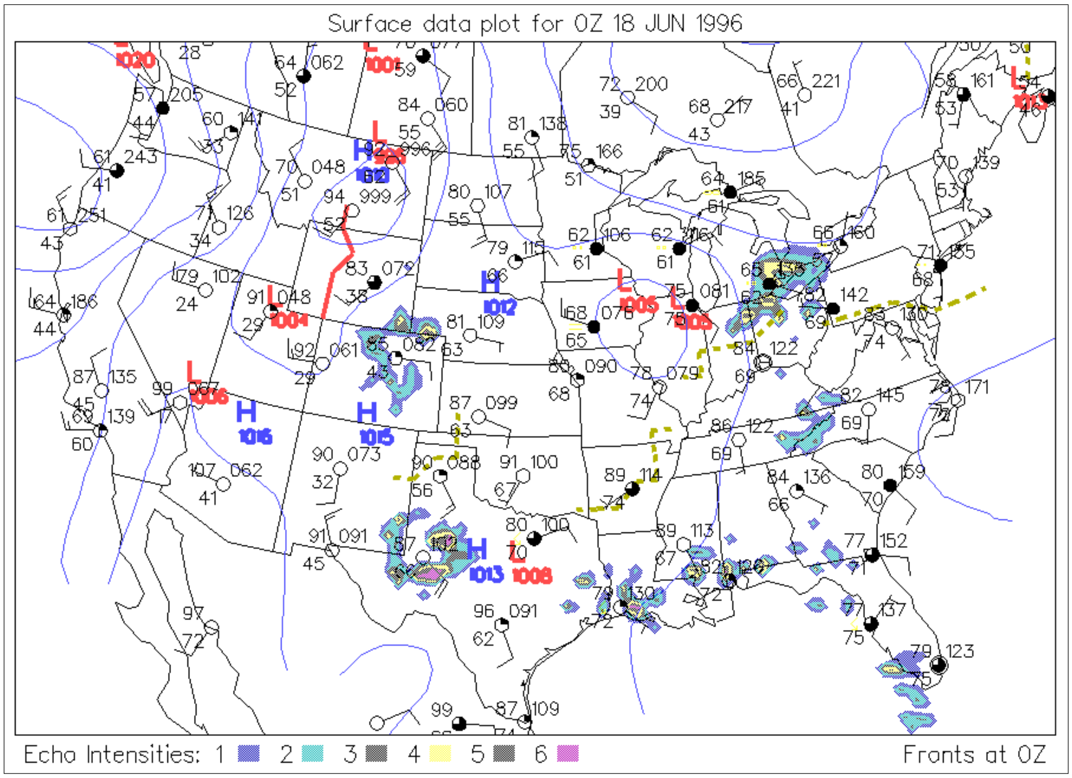

Figure A.4: 0000 UTC 18 June 1996 synoptic surface chart.

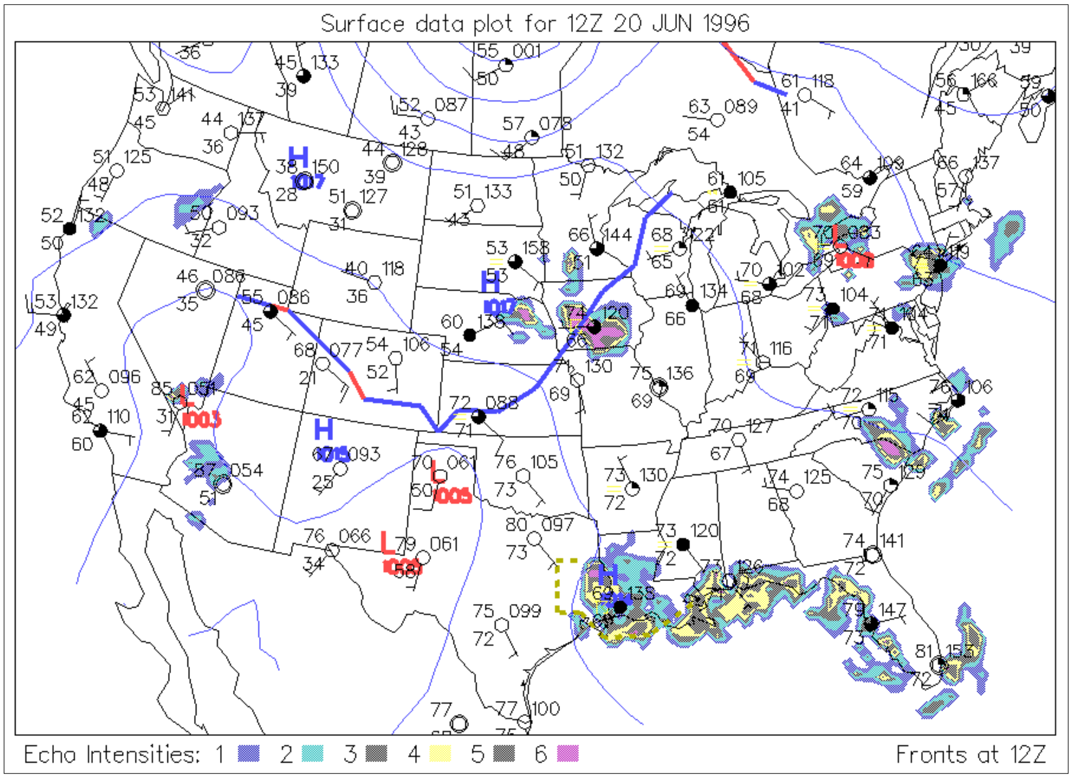

Figure A.5: 1200 UTC 20 June 1996 synoptic surface chart.

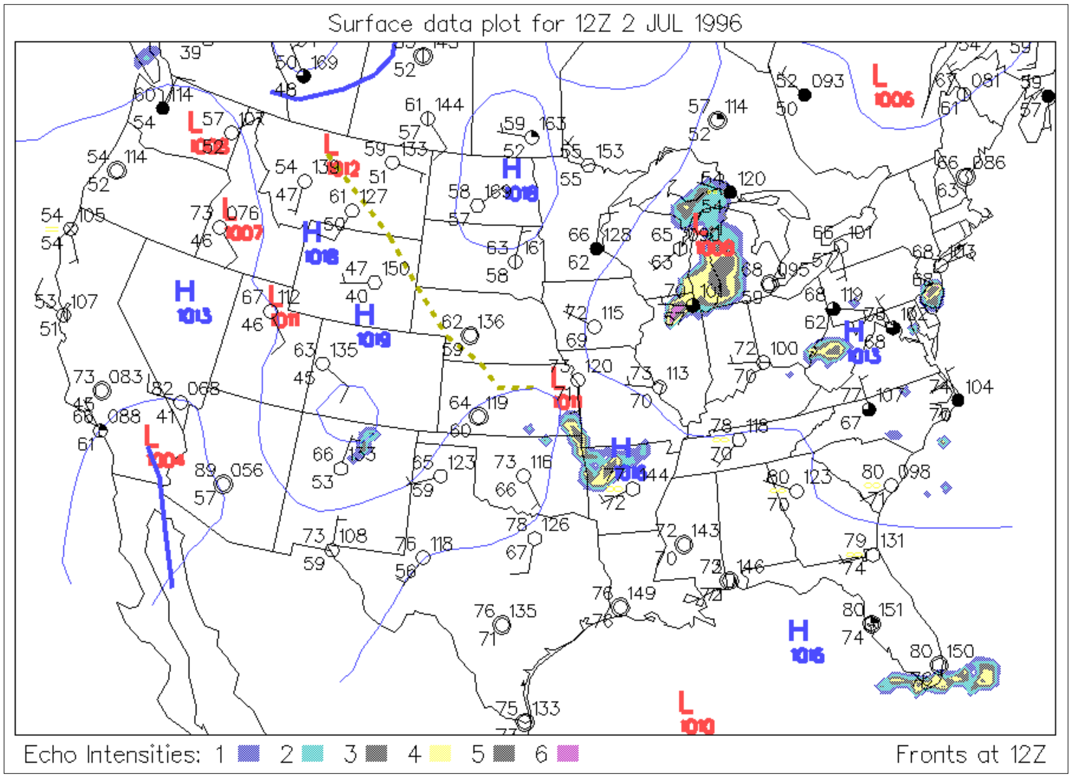

Figure A.6: 1200 UTC 02 July 1996 synoptic surface chart.

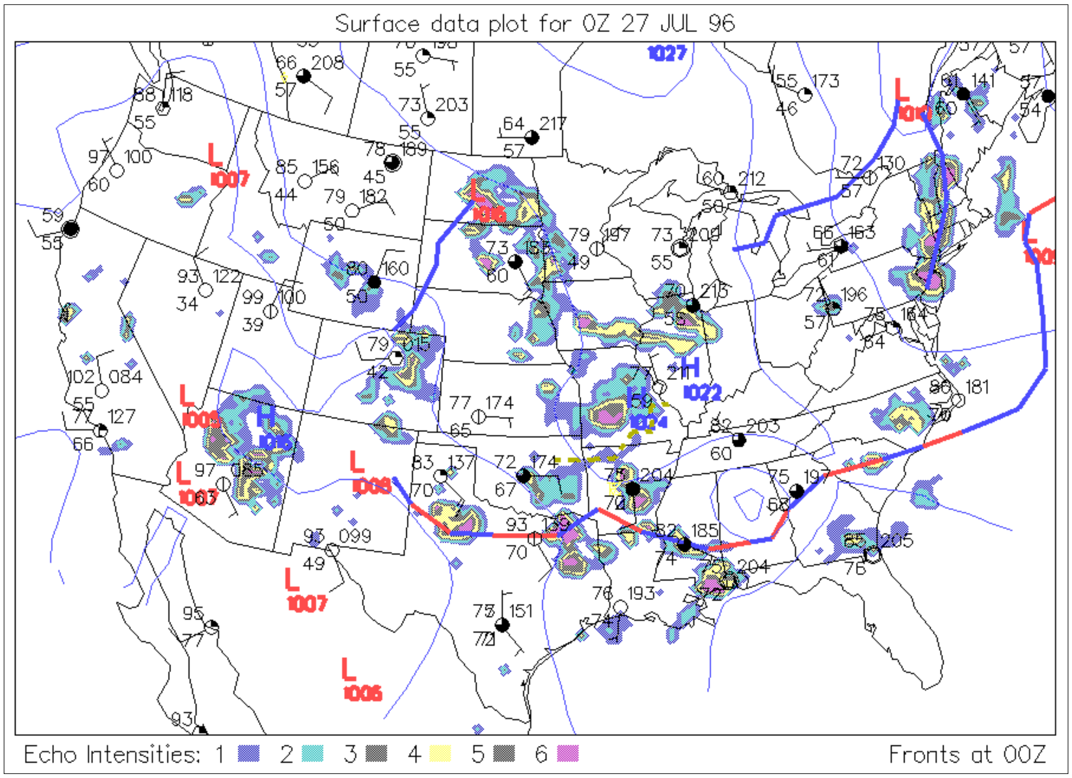

Figure A.7: 0000 UTC 27 July 1996 synoptic surface chart.

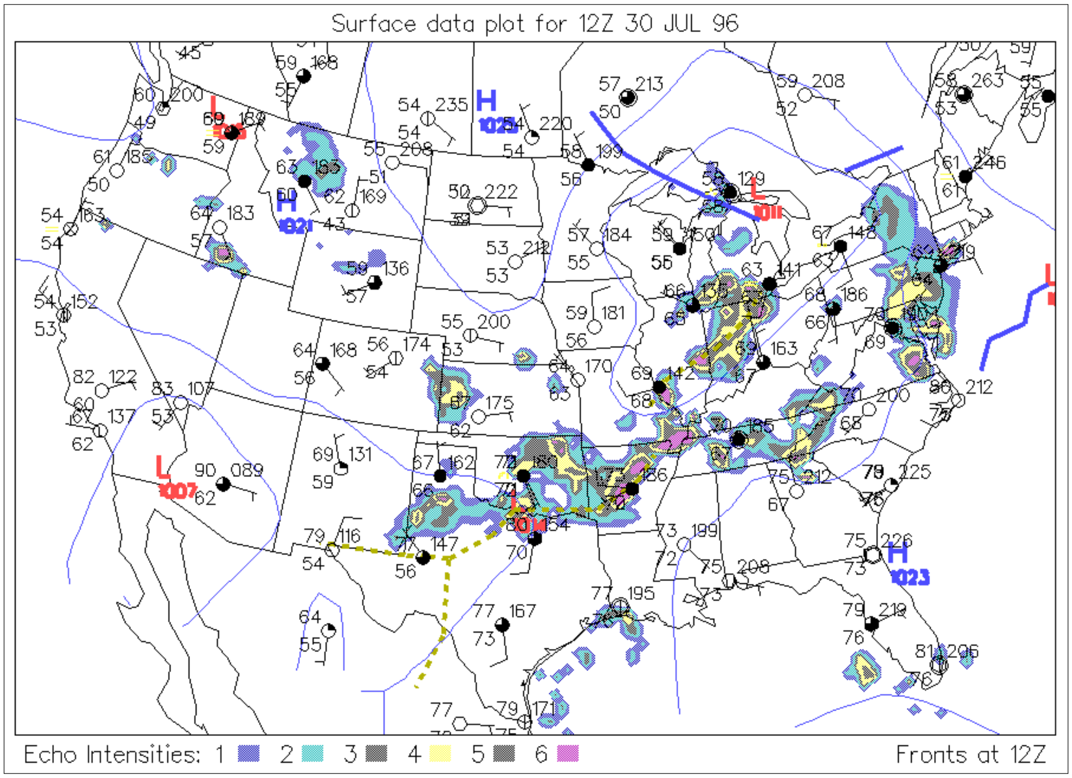

Figure A.8: 1200 UTC 30 July 1996 synoptic surface chart.

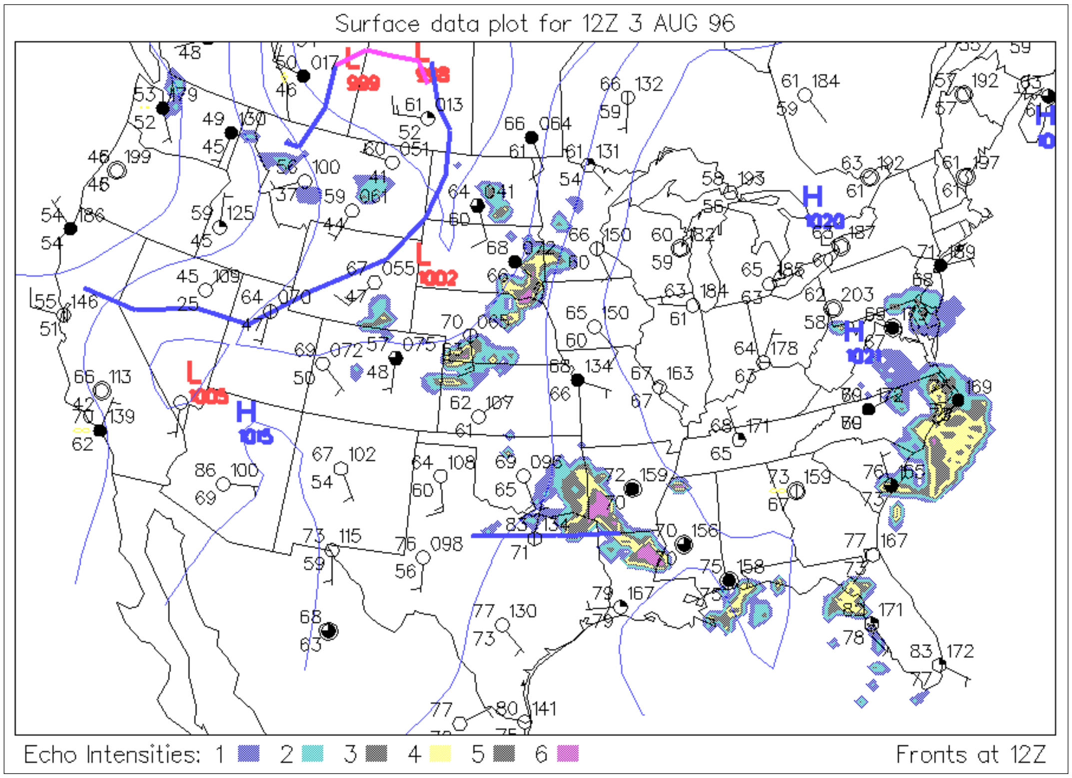

Figure A.9: 1200 UTC 03 August 1996 synoptic surface chart.

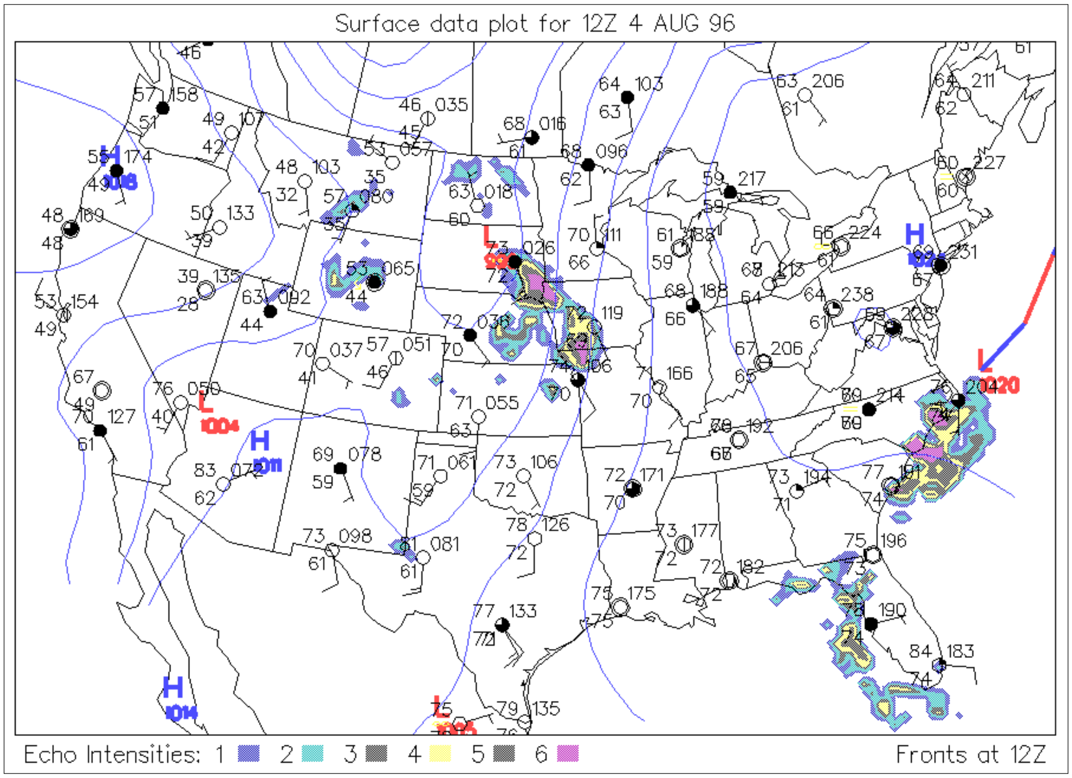

Figure A.10: 1200 UTC 04 August 1996 synoptic surface chart.

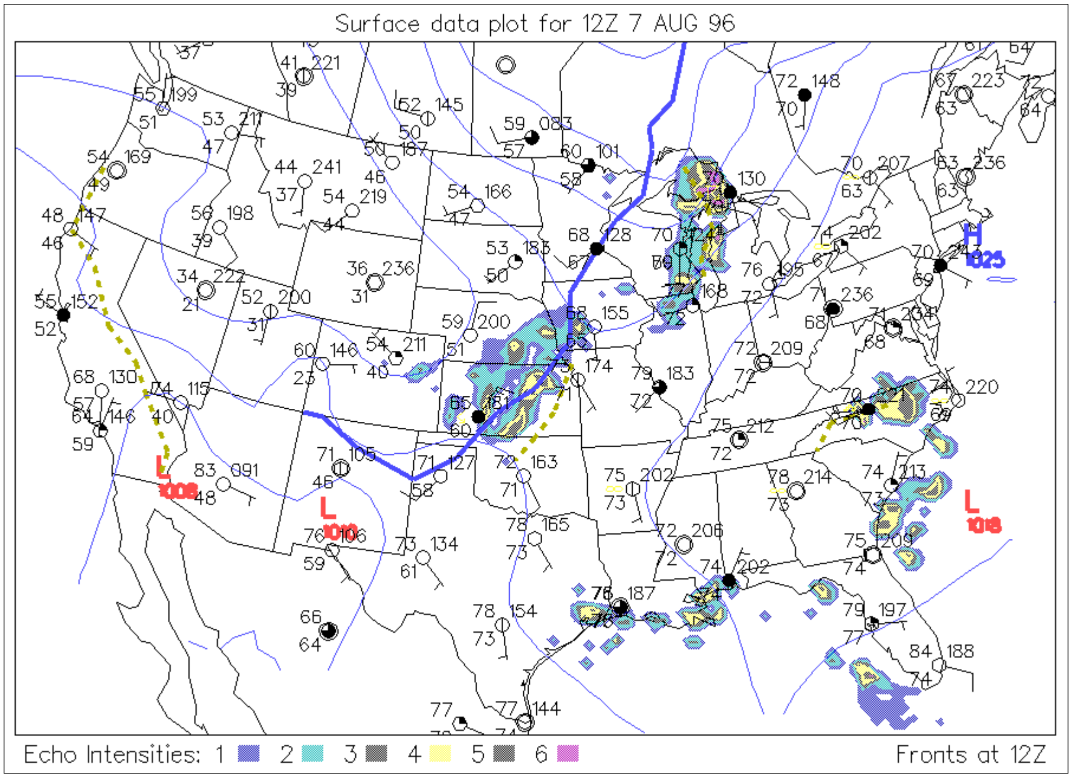

Figure A.11: 1200 UTC 07 August 1996 synoptic surface chart.

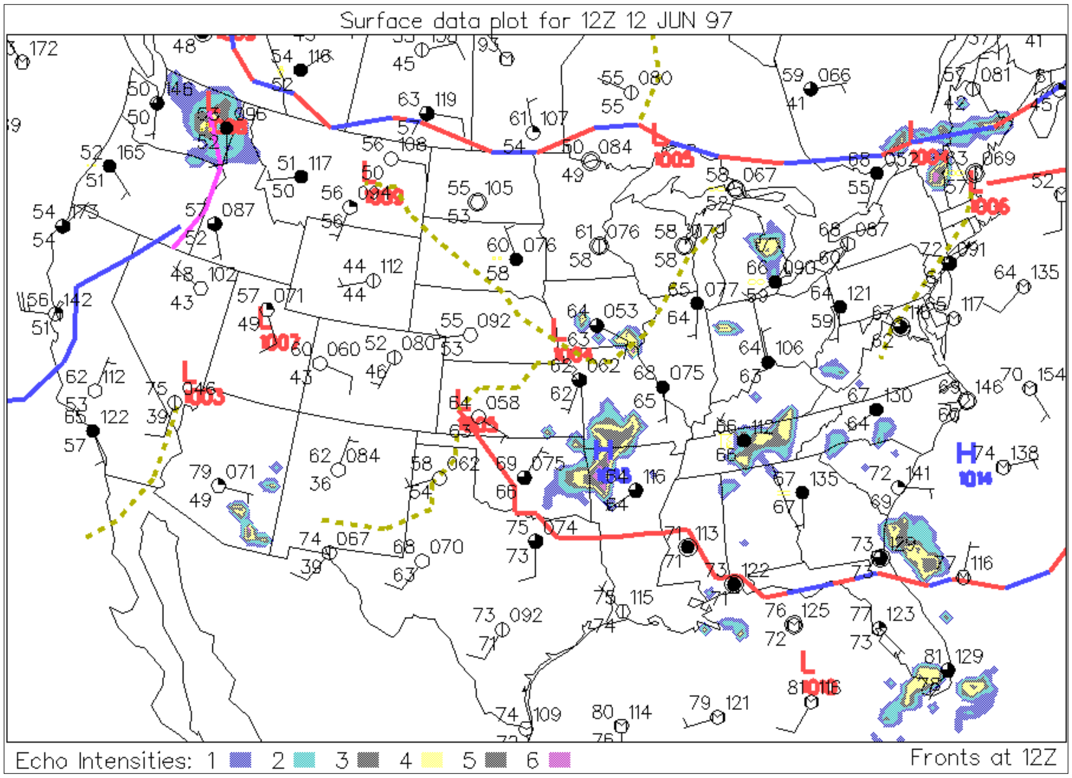

Figure A.12: 1200 UTC 12 June 1997 synoptic surface chart.

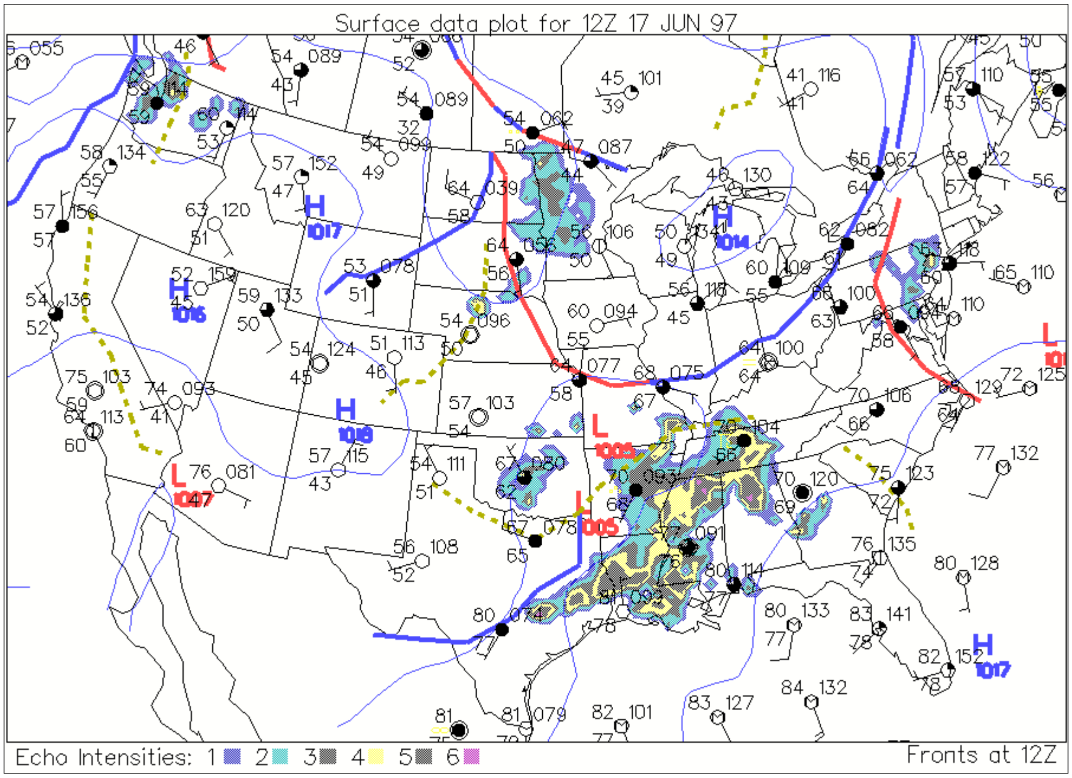

Figure A.13: 1200 UTC 17 June 1997 synoptic surface chart.

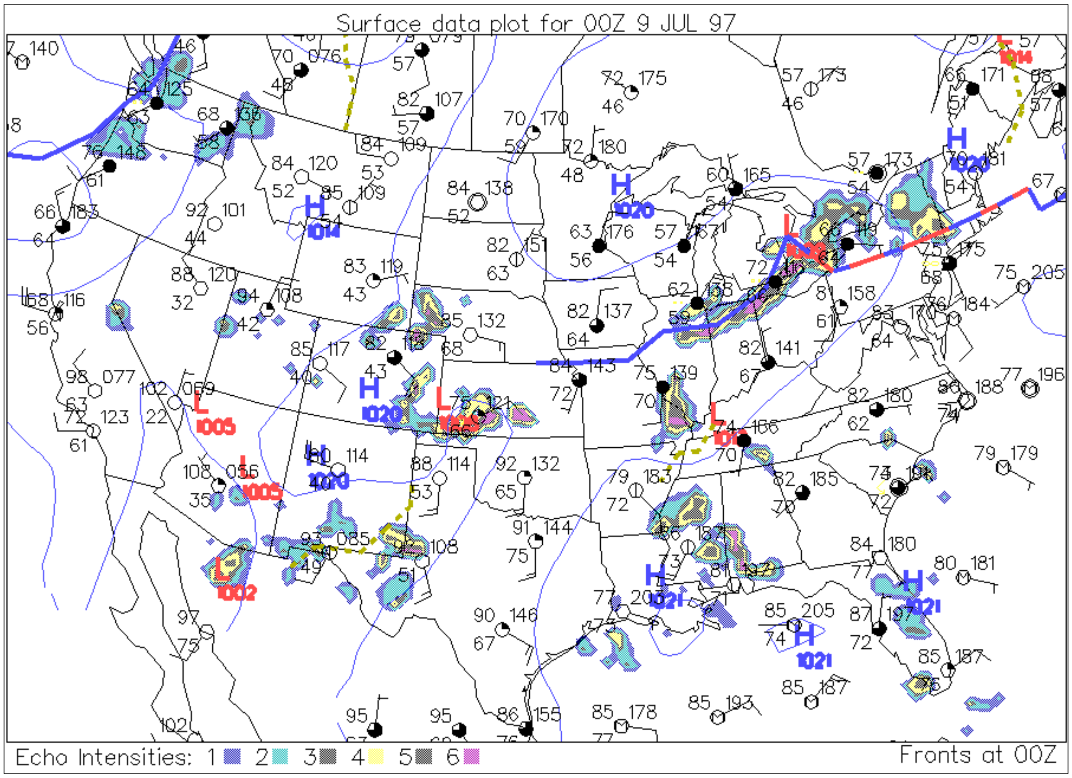

Figure A.14: 0000 UTC 09 July 1997 synoptic surface chart.

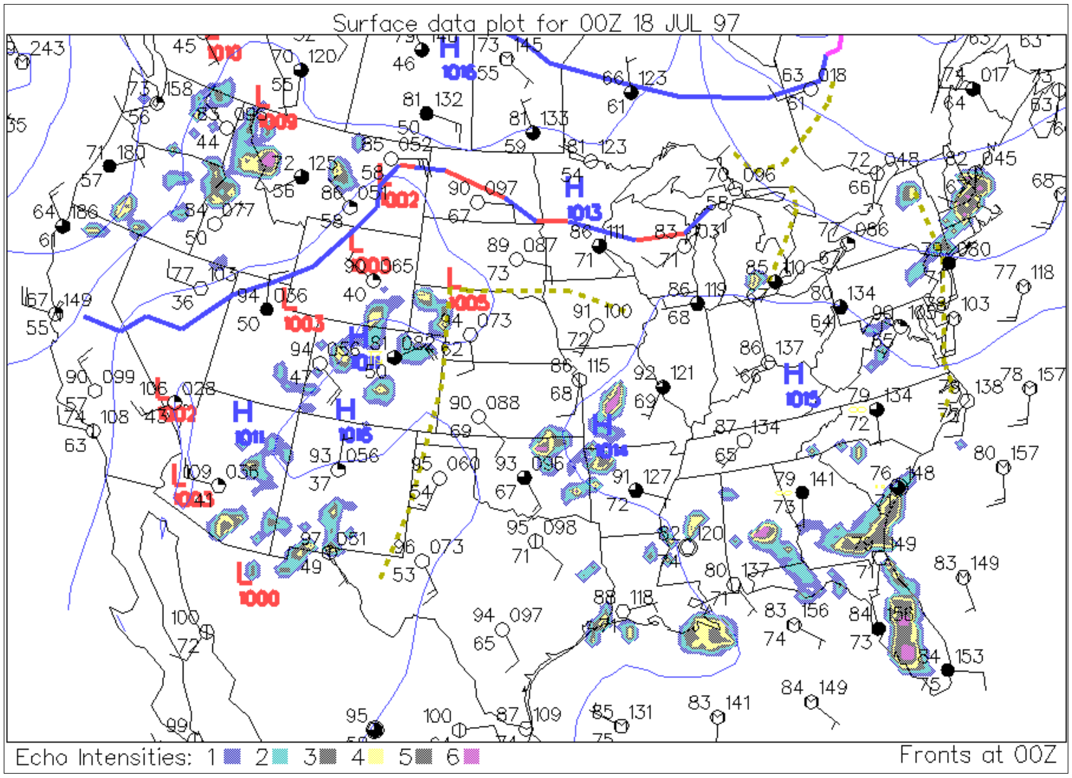

Figure A.15: 0000 UTC 18 July 1997 synoptic surface chart.

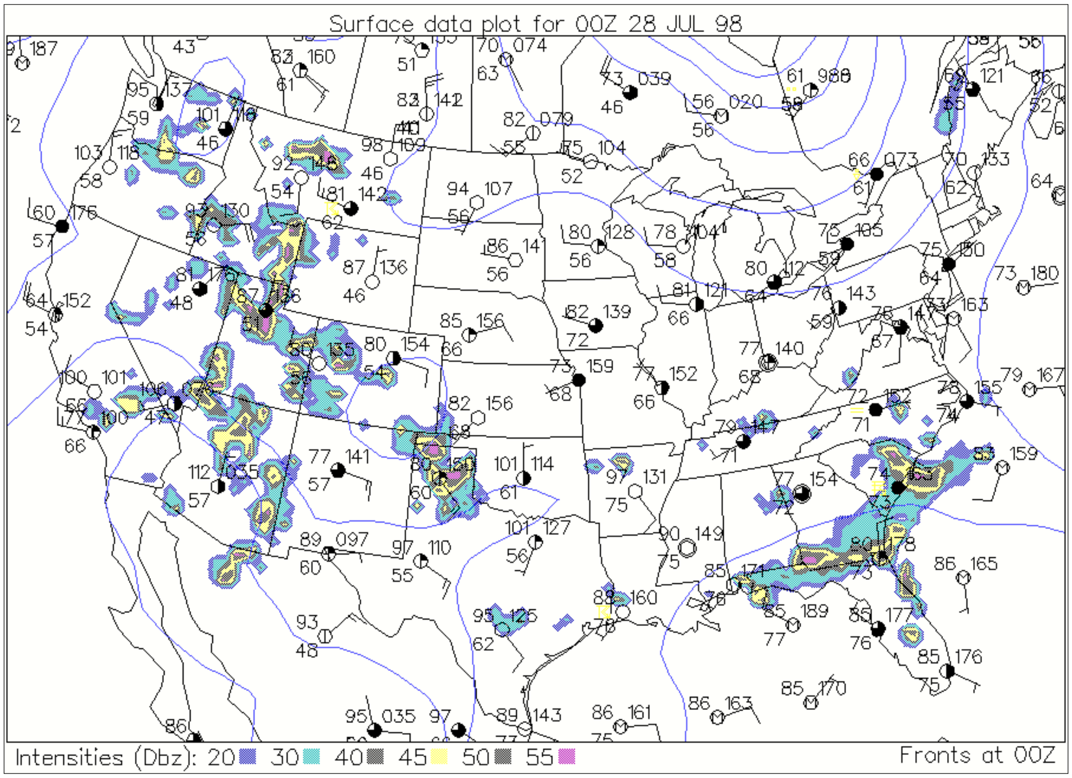

Figure A.16: 0000 UTC 28 July 1998 synoptic surface chart.

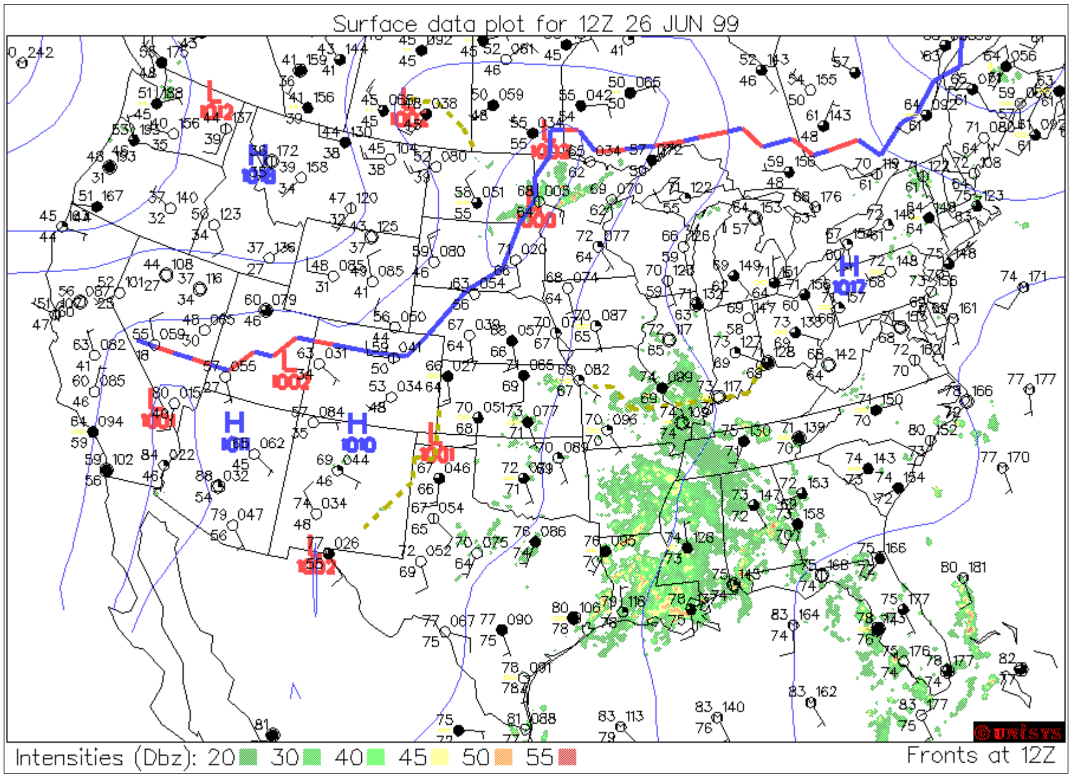

Figure A.17: 1200 UTC 26 June 1999 synoptic surface chart.

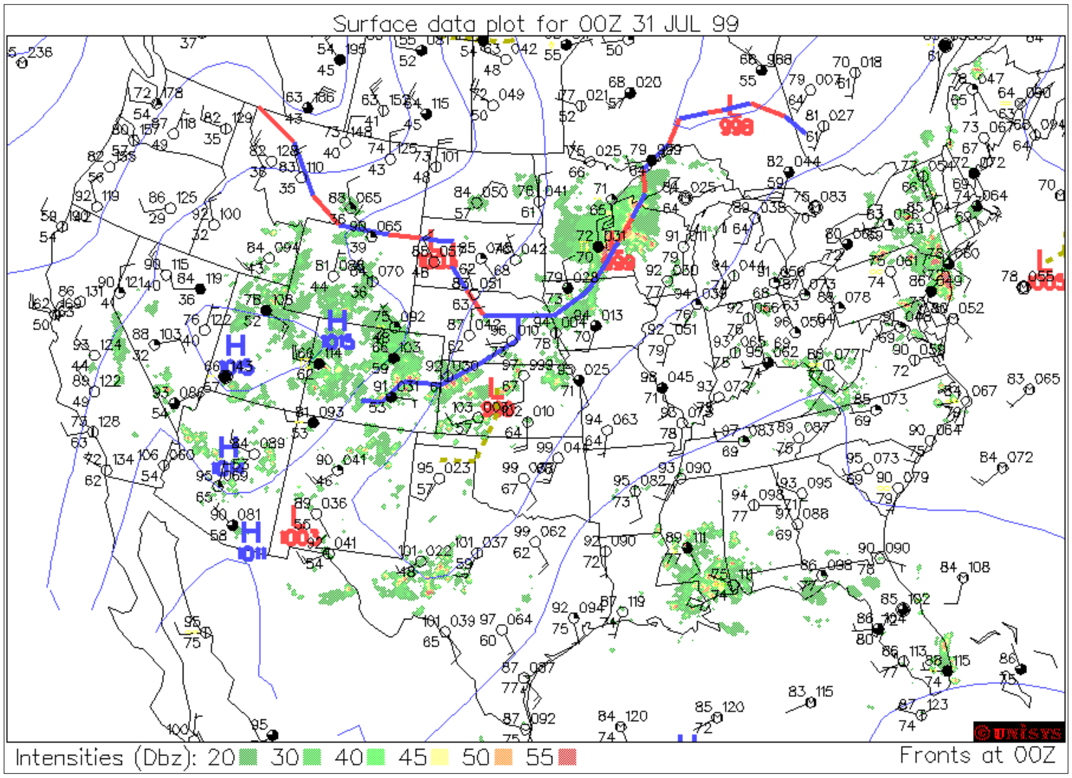

Figure A.18: 0000 UTC 31 July 1999 synoptic surface chart.

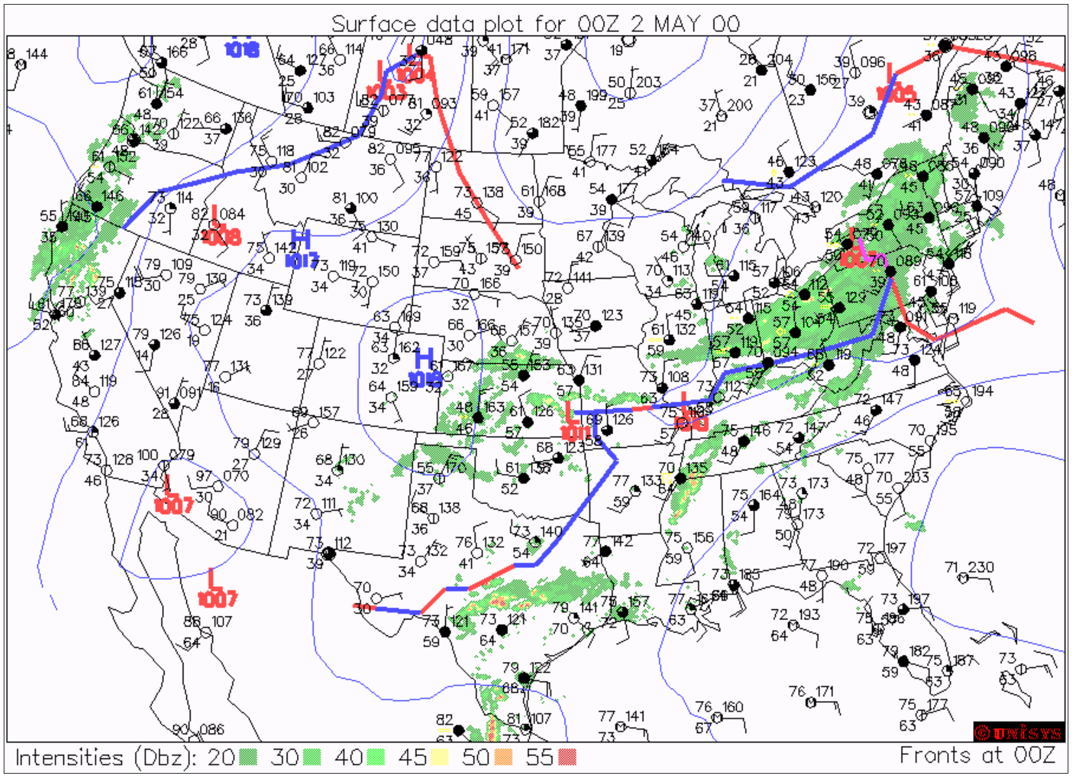

Figure A.19: 0000 UTC 02 May 2000 synoptic surface chart.

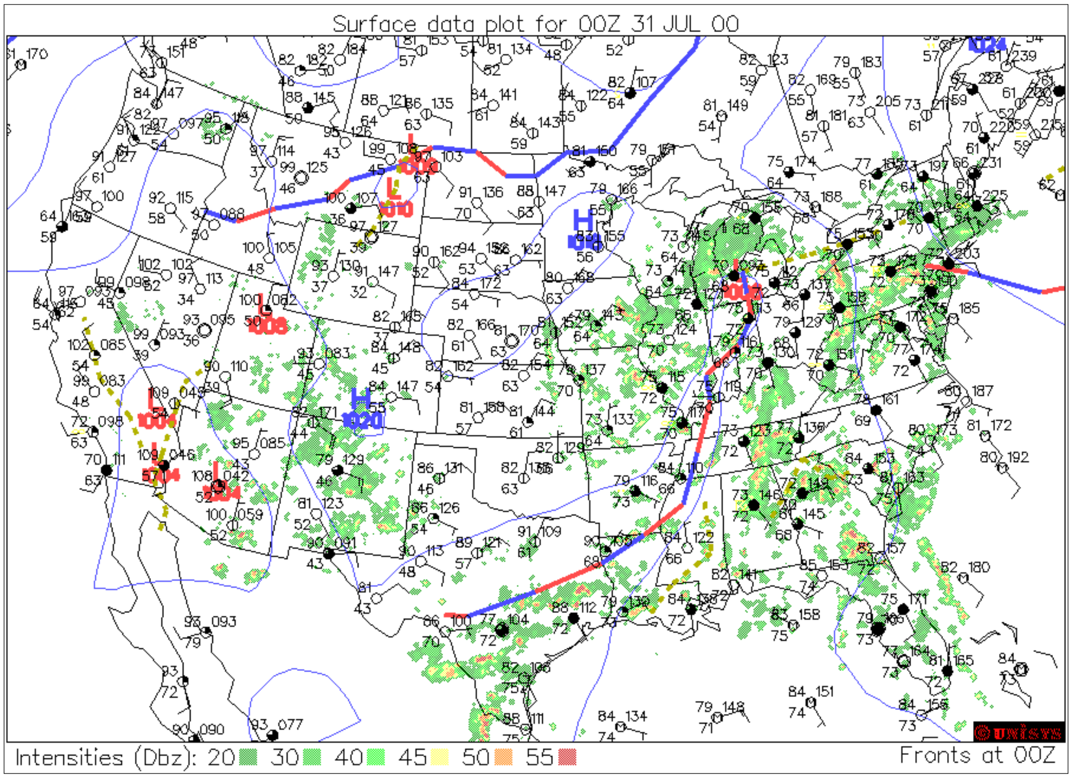

Figure A.20: 0000 UTC 31 July 2000 synoptic surface chart.

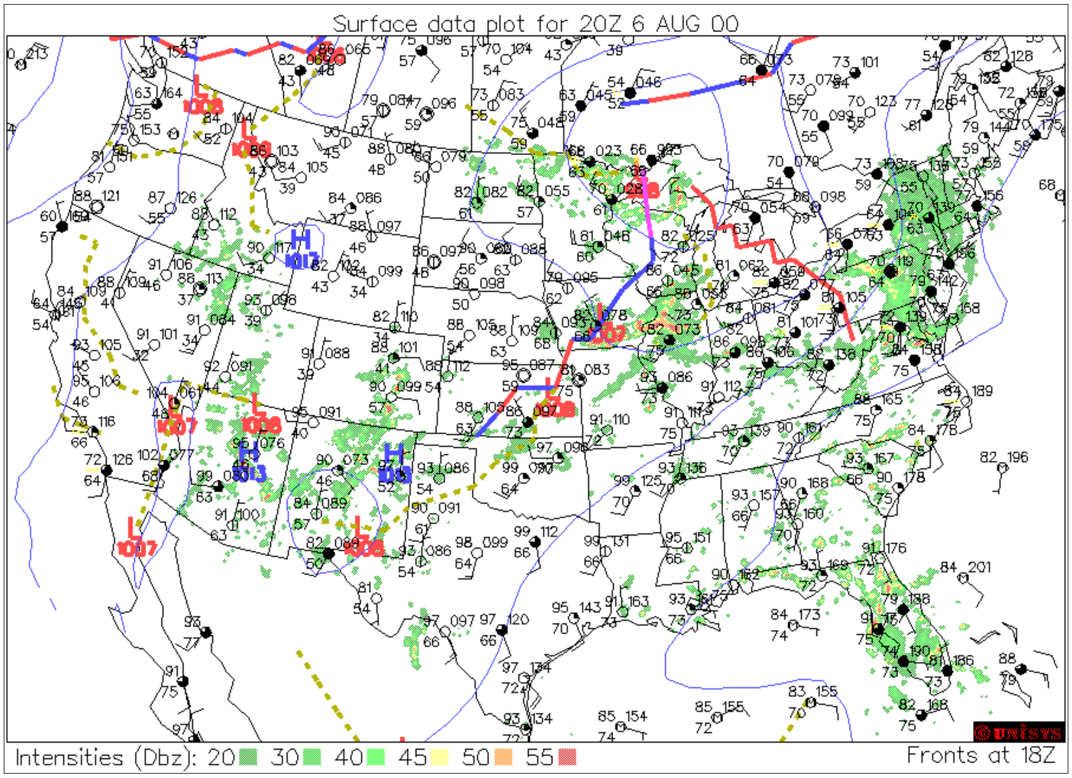

Figure A.21: 2000 UTC 06 August 2000 synoptic surface chart.

APPENDIX B

RADAR REFLECTIVITY IMAGES

This appendix includes GHRC 2–km 15–min reflectivity images for the initiation times of each event. Samples of the GHRC reflectivity data are shown in Chapter 3 (Figures 3.1 and 3.4). Figure 3.1 shows the format of the data when viewed online (http://ghrc.nsstc.nasa.gov) while Figure 3.4 shows the format when viewed with IDL 5.5 as in this project.

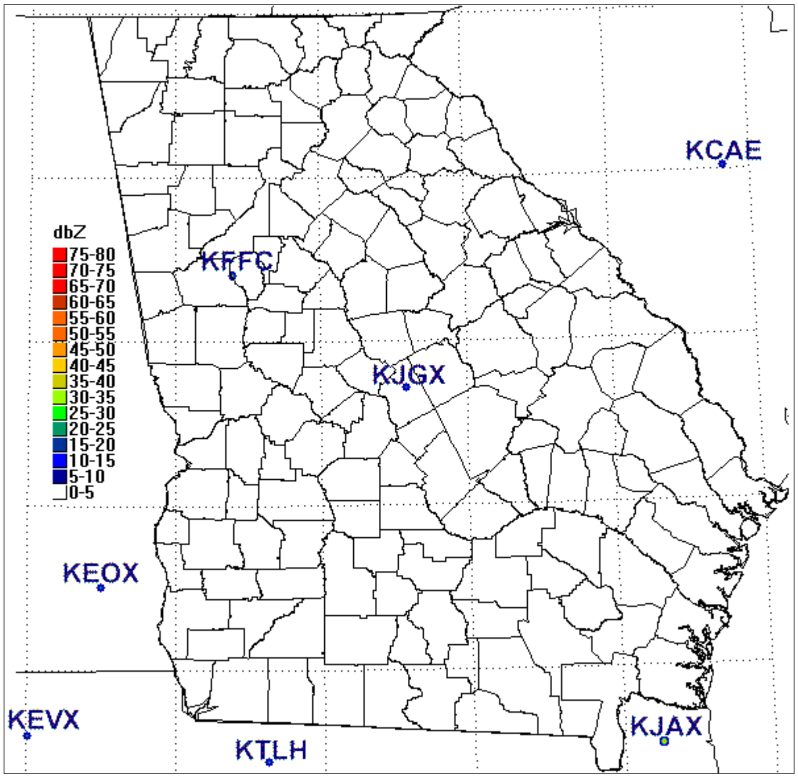

Figure B.1: Labeled radar sites visible in the GHRC 2–km 15–min reflectivity. data.

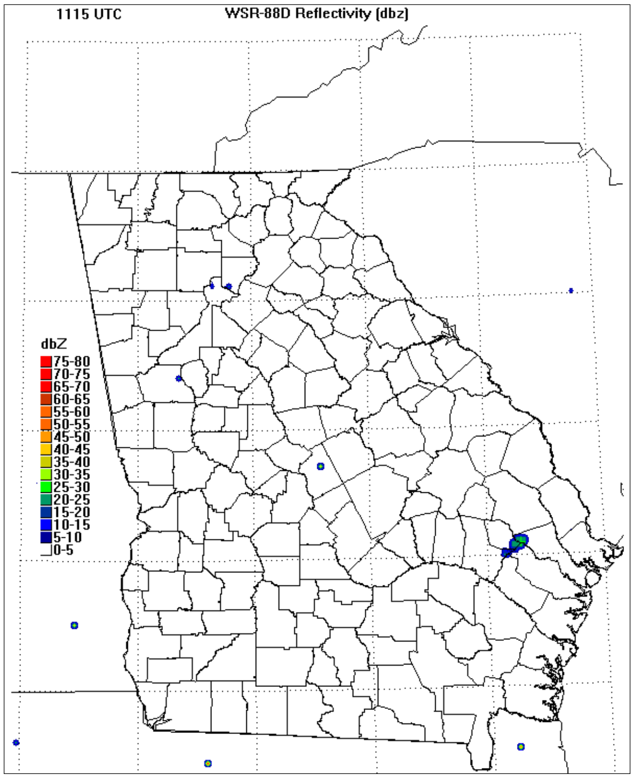

Figure B.2: 1115 UTC 09 May 1996 radar reflectivity.

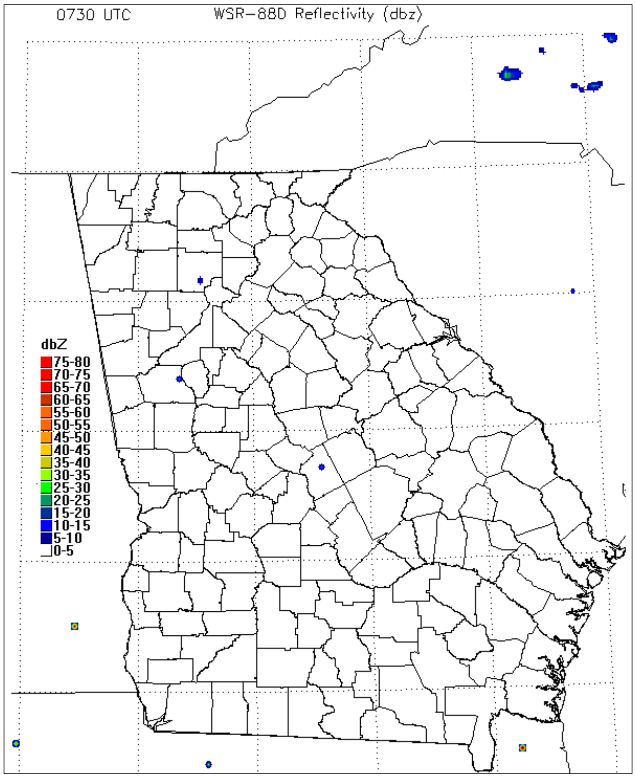

Figure B.3: 0730 UTC 11 May 1996 radar reflectivity.

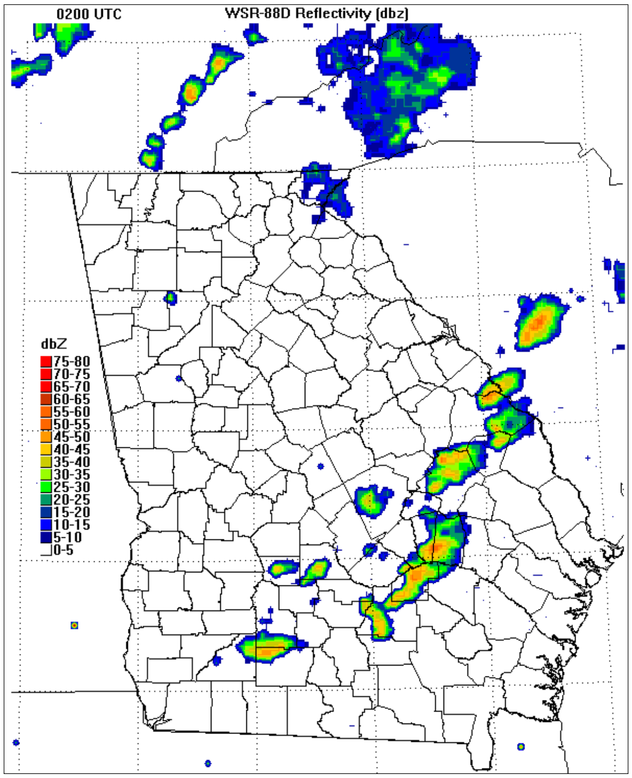

Figure B.4: 0200 UTC 11 June 1996 radar reflectivity.

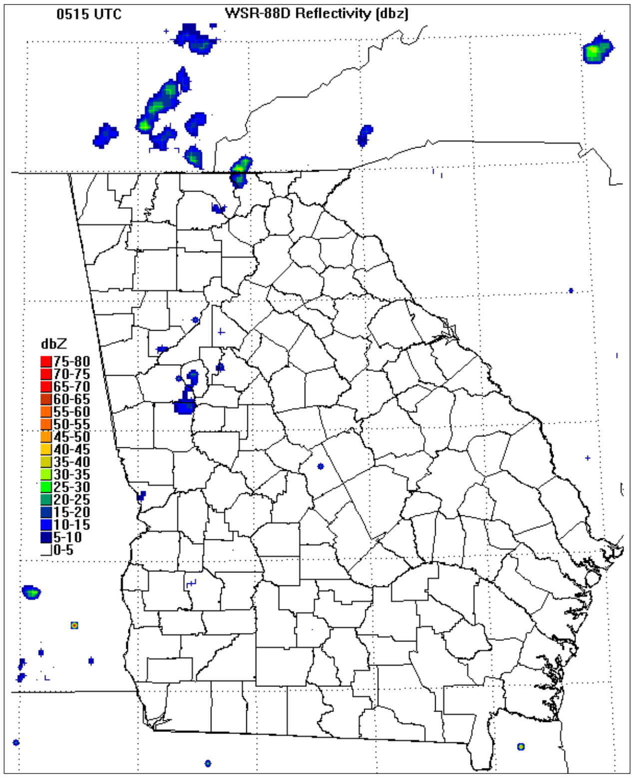

Figure B.5: 0515 UTC 18 June 1996 radar reflectivity.

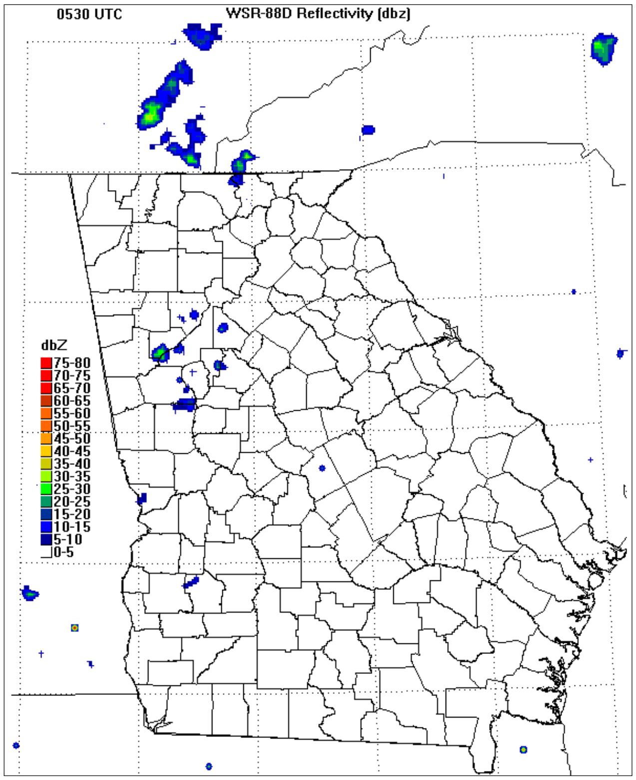

Figure B.6: 0530 UTC 18 June 1996 radar reflectivity.

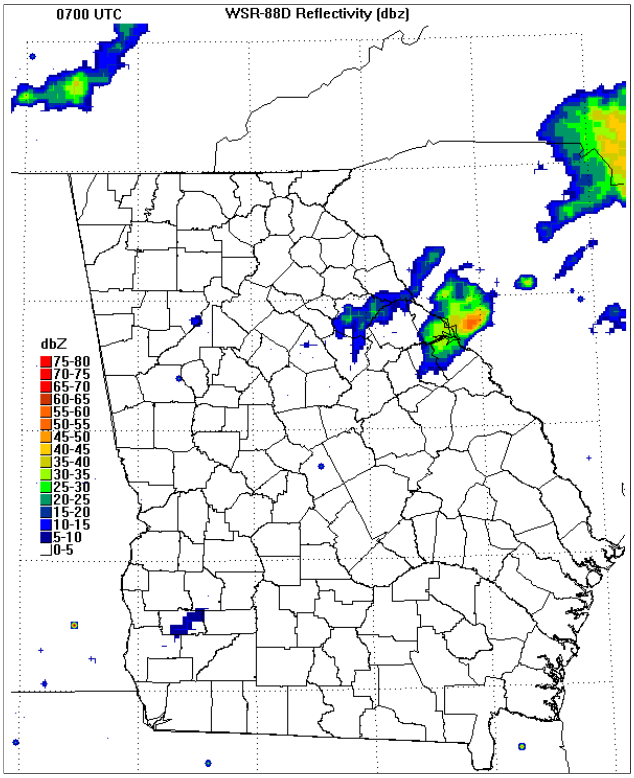

Figure B.7: 0700 UTC 20 June 1996 radar reflectivity.

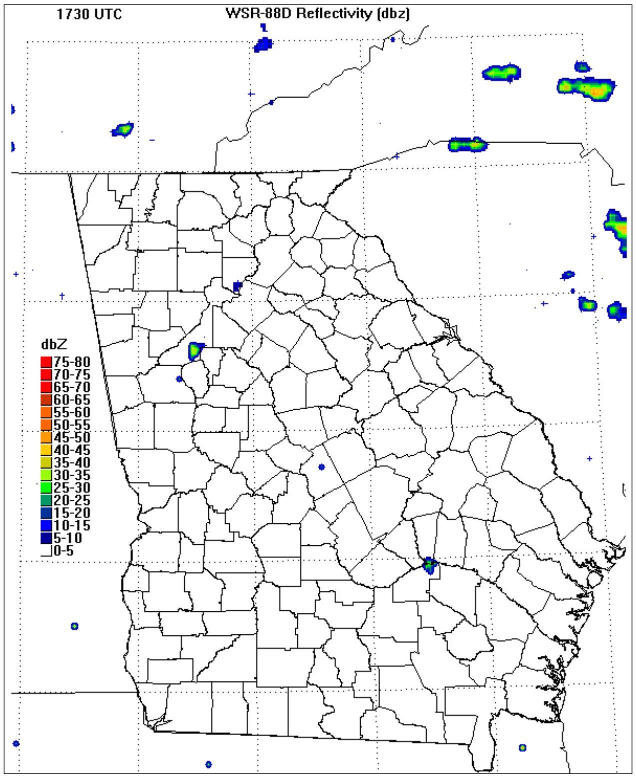

Figure B.8: 1730 UTC 02 July 1996 radar reflectivity.

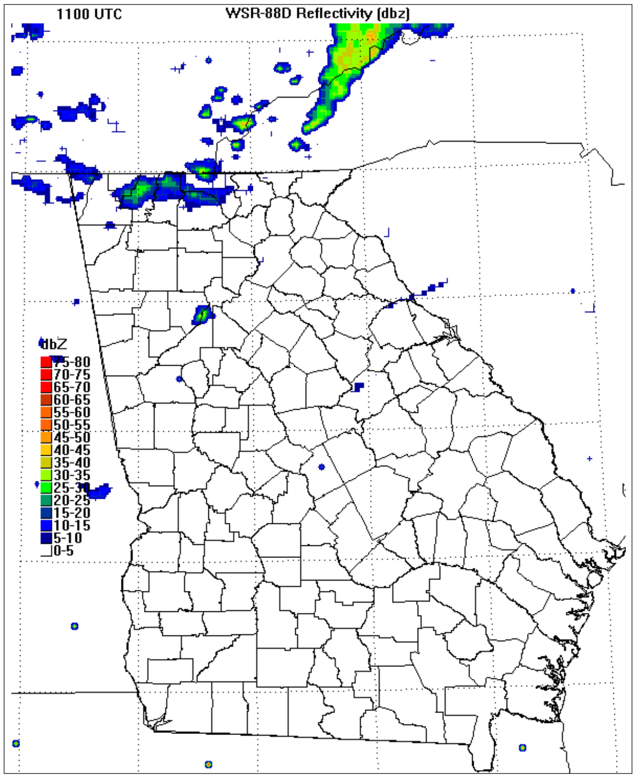

Figure B.9: 1100 UTC 30 July 1996 radar reflectivity.

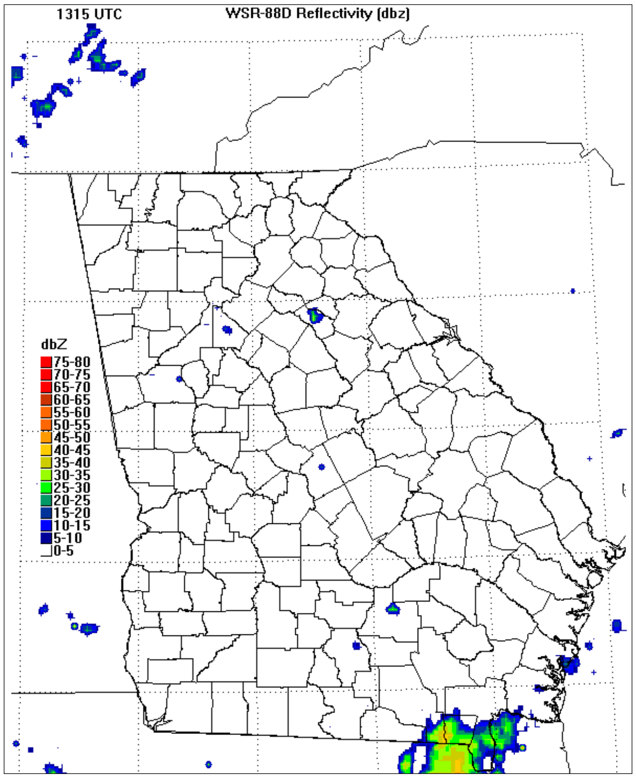

Figure B.10: 1315 UTC 03 August 1996 radar reflectivity.

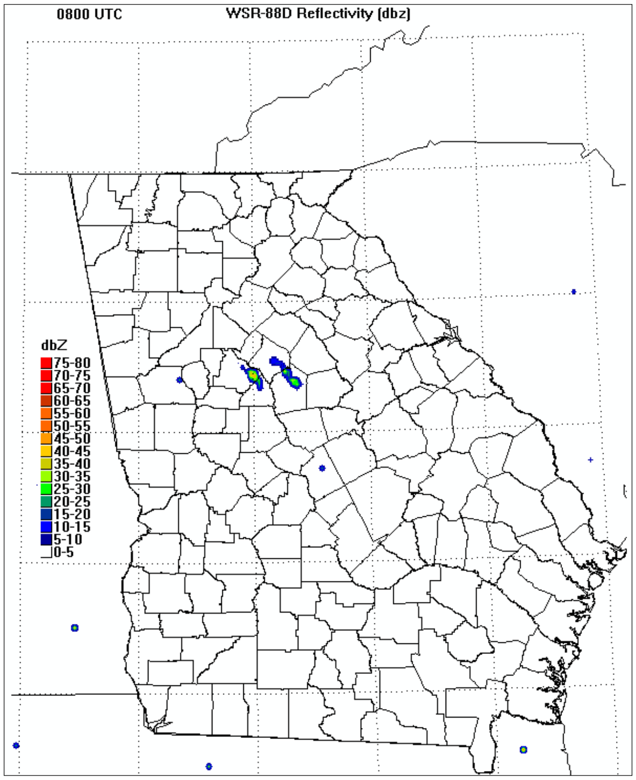

Figure B.11: 0800 UTC 04 August 1996 radar reflectivity.

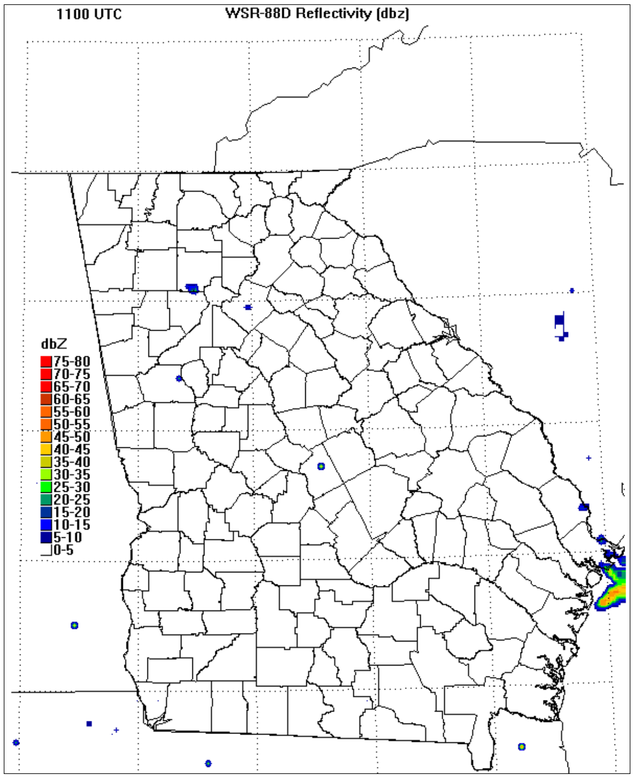

Figure B.12: 1100 UTC 07 August 1996 radar reflectivity.

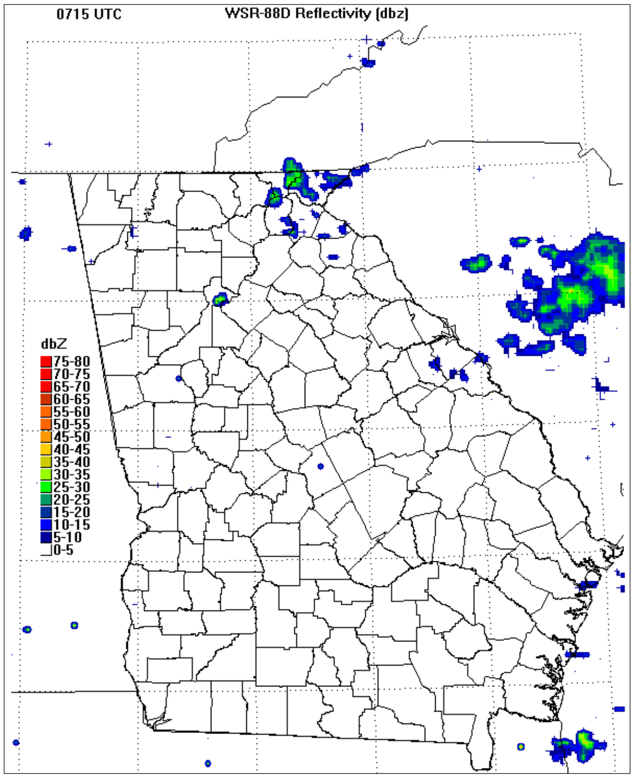

Figure B.13: 0715 UTC 12 June 1997 radar reflectivity.

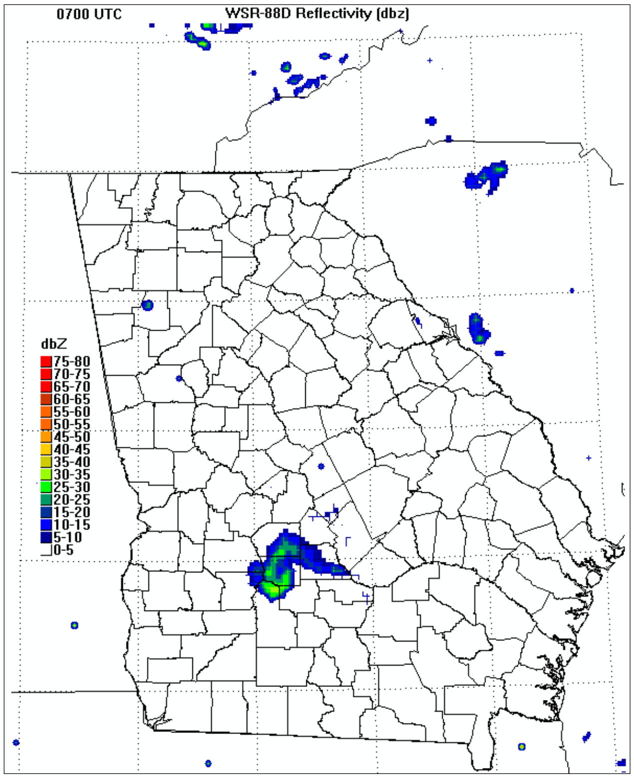

Figure B.14: 0700 UTC 17 June 1997 radar reflectivity.

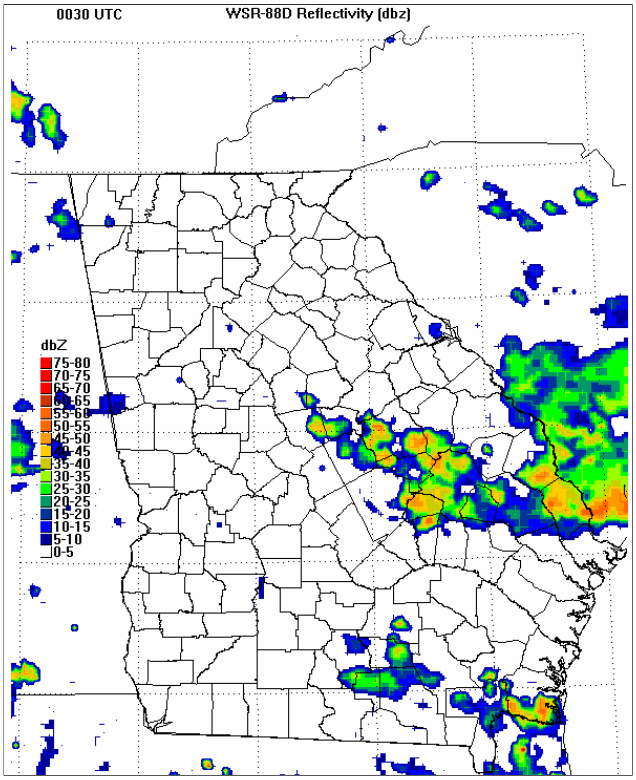

Figure B.15: 0030 UTC 09 July 1997 radar reflectivity.

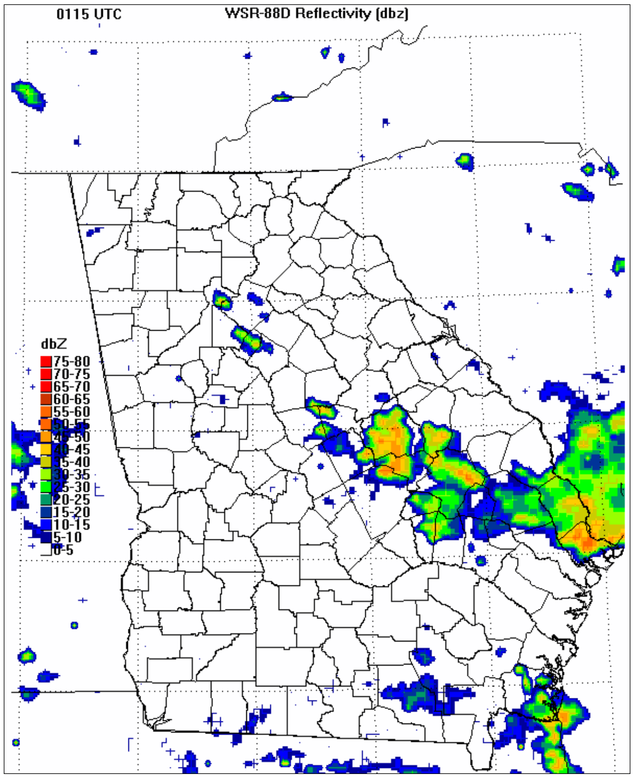

Figure B.16: 0115 UTC 09 July 1997 radar reflectivity.

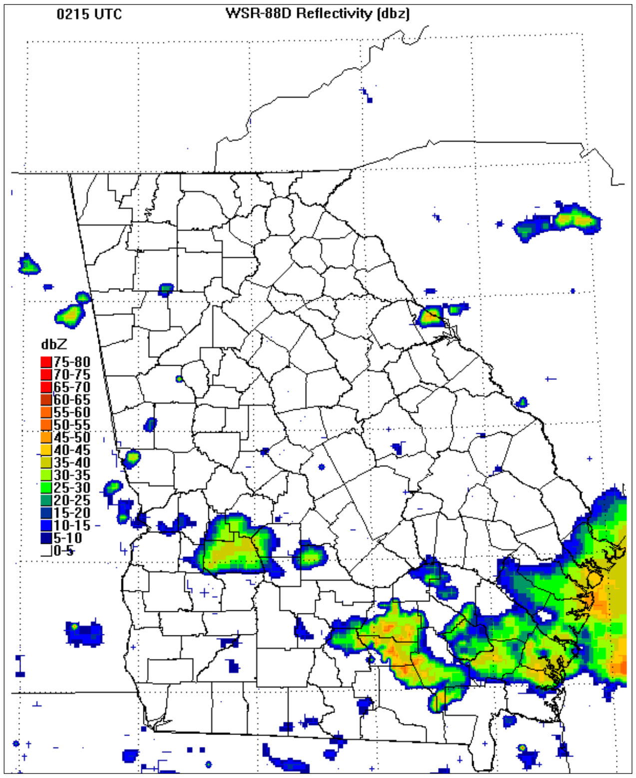

Figure B.17: 0215 UTC 18 July 1997 radar reflectivity.

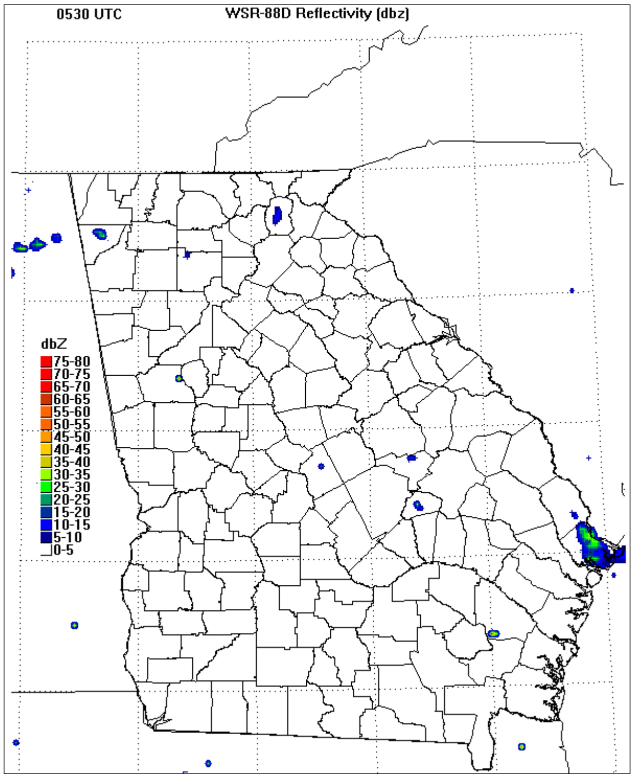

Figure B.18: 0530 UTC 18 July 1997 radar reflectivity.

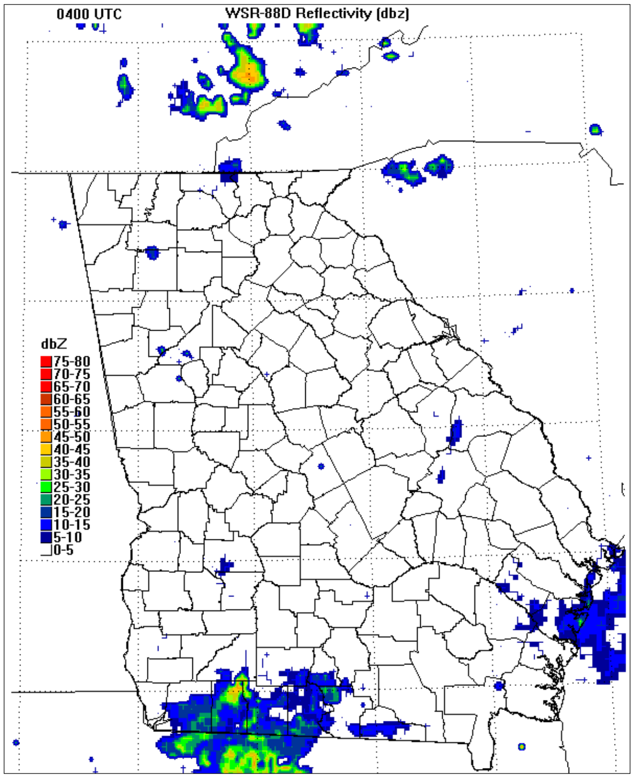

Figure B.19: 0400 UTC 28 July 1998 radar reflectivity.

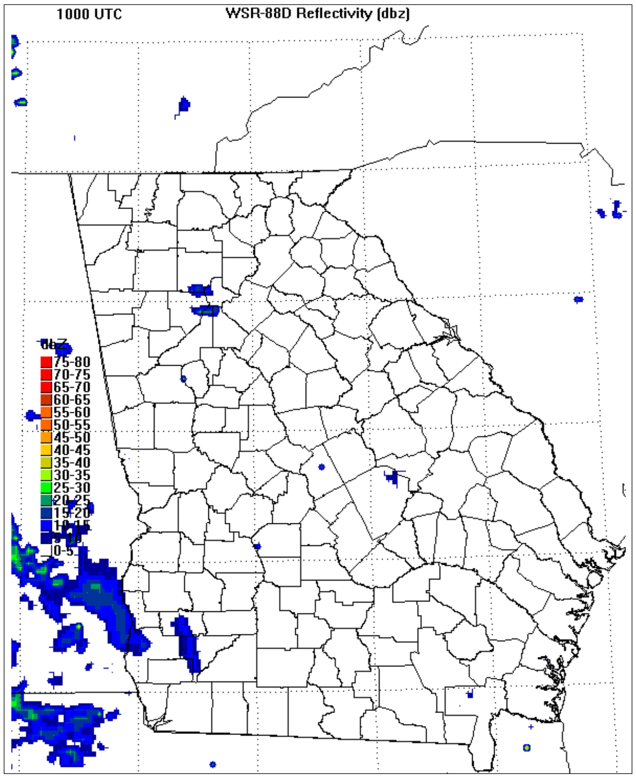

Figure B.20: 1000 UTC 26 June 1999 radar reflectivity.

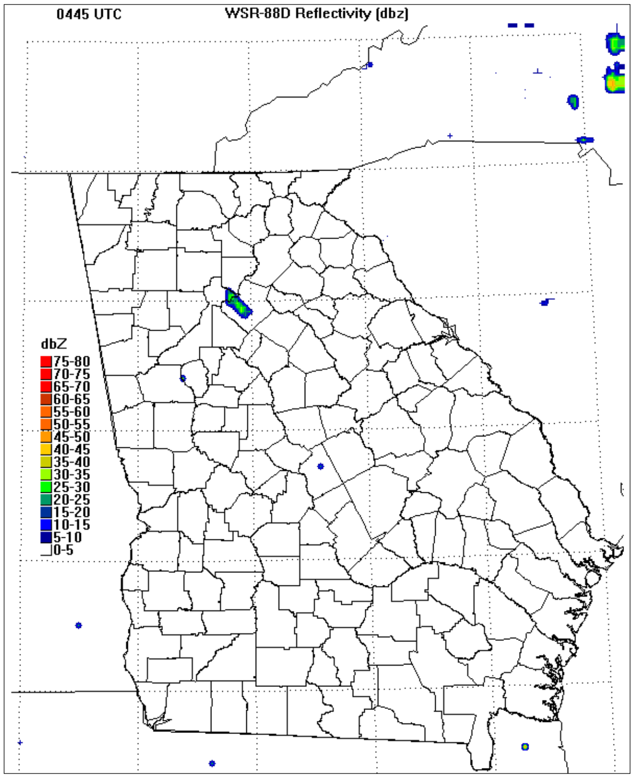

Figure B.21: 0445 UTC 31 July 1999 radar reflectivity.

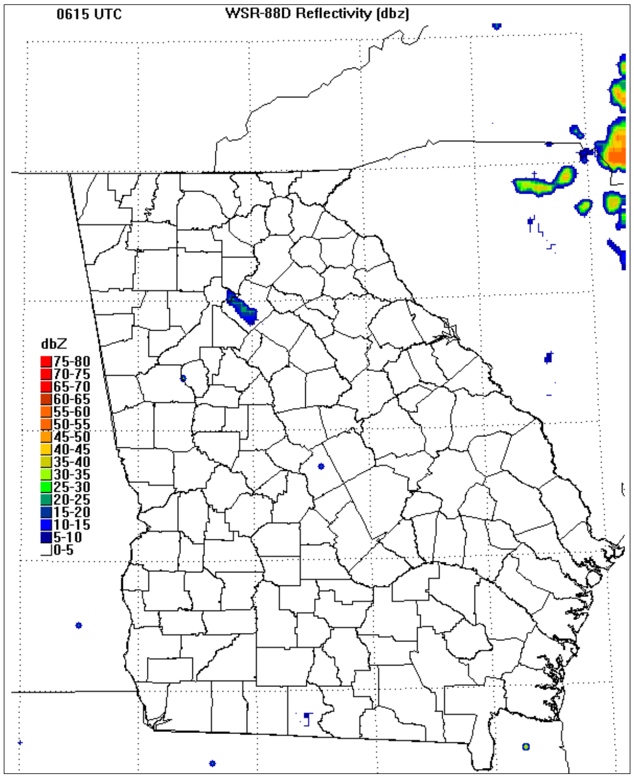

Figure B.22: 0615 UTC 31 July 1999 radar reflectivity.

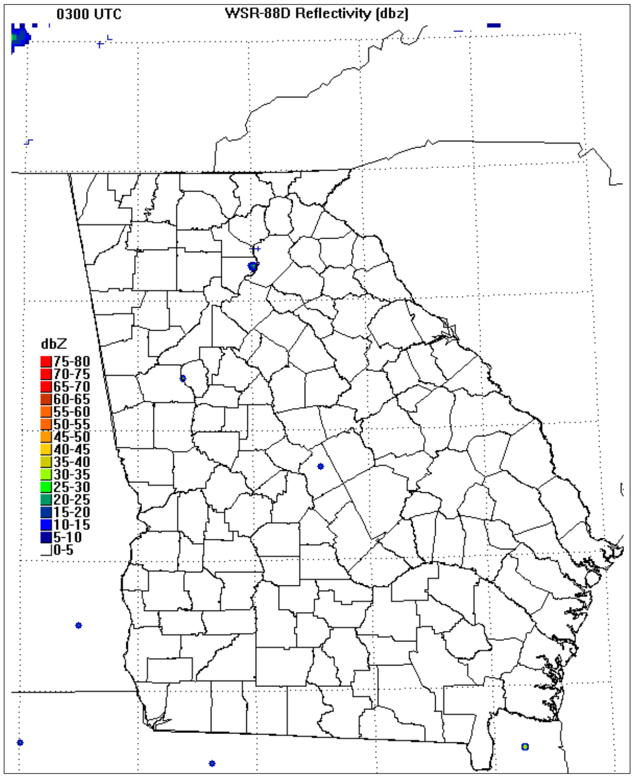

Figure B.23: 0300 UTC 02 May 2000 radar reflectivity.

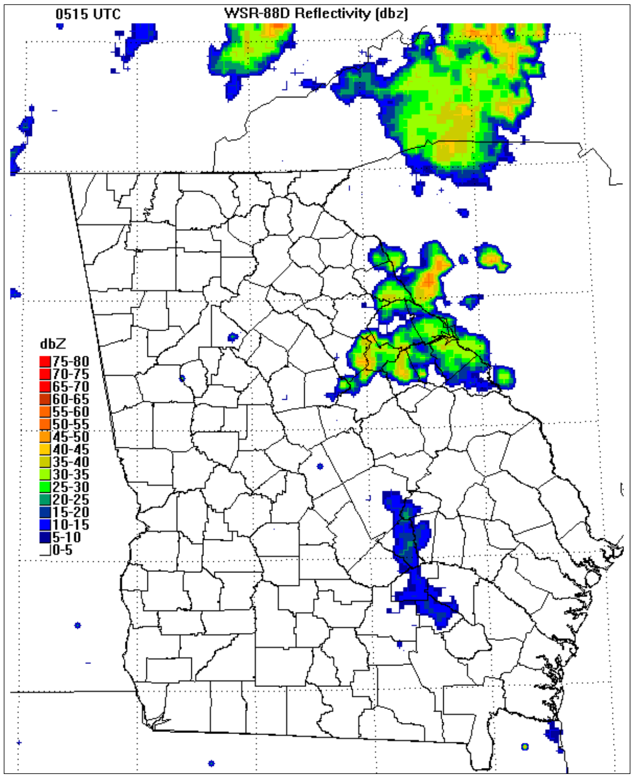

Figure B.24: 0515 UTC 31 July 2000 radar reflectivity.

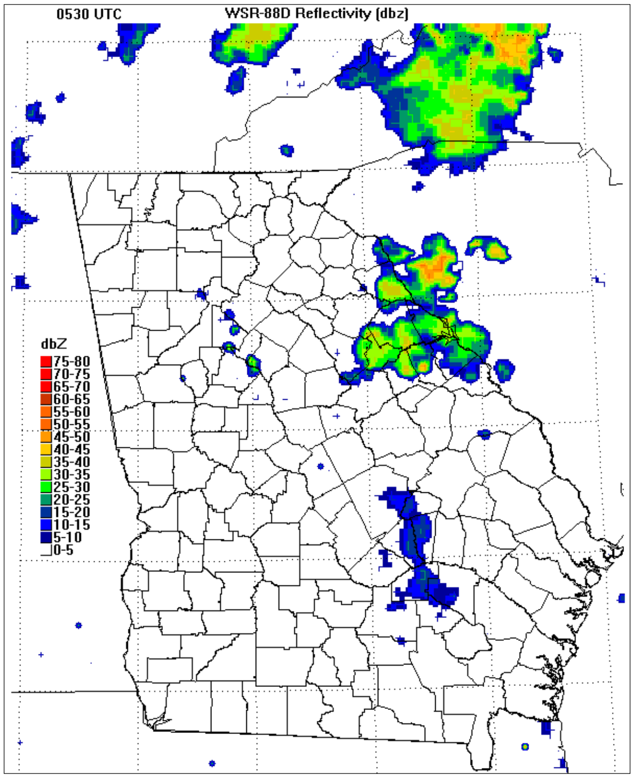

Figure B.25: 0530 UTC 31 July 2000 radar reflectivity.

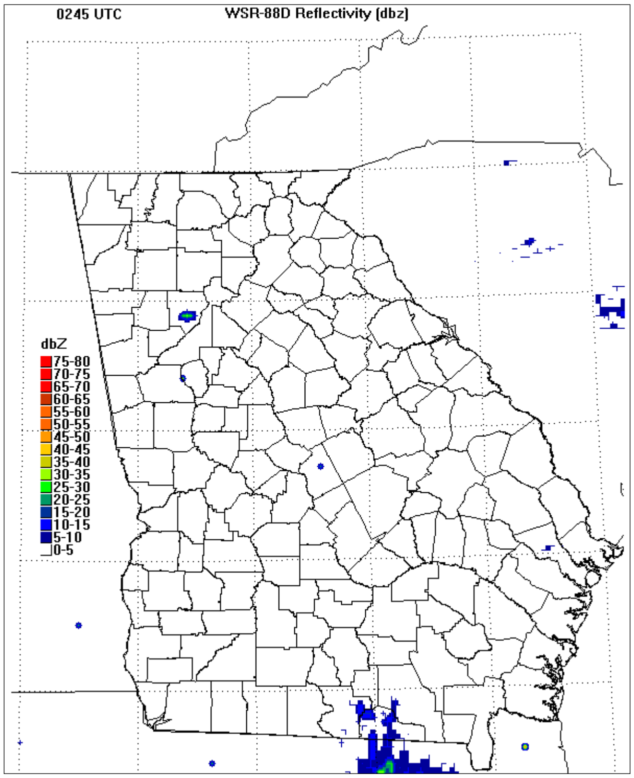

Figure B.26: 0245 UTC 06 August 2000 radar reflectivity.

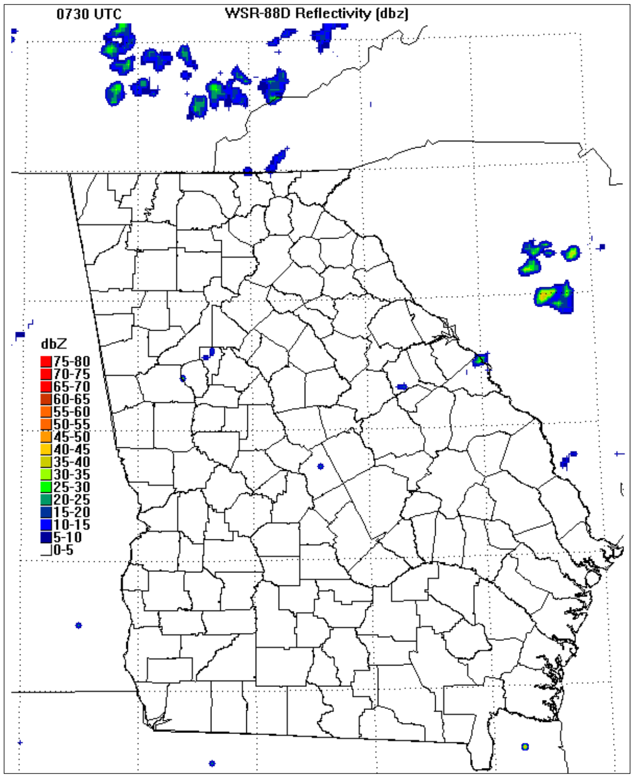

Figure B.27: 0730 UTC 06 August 2000 radar reflectivity.

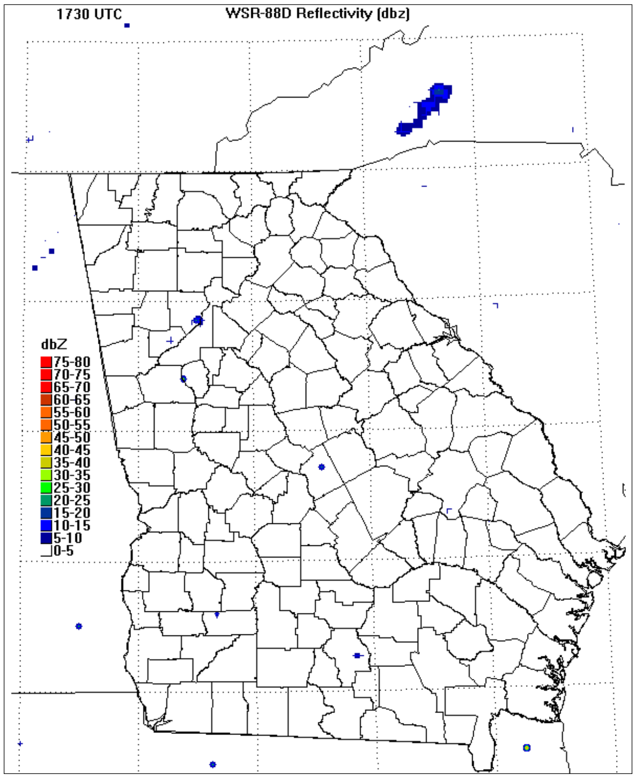

Figure B.28: 1730 UTC 06 August 2000 radar reflectivity.

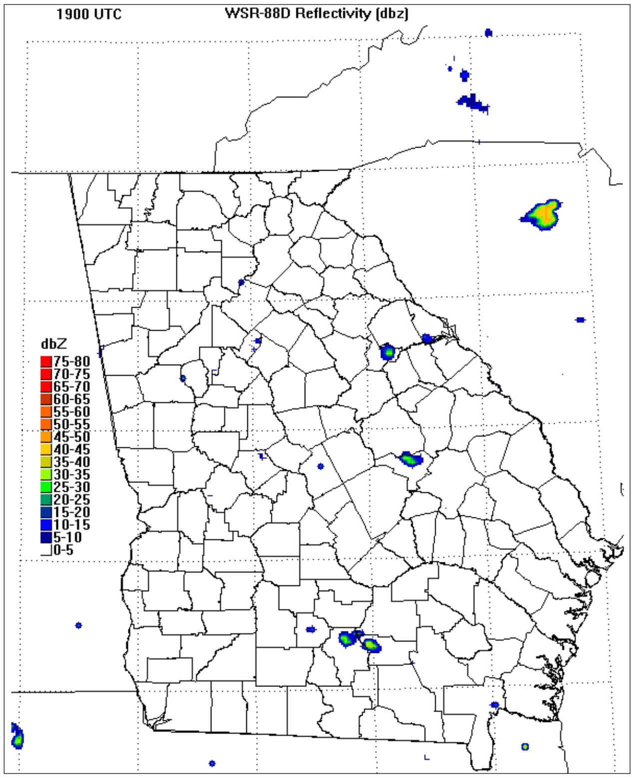

Figure B.29: 1900 UTC 06 August 2000 radar reflectivity.

APPENDIX C

SURFACE STATION PLOTS

This appendix includes hourly surface meteorological charts based on data from surface weather stations around Atlanta. Only data from the GAEMN stations were available before July 1996; therefore, surface data from the first nine events is not included here.

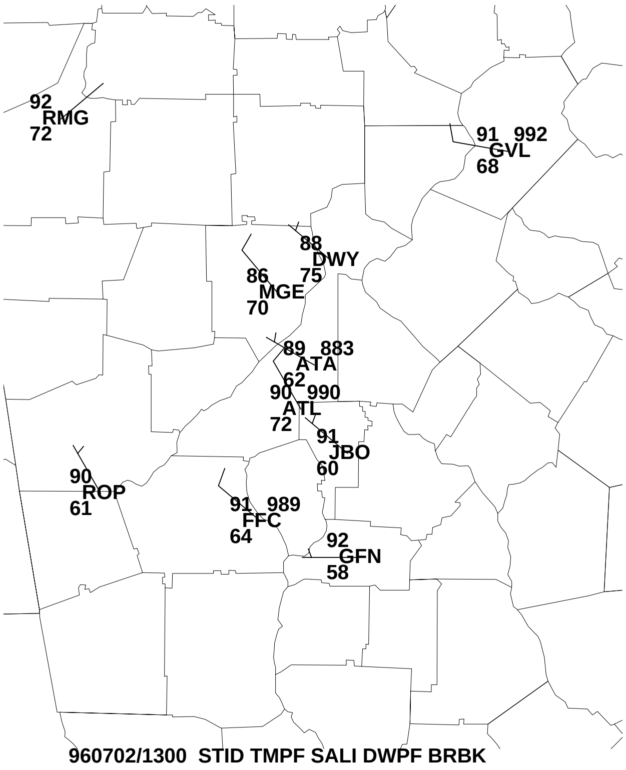

Figure C.1: 1700 UTC 02 July 1996 surface station plots.

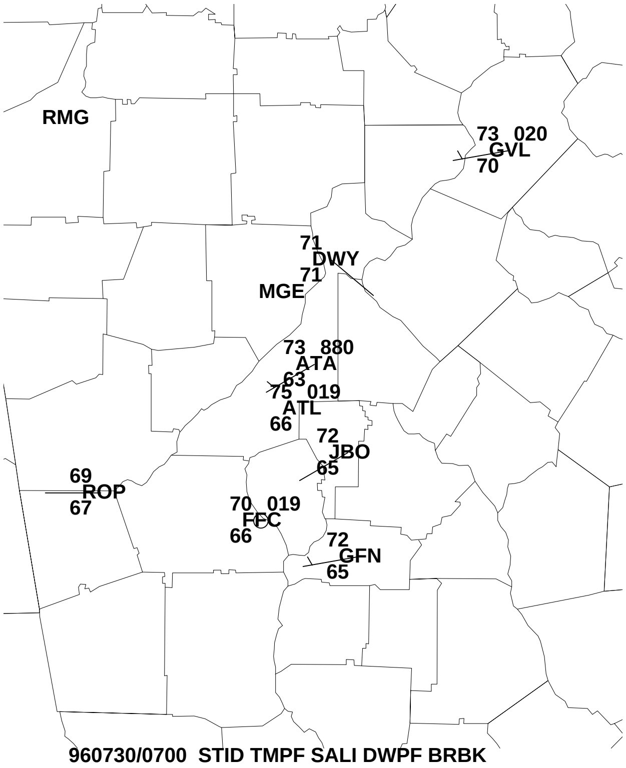

Figure C.2: 1100 UTC 30 July 1996 surface station plots.

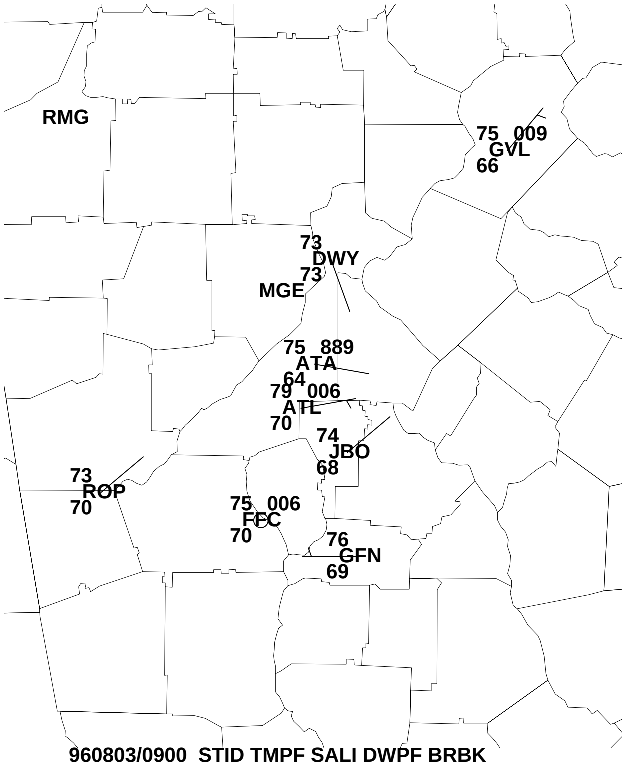

Figure C.3: 1300 UTC 03 August 1996 surface station plots.

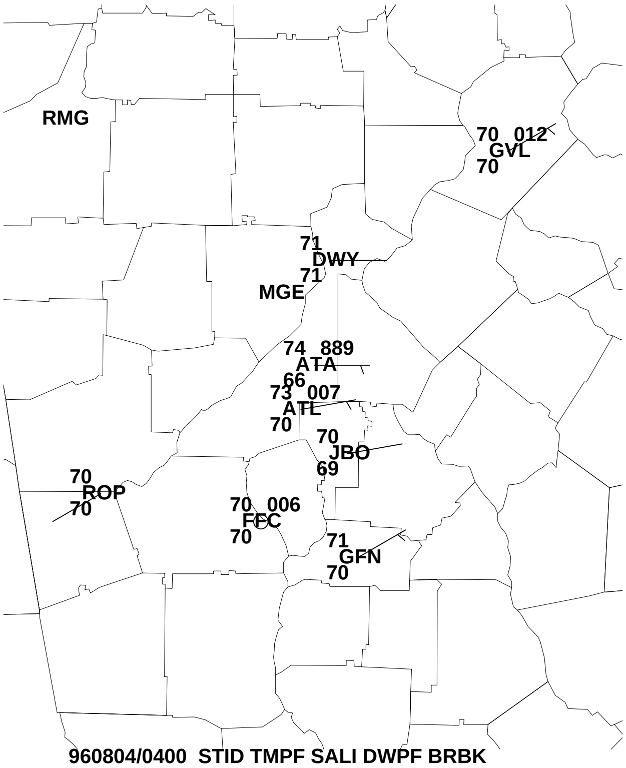

Figure C.4: 0800 UTC 04 August 1996 surface station plots.

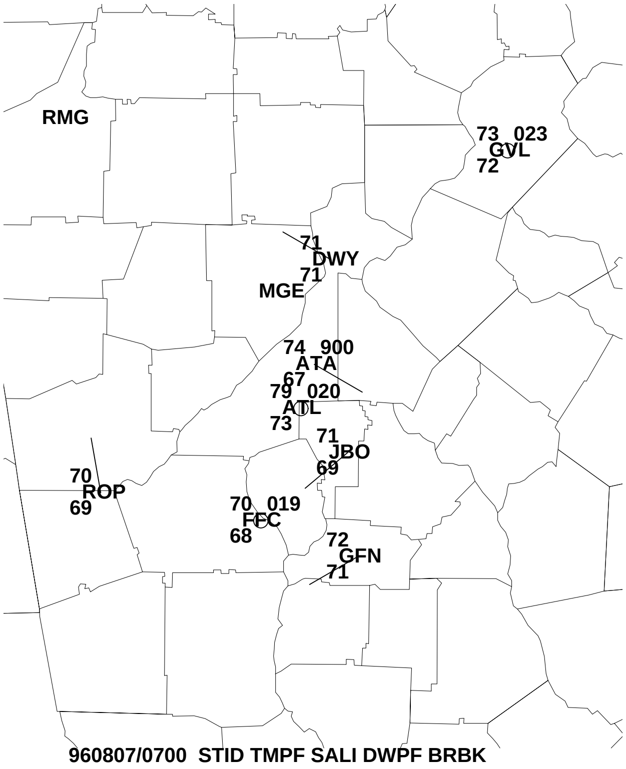

Figure C.5: 1100 UTC 07 August 1996 surface station plots.

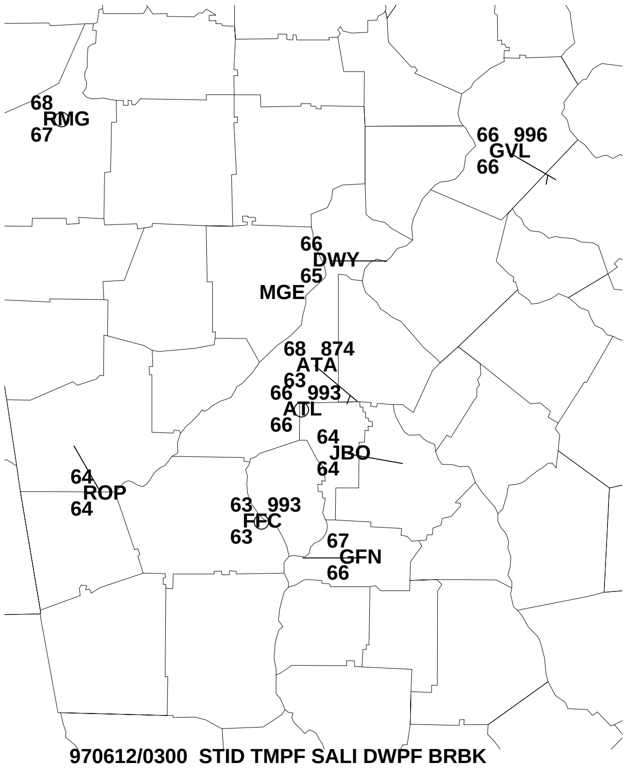

Figure C.6: 0700 UTC 12 June 1997 surface station plots.

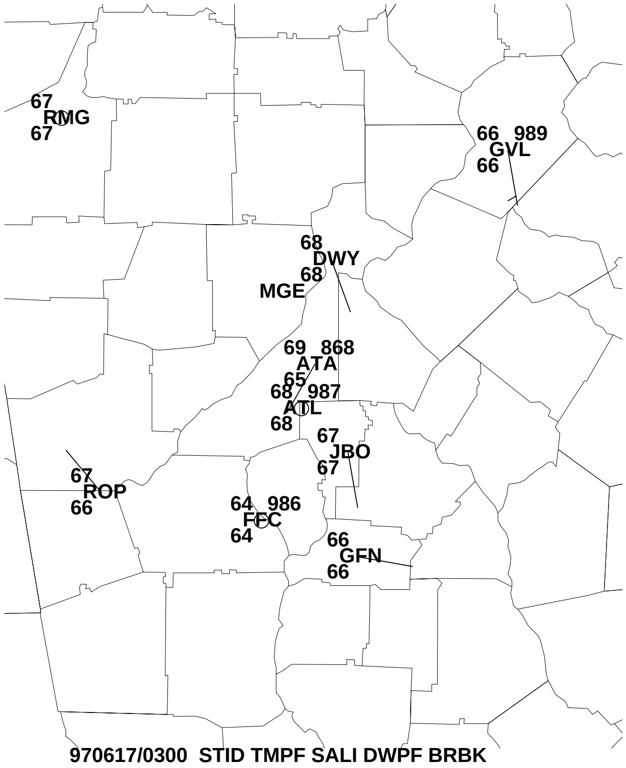

Figure C.7: 0700 UTC 17 June 1997 surface station plots.

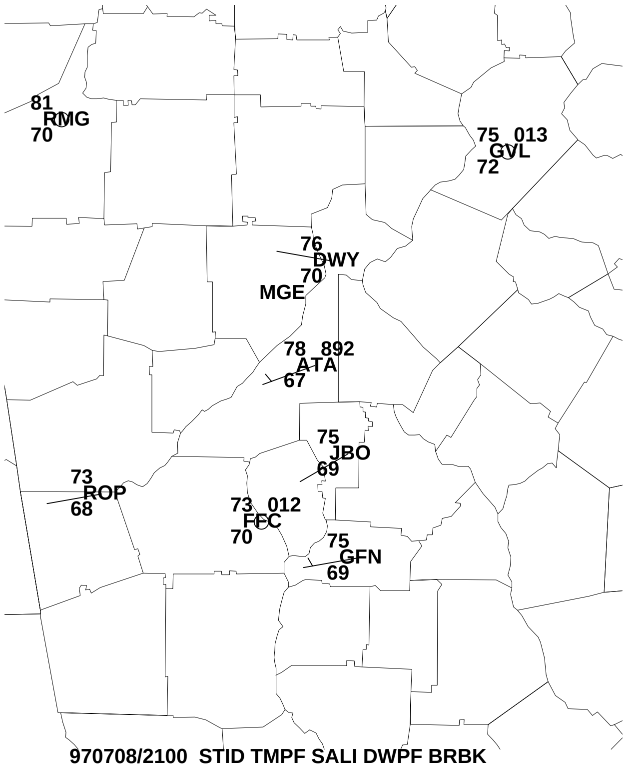

Figure C.8: 0000 UTC 09 July 1997 surface station plots.

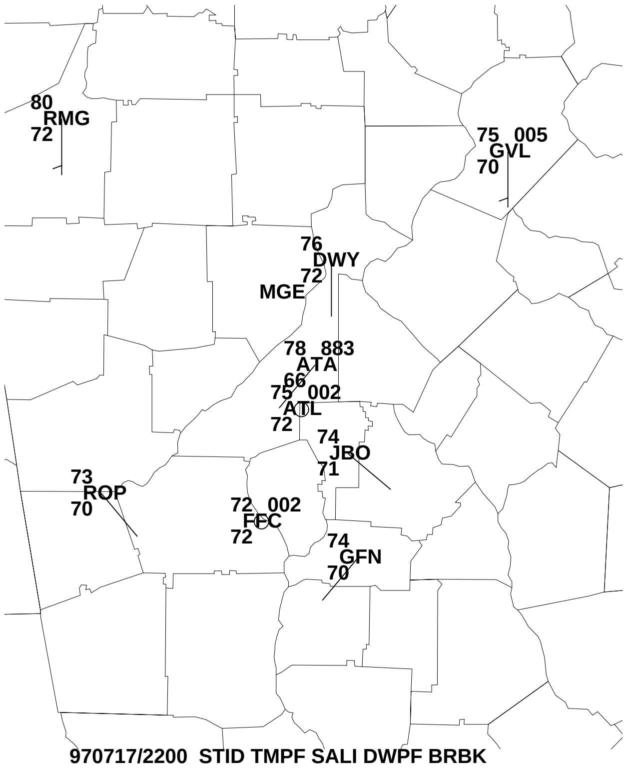

Figure C.9: 0200 UTC 18 July 1997 surface station plots.

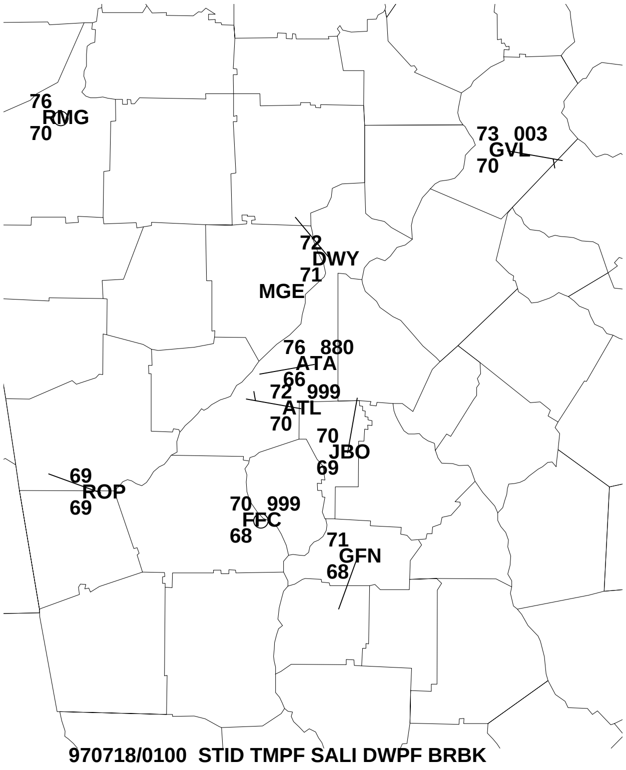

Figure C.10: 0500 UTC 18 July 1997 surface station plots.

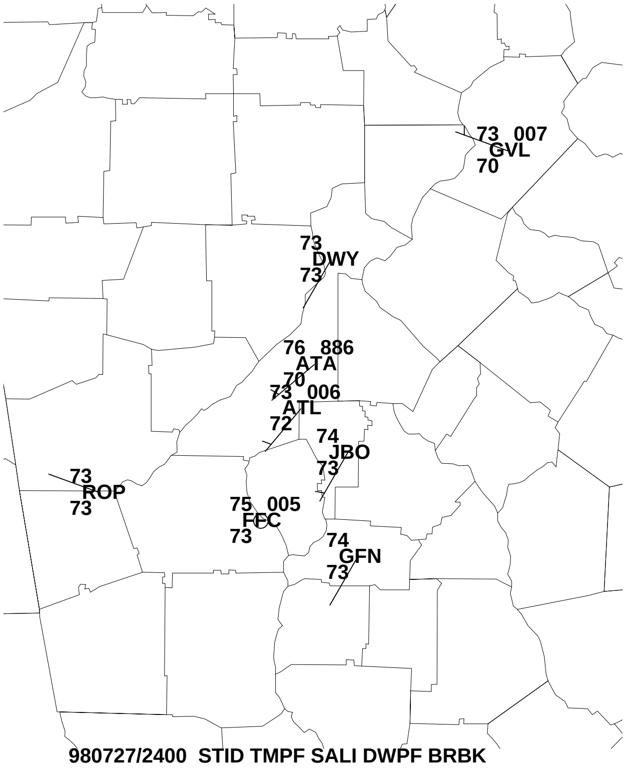

Figure C.11: 0400 UTC 28 July 1998 surface station plots.

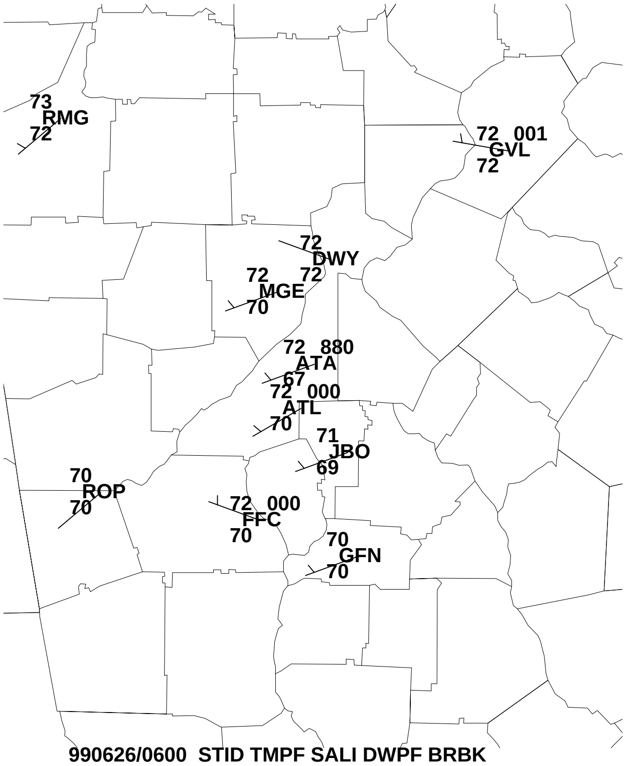

Figure C.12: 1000 UTC 26 June 1999 surface station plots.

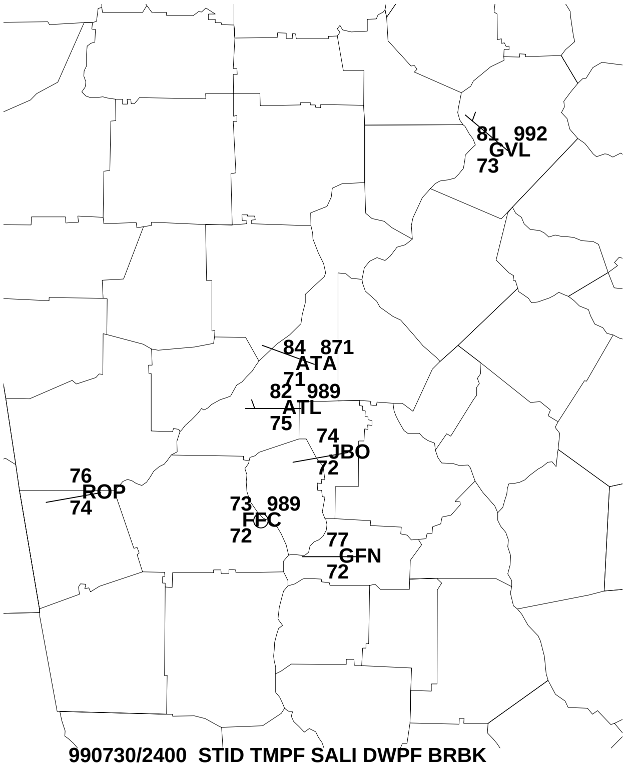

Figure C.13: 0400 UTC 31 July 1999 surface station plots.

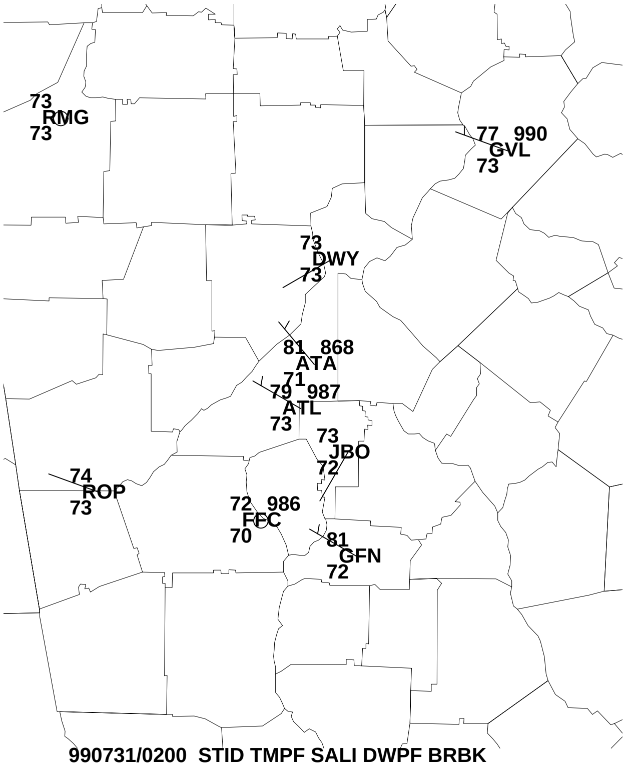

Figure C.14: 0600 UTC 31 July 1999 surface station plots.

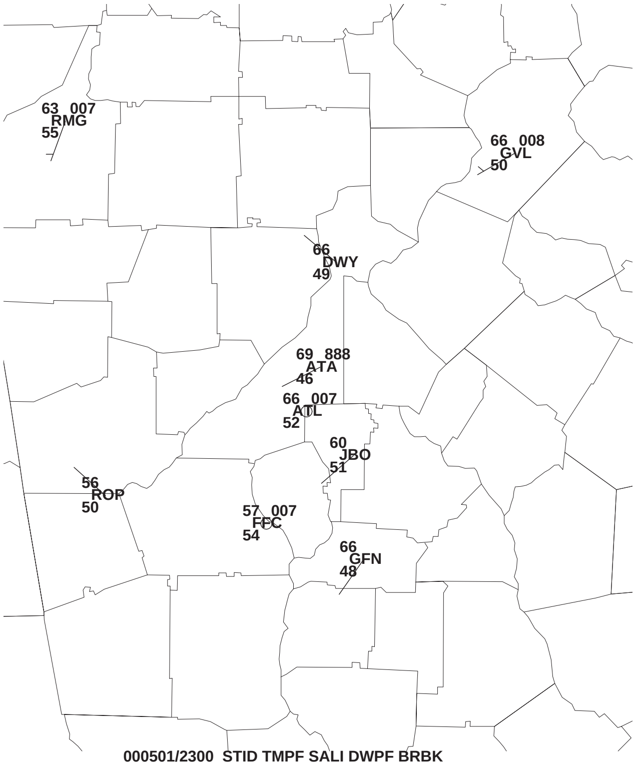

Figure C.15: 0300 UTC 02 May 2000 surface station plots.

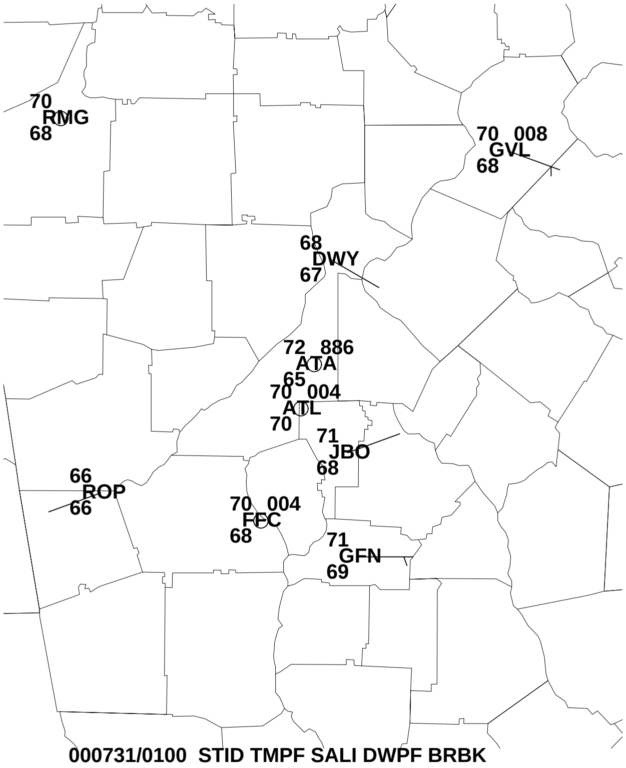

Figure C.16: 0500 UTC 31 July 2000 surface station plots.

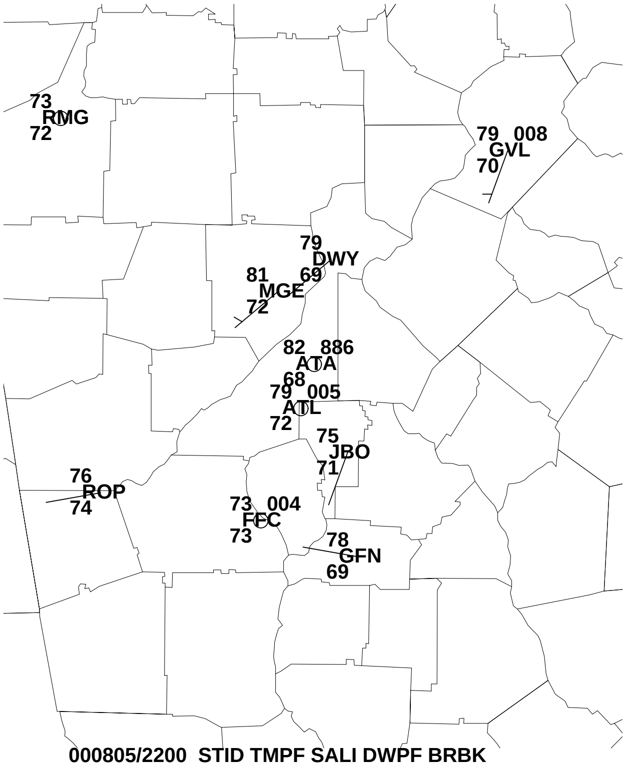

Figure C.17: 0200 UTC 06 August 2000 surface station plots.

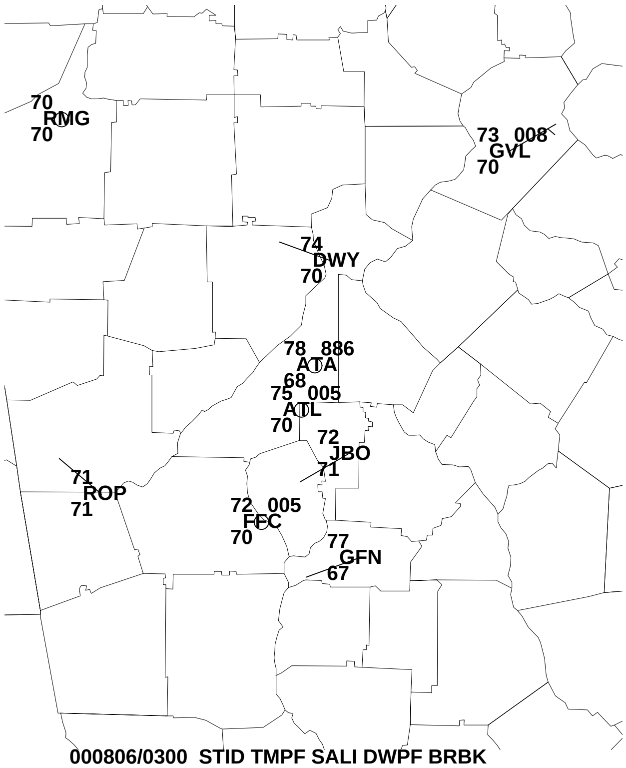

Figure C.18: 0700 UTC 06 August 2000 surface station plots.

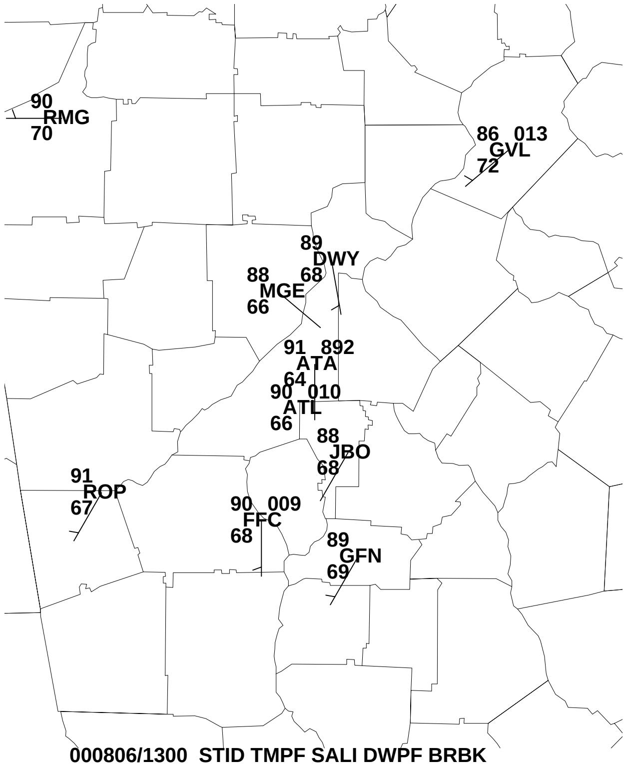

Figure C.19: 1700 UTC 06 August 2000 surface station plots.

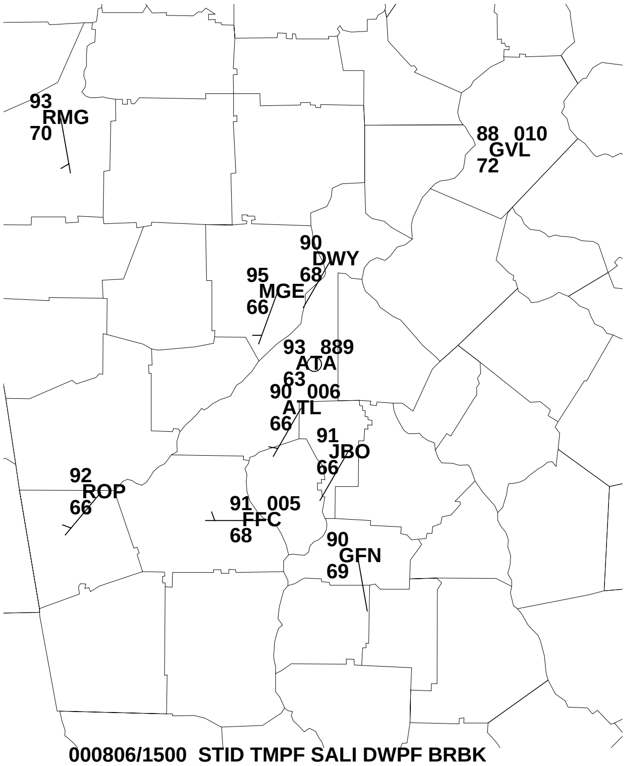

Figure C.20: 1900 UTC 06 August 2000 surface station plots.

APPENDIX D

URBAN–RURAL TEMPERATURE DIFFERENCE GRAPHS

This appendix includes graphs of the urban–rural temperature differences (based on ATA–ROP temperature differences) for a 24–hour period leading up to each UHI–initiated precipitation event.

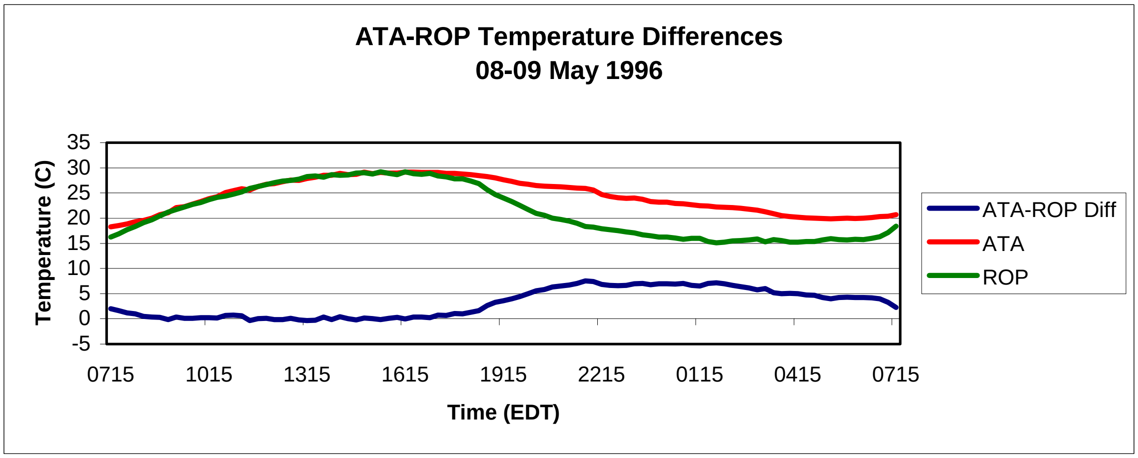

Figure D.1: Urban–rural temperature differences from 1115 UTC 08 May 1996 to 1115 UTC 09 May 1996.

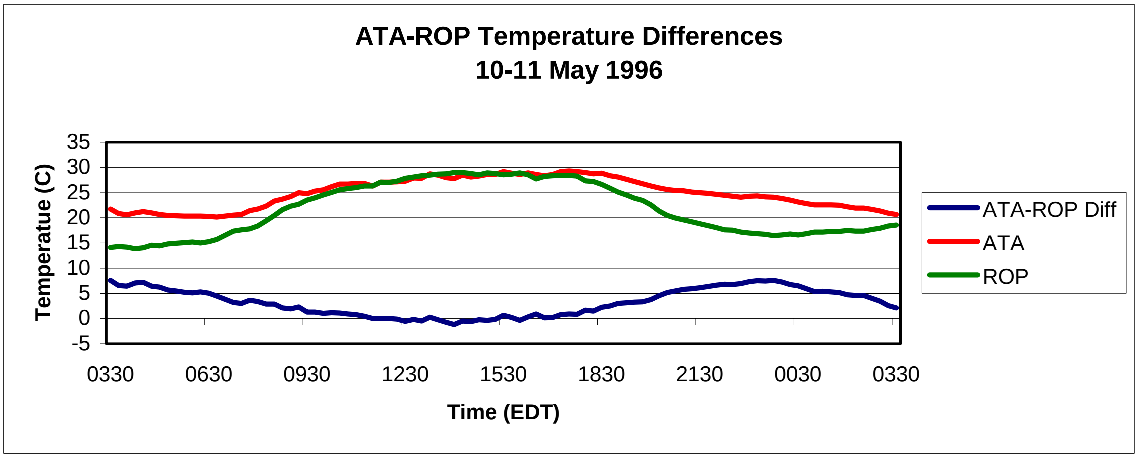

Figure D.2: Urban–rural temperature differences from 0730 UTC 10 May 1996 to 0730 UTC 11 May 1996.

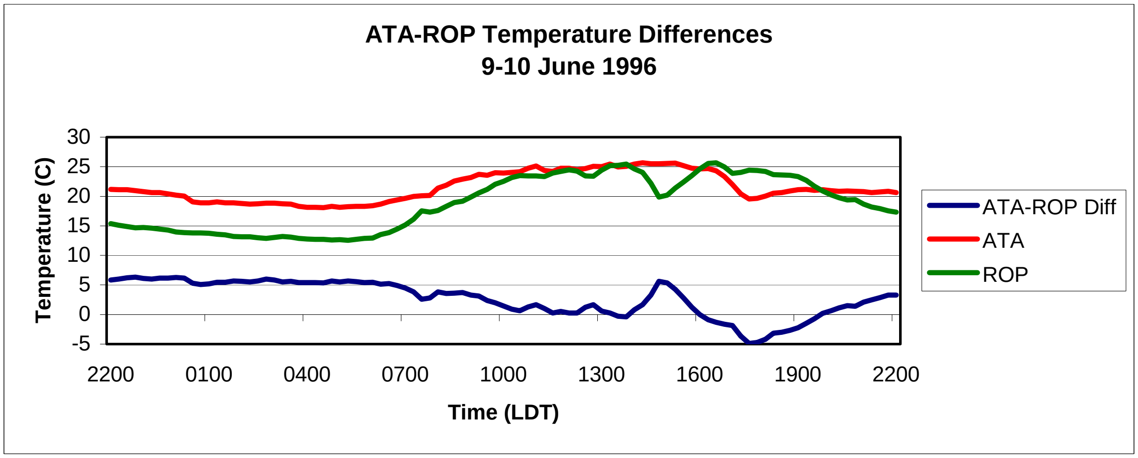

Figure D.3: Urban–rural temperature differences from 0200 UTC 10 June 1996 to 0200 UTC 11 June 1996.

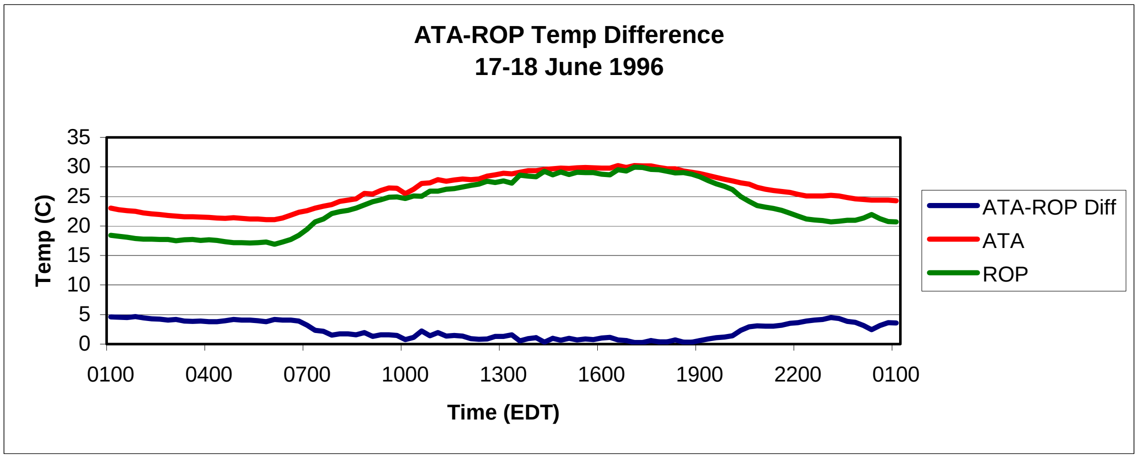

Figure D.4: Urban–rural temperature differences from 0500 UTC 17 June 1996 to 0500 UTC 18 June 1996.

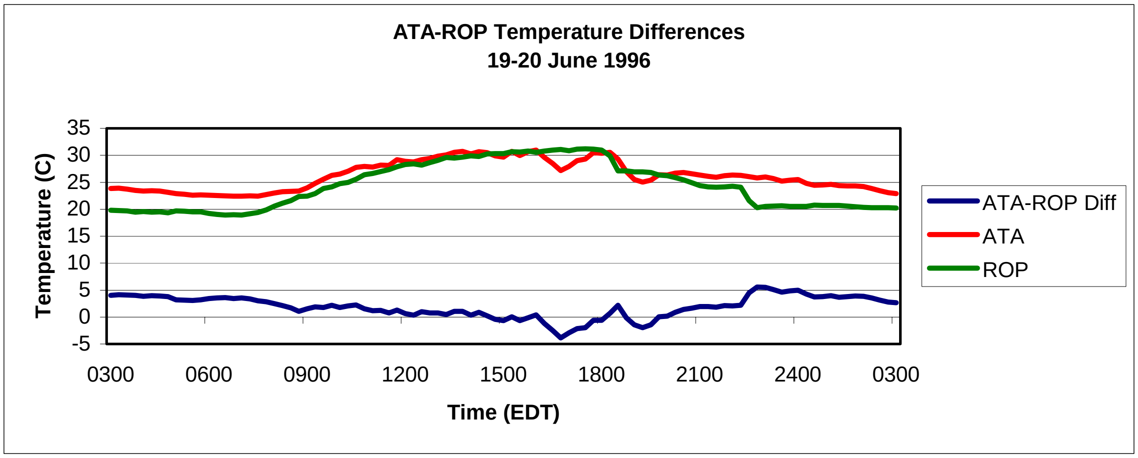

Figure D.5: Urban–rural temperature differences from 0700 UTC 19 June 1996 to 0700 UTC 20 June 1996.

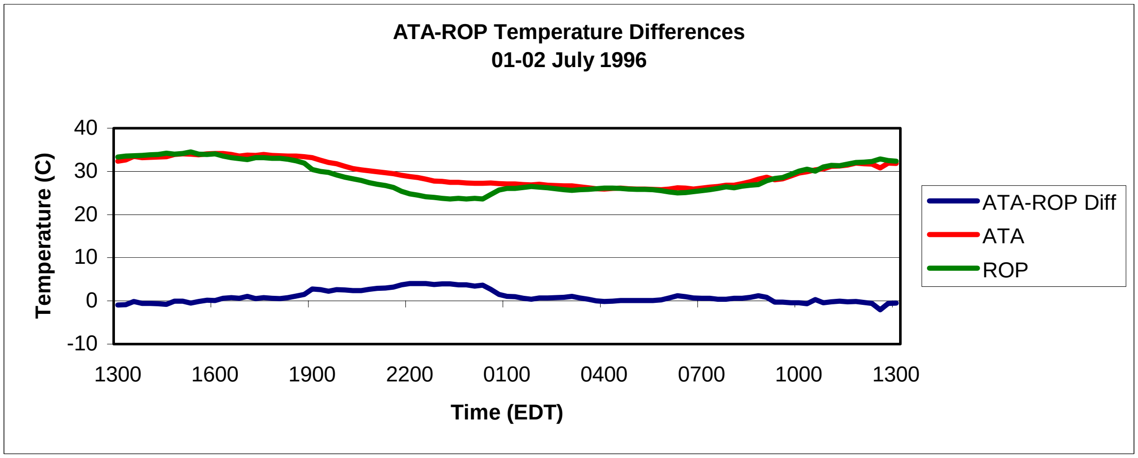

Figure D.6: Urban–rural temperature differences from 1700 UTC 01 July 1996 to 1700 UTC 02 July 1996.

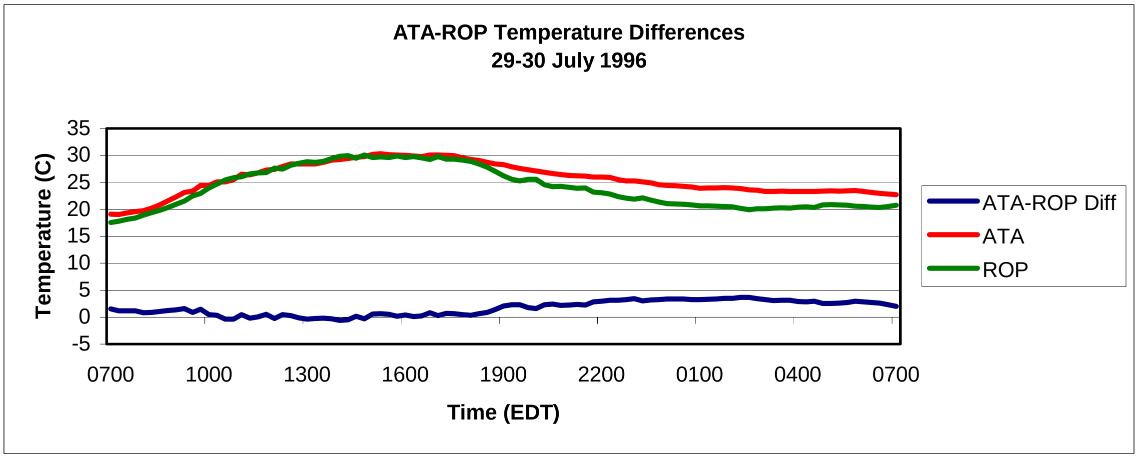

Figure D.7: Urban–rural temperature differences from 1100 UTC 29 July 1996 to 1100 UTC 30 July 1996.

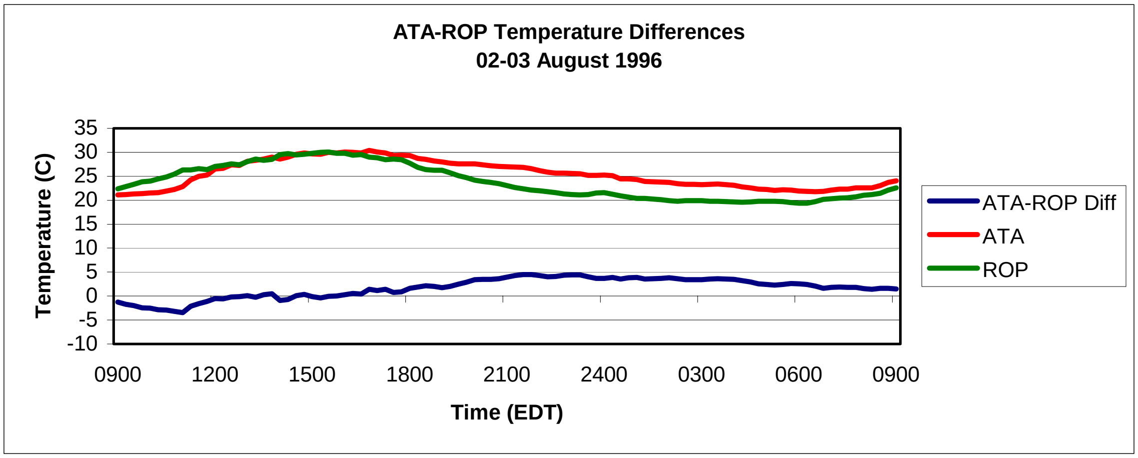

Figure D.8: Urban–rural temperature differences from 1300 UTC 02 August 1996 to 1300 UTC 03 August 1996.

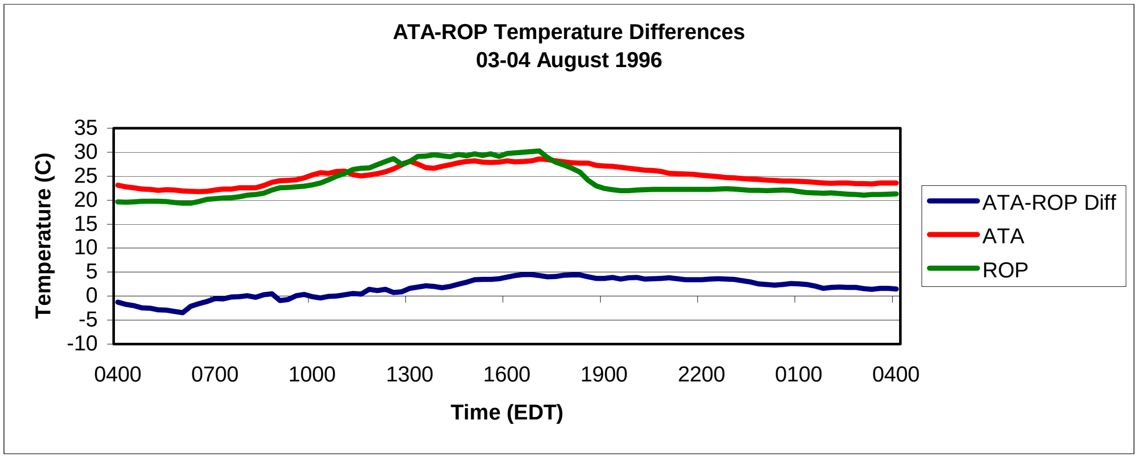

Figure D.9: Urban–rural temperature differences from 0800 UTC 03 August 1996 to 0800 UTC 04 August 1996.

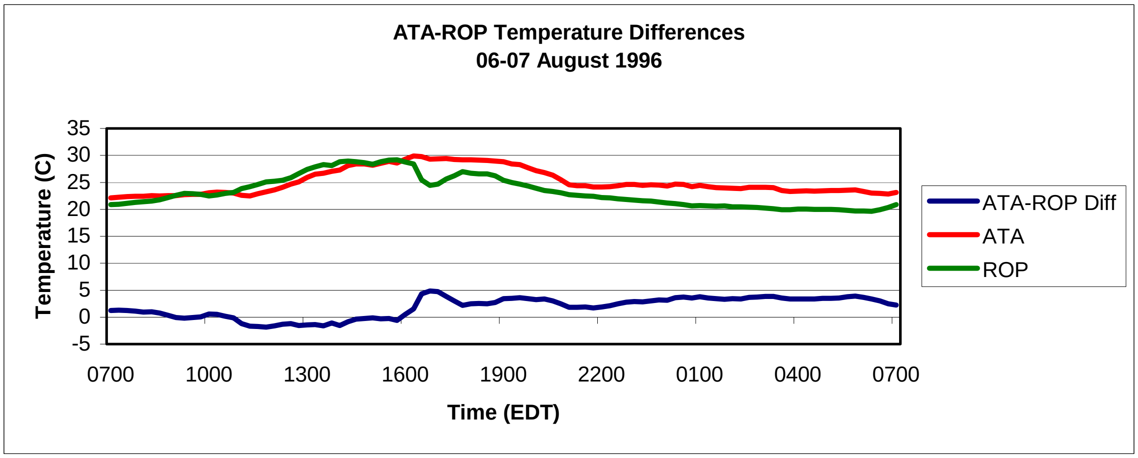

Figure D.10: Urban–rural temperature differences from 1100 UTC 06 August 1996 to 1100 UTC 07 August 1996.

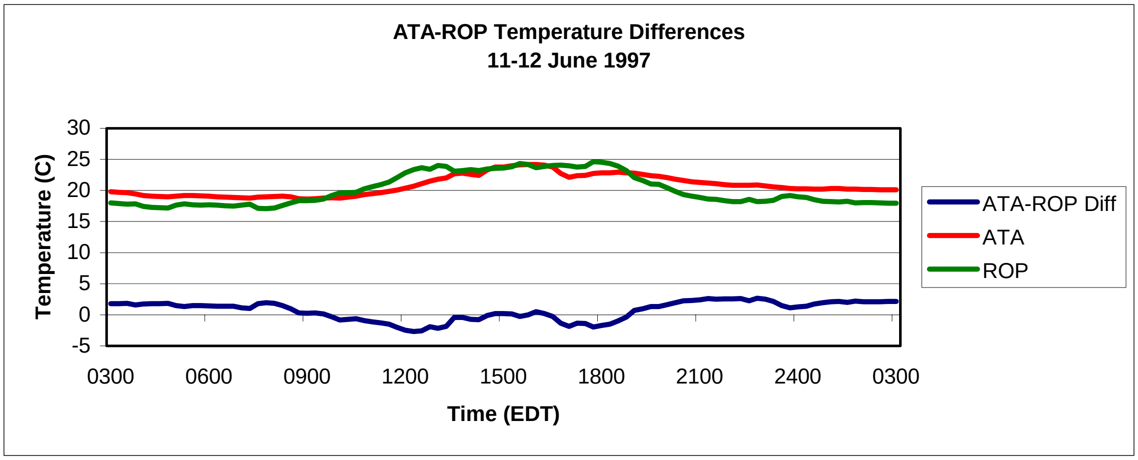

Figure D.11: Urban–rural temperature differences from 0700 UTC 11 June 1997 to 0700 UTC 12 June 1997.

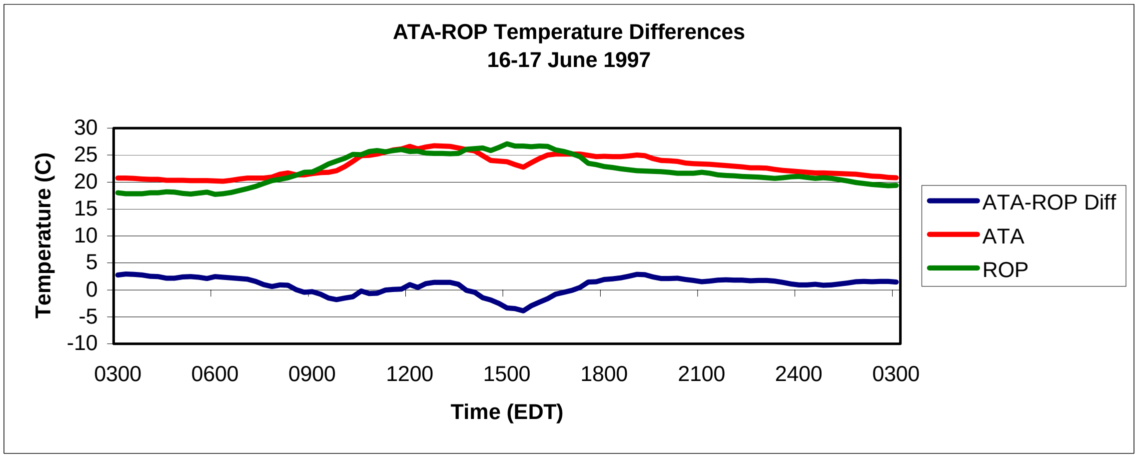

Figure D.12: Urban–rural temperature differences from 0700 UTC 16 June 1997 to 0700 UTC 17 June 1997.

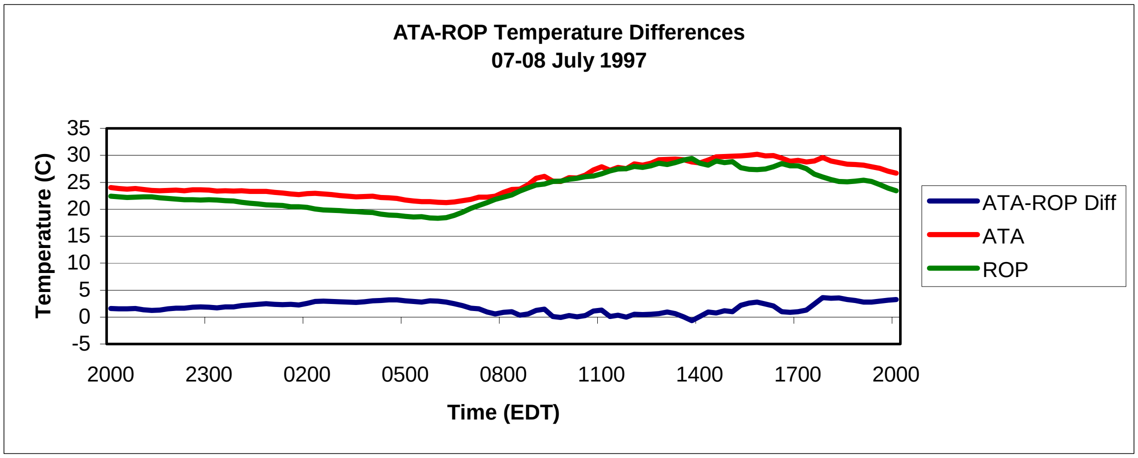

Figure D.13: Urban–rural temperature differences from 0000 UTC 08 July 1997 to 0000 UTC 09 July 1997.

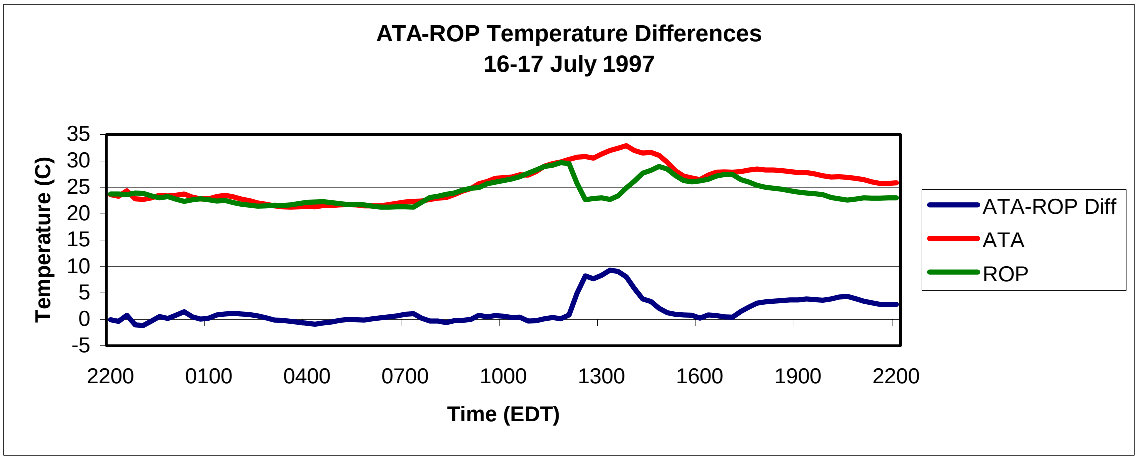

Figure D.14: Urban–rural temperature differences from 0200 UTC 17 July 1997 to 0200 UTC 18 July 1997.

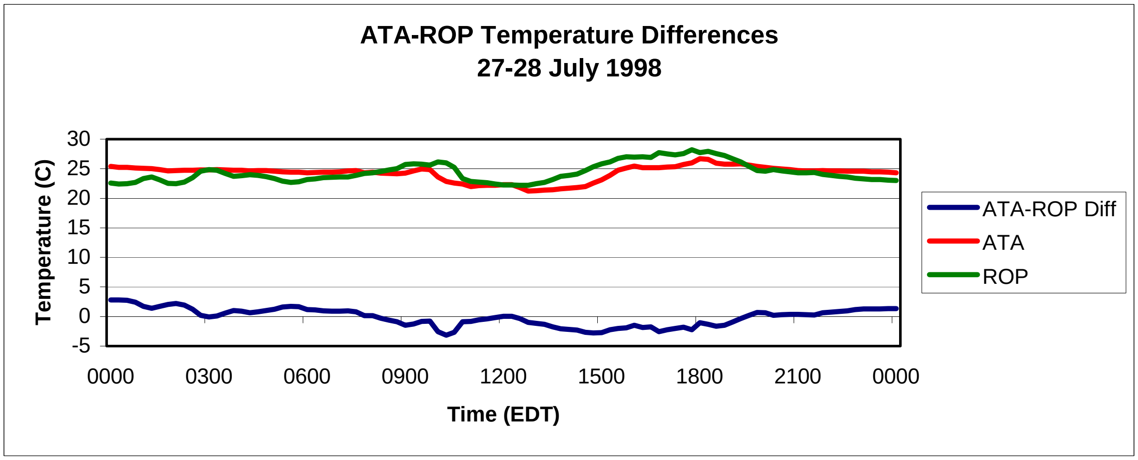

Figure D.15: Urban–rural temperature differences from 0400 UTC 27 July 1998 to 0400 UTC 28 July 1998.

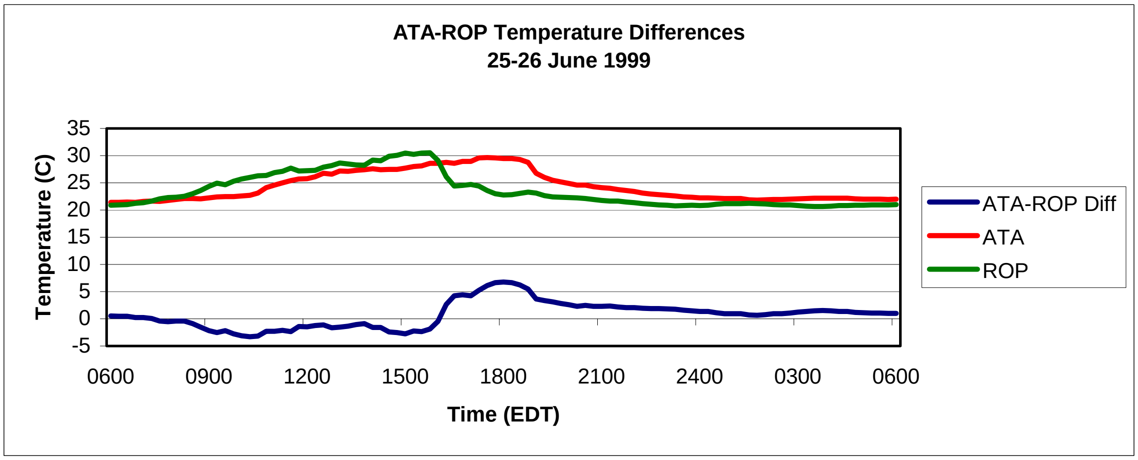

Figure D.16: Urban–rural temperature differences from 1000 UTC 25 June 1999 to 1000 UTC 26 June 1999.

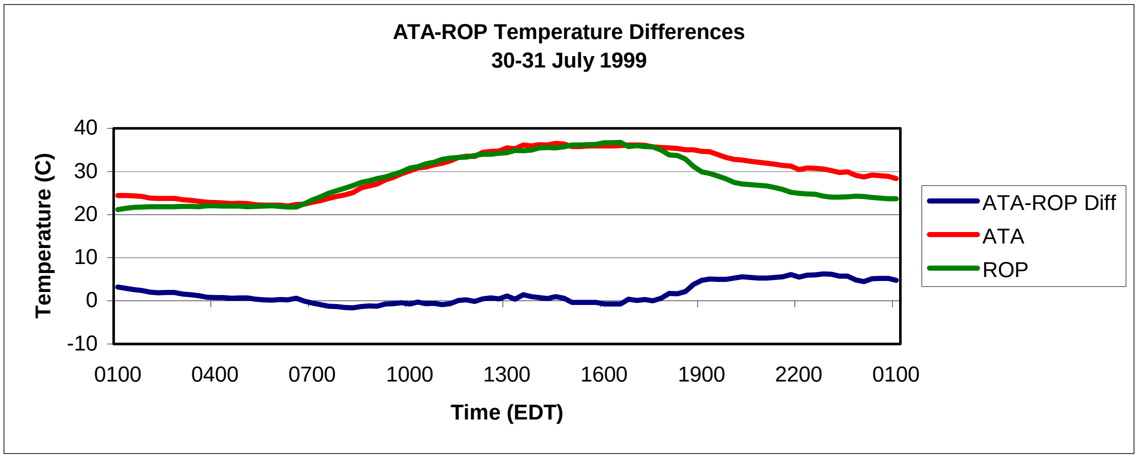

Figure D.17: Urban–rural temperature differences from 0500 UTC 30 July 1999 to 0500 UTC 31 July 1999.

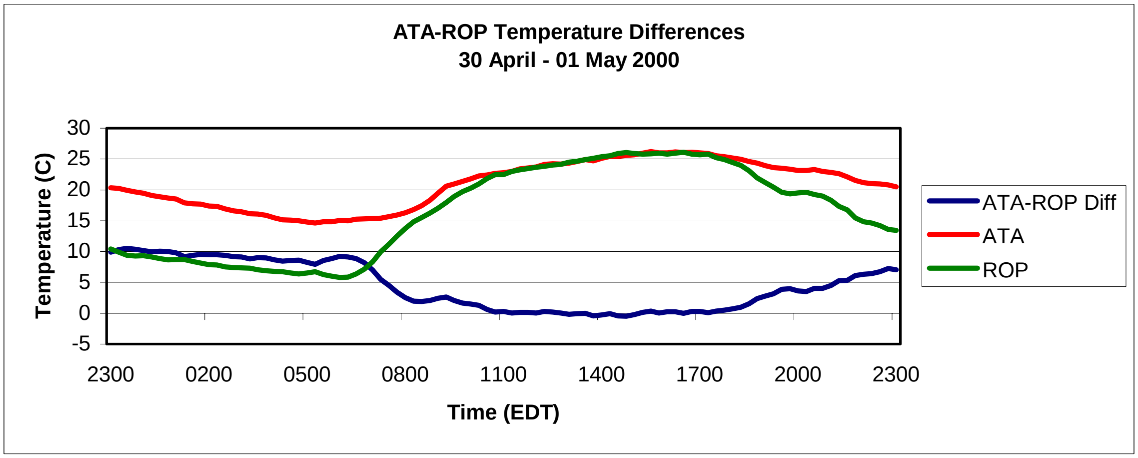

Figure D.18: Urban–rural temperature differences from 0300 UTC 01 May 2000 to 0300 UTC 02 May 2000.

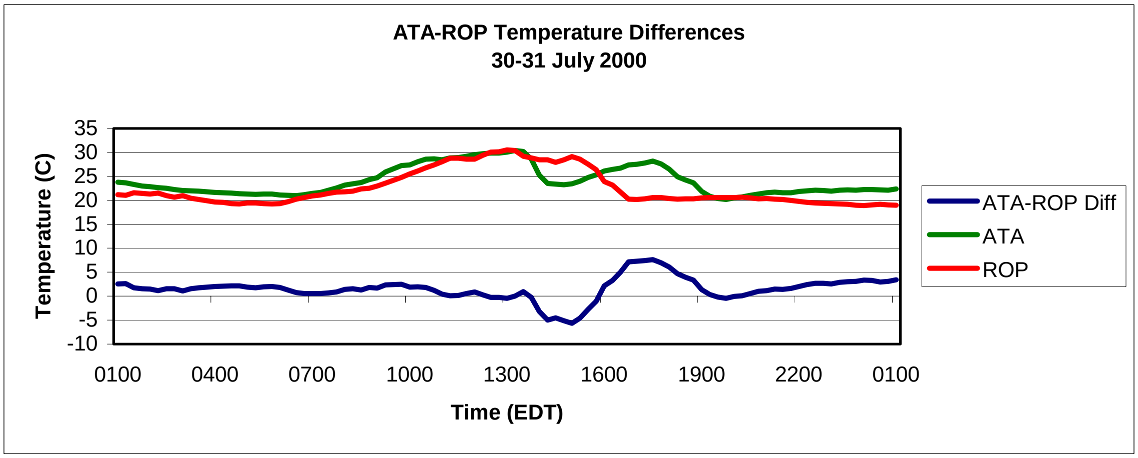

Figure D.19: Urban–rural temperature differences from 0500 UTC 30 July 2000 to 0500 UTC 31 July 2000.

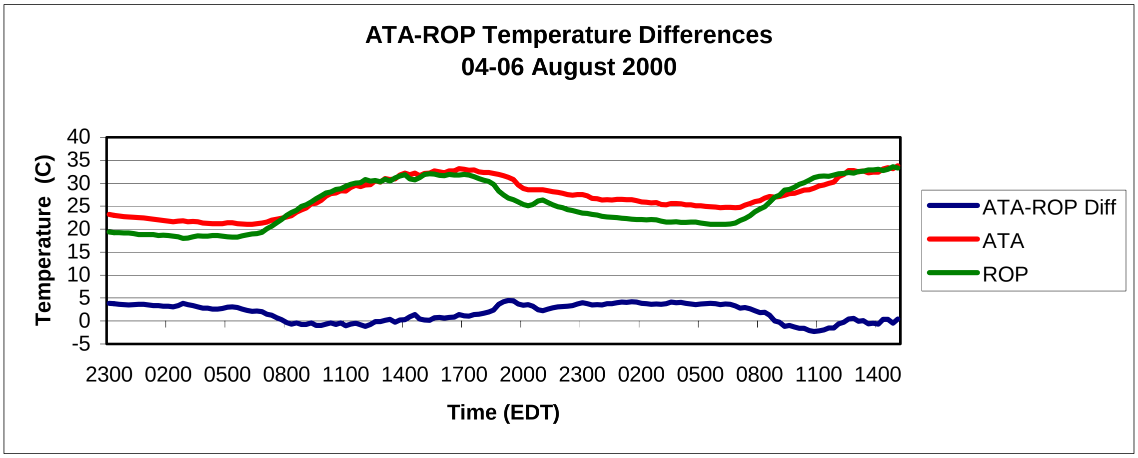

Figure D.20: Urban–rural temperature differences from 0300 UTC 05 August 2000 to 1900 UTC 06 August 2000.

APPENDIX E

SKEW–T / LOG–P DIAGRAM.S

This appendix includes skew–T / log–P diagrams based on sounding data from FFC. Diagrams are plotted for each observation time immediately before and immediately after the beginning each UHI–induced precipitation event. However, only the 12 UTC data was available for 26 June 1999. Also, no data was available for the following times: 00 UTC, 06 August 2000, 00 UTC, 31 July 2000, and 12 UTC, 31 July 2000.

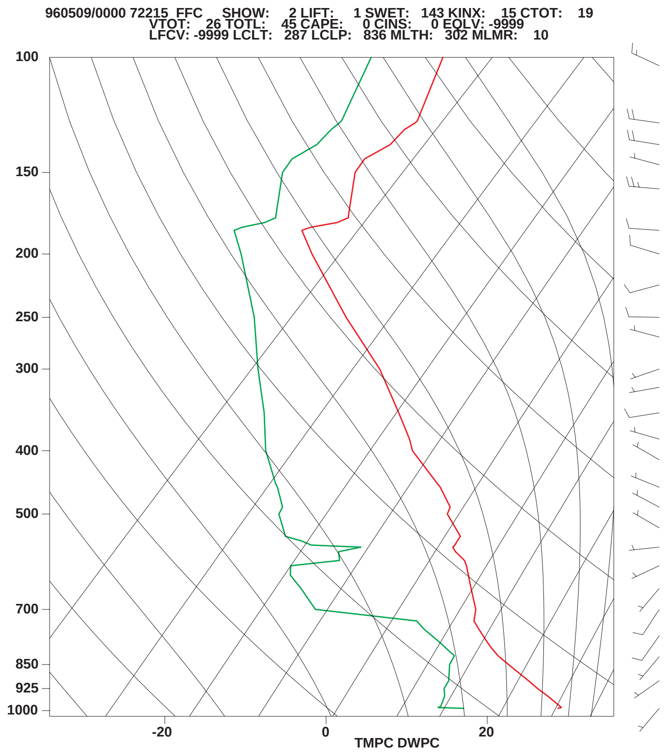

Figure E.1: 0000 UTC 09 May 1996 skew–T / log–P diagram.

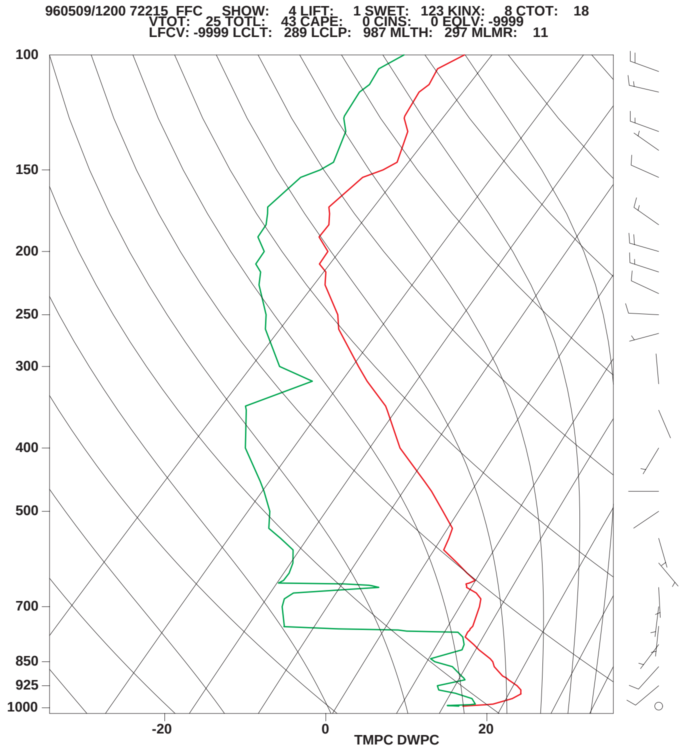

Figure E.2: 1200 UTC 09 May 1996 skew–T / log–P diagram.

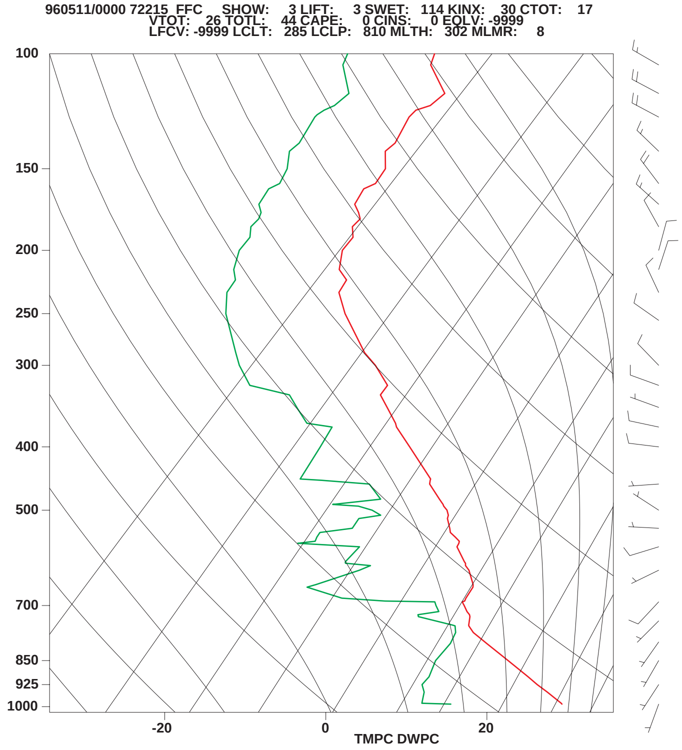

Figure E.3: 0000 UTC 11 May 1996 skew–T / log–P diagram.

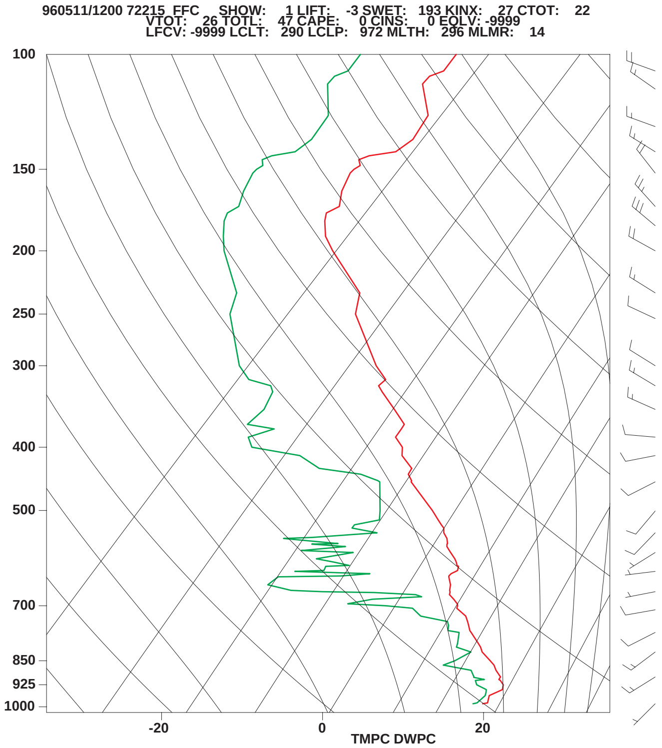

Figure E.4: 1200 UTC 11 May 1996 skew–T / log–P diagram.

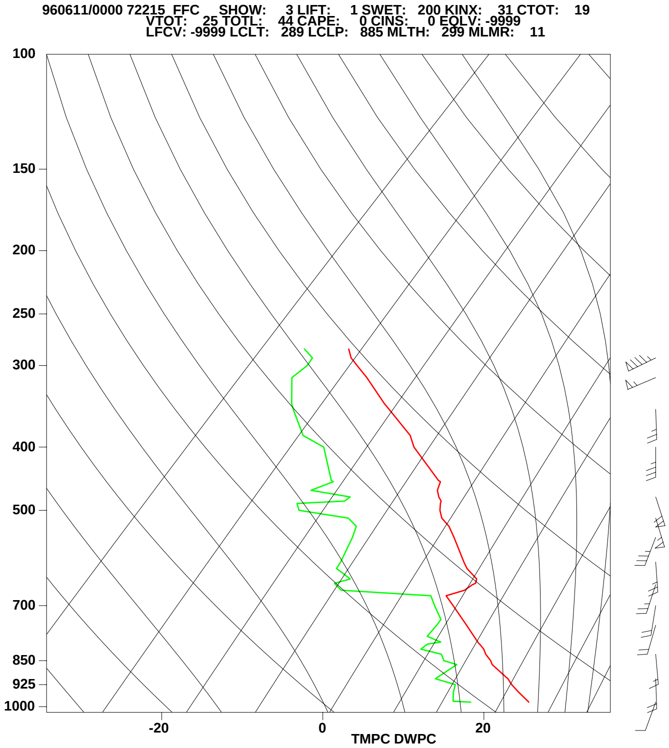

Figure E.5: 0000 UTC 11 June 1996 skew–T / log–P diagram.

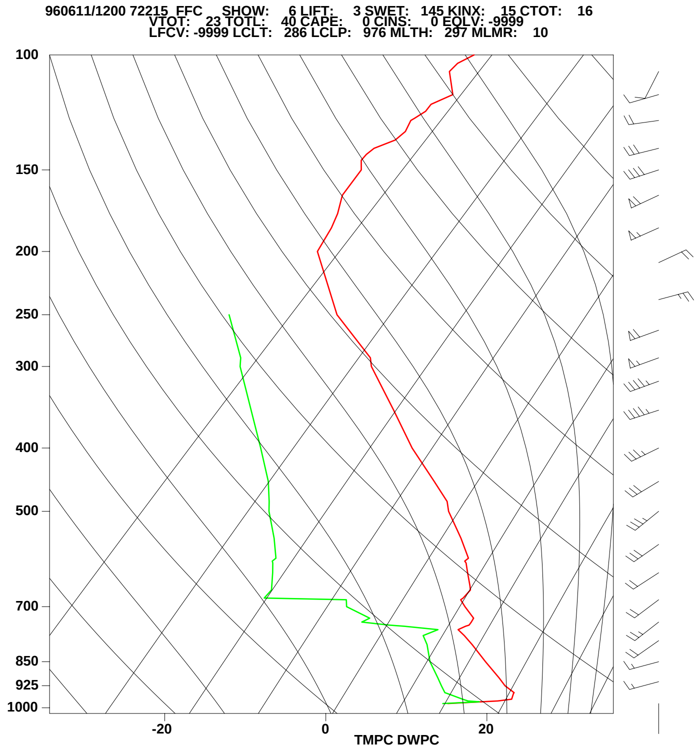

Figure E.6: 1200 UTC 11 June 1996 skew–T / log–P diagram.

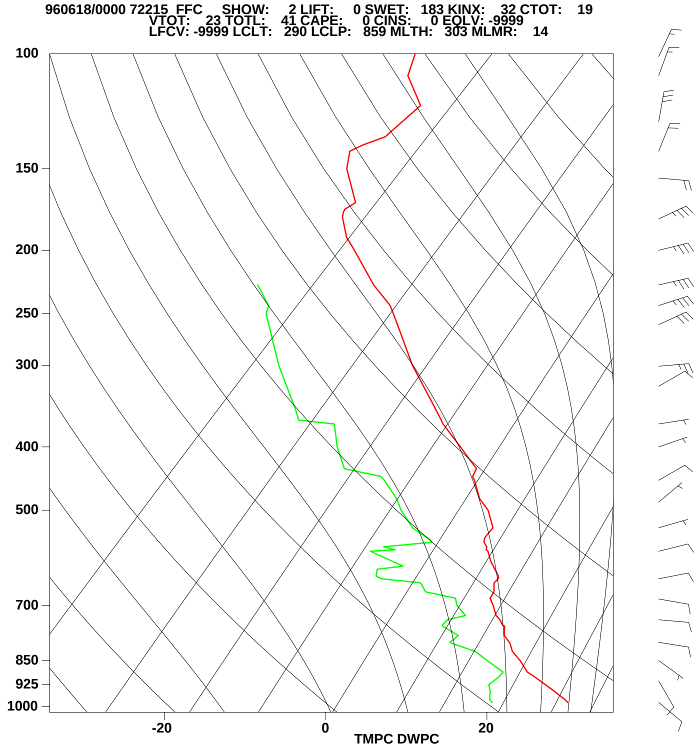

Figure E.7: 0000 UTC 18 June 1996 skew–T / log–P diagram.

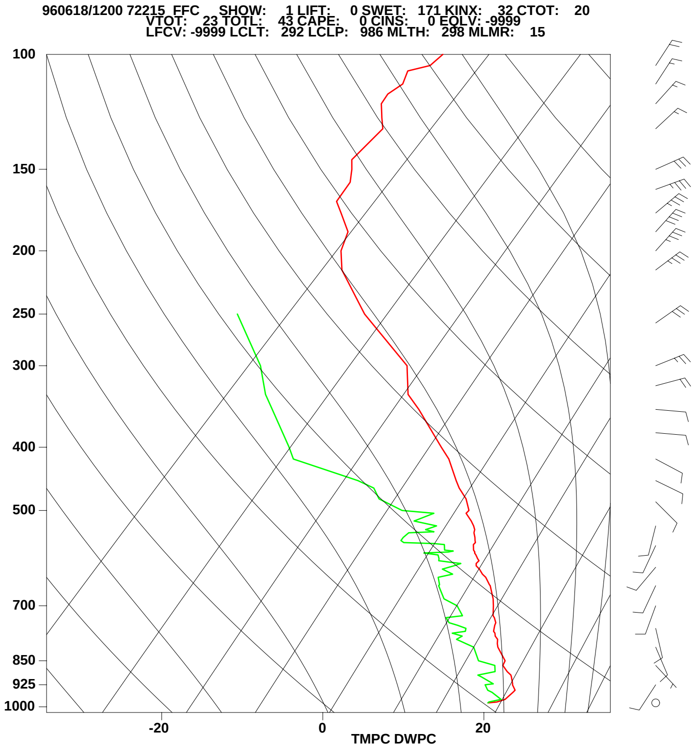

Figure E.8: 1200 UTC 18 June 1996 skew–T / log–P diagram.

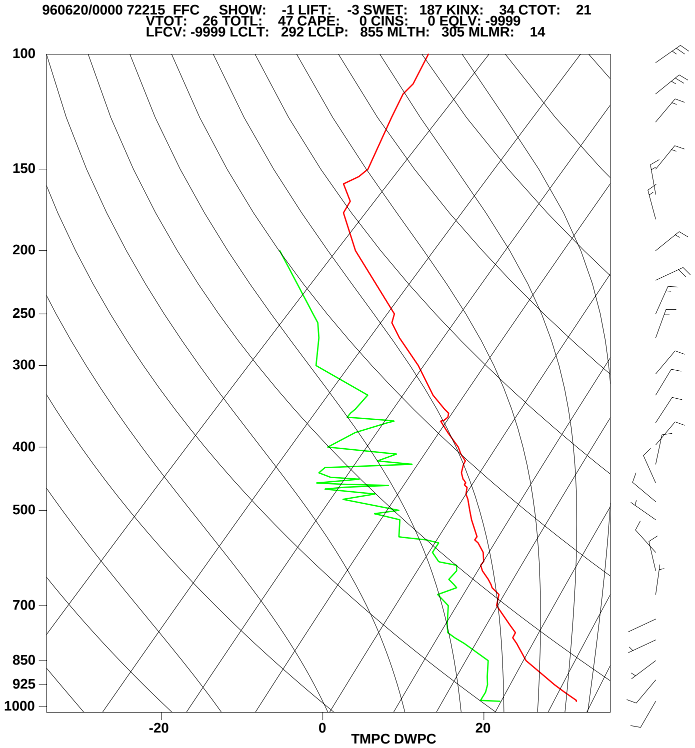

Figure E.9: 0000 UTC 20 June 1996 skew–T / log–P diagram.

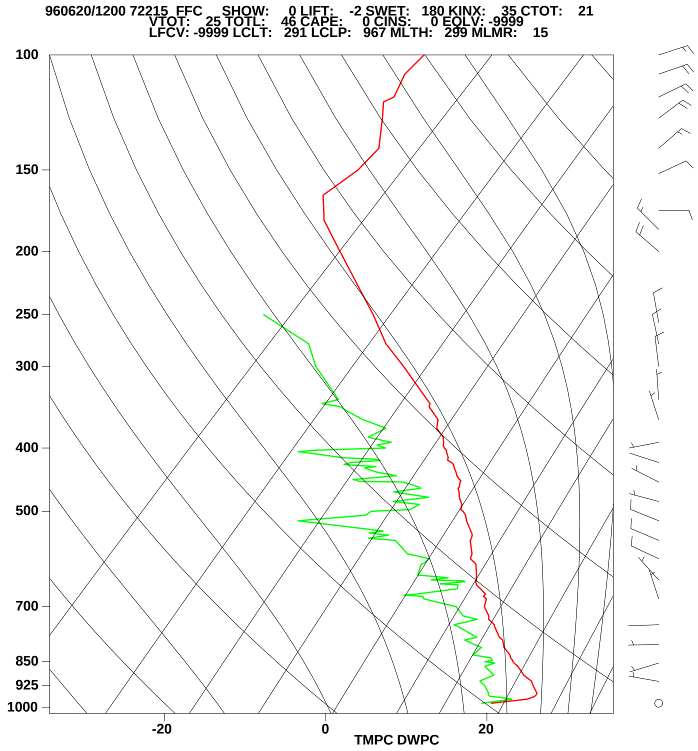

Figure E.10: 1200 UTC 20 June 1996 skew–T / log–P diagram.

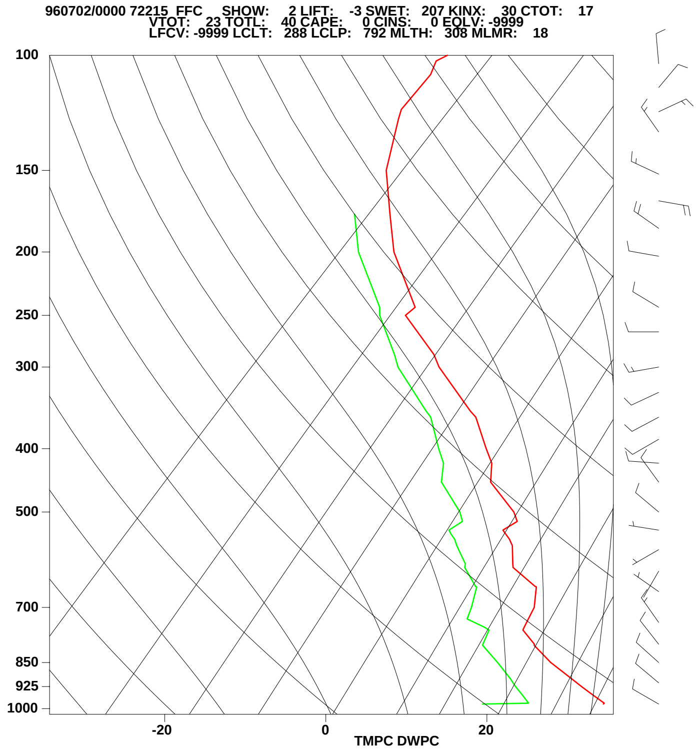

Figure E.11: 0000 UTC 02 July 1996 skew–T / log–P diagram.

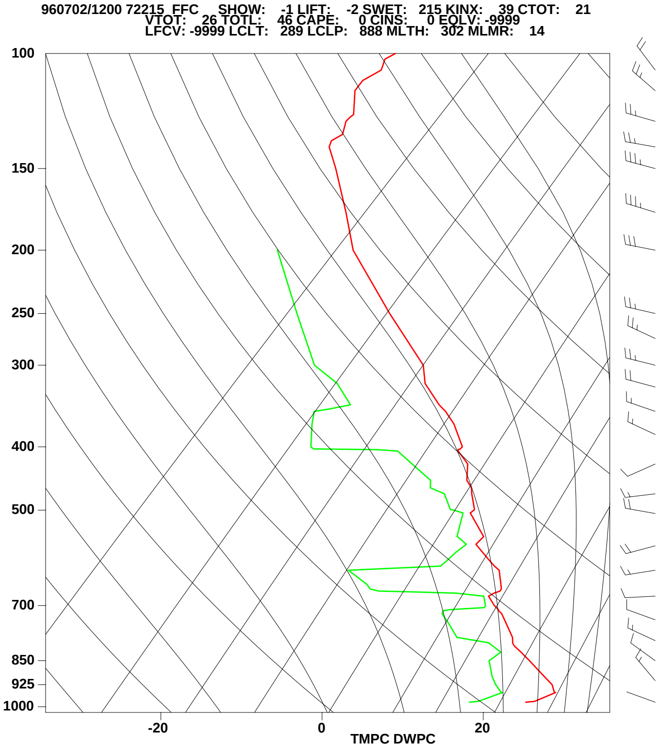

Figure E.12: 1200 UTC 02 July 1996 skew–T / log–P diagram.

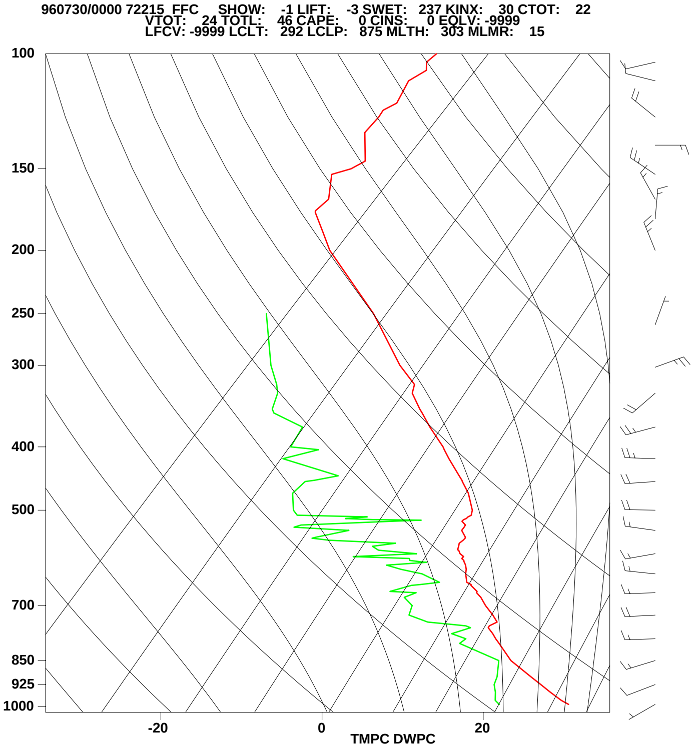

Figure E.13: 0000 UTC 30 July 1996 skew–T / log–P diagram.

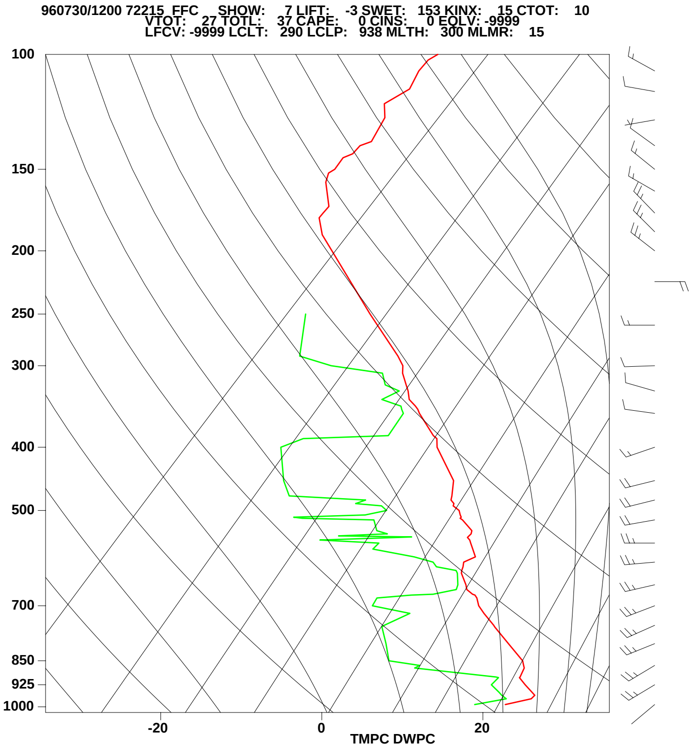

Figure E.14: 1200 UTC 30 July 1996 skew–T / log–P diagram.

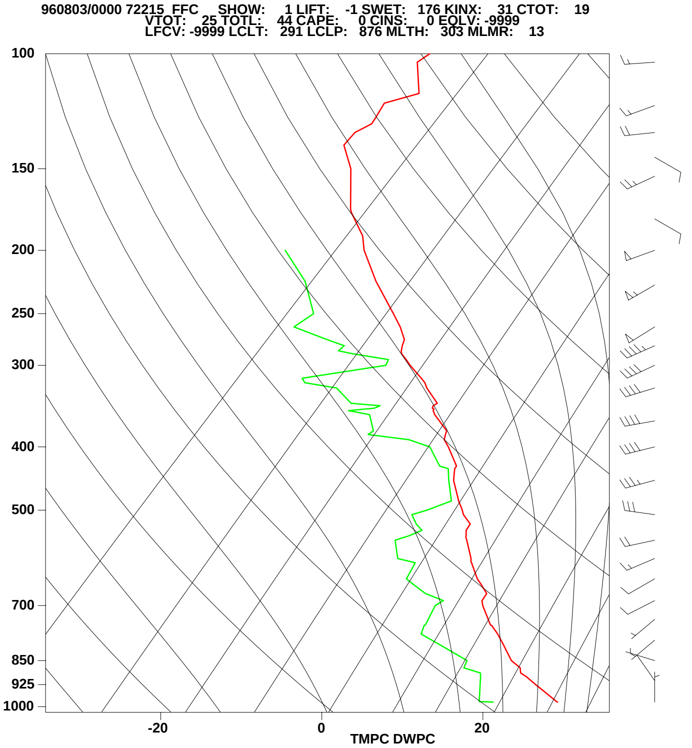

Figure E.15: 0000 UTC 03 August 1996 skew–T / log–P diagram.

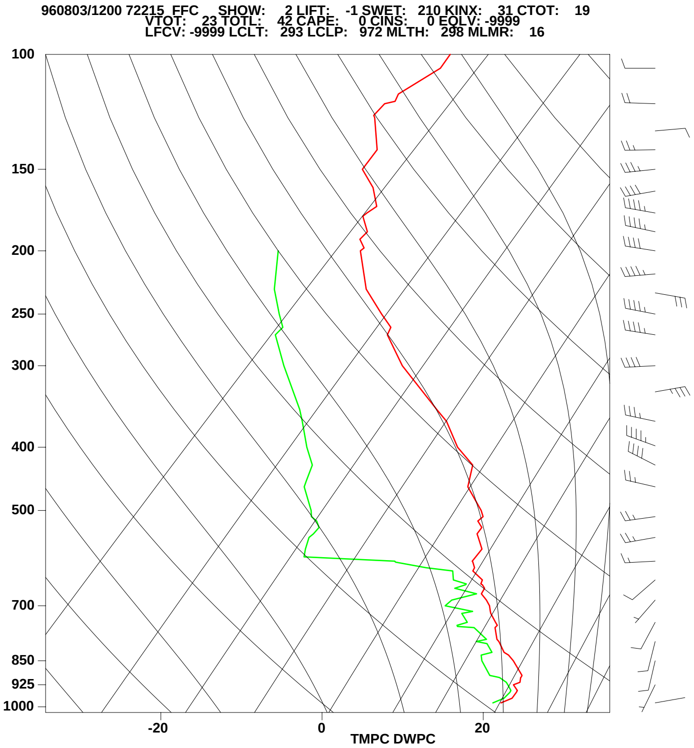

Figure E.16: 1200 UTC 03 August 1996 skew–T / log–P diagram.

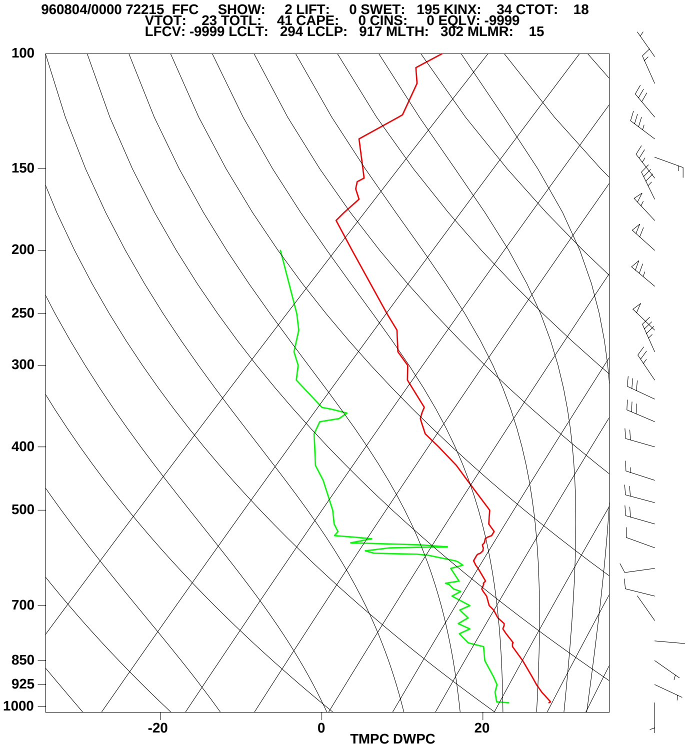

Figure E.17: 0000 UTC 04 August 1996 skew–T / log–P diagram.

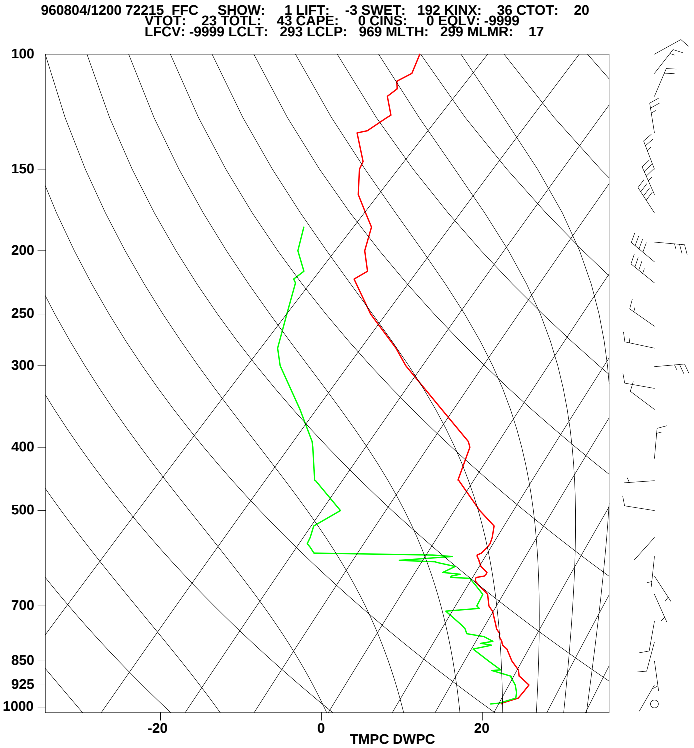

Figure E.18: 1200 UTC 04 August 1996 skew–T / log–P diagram.

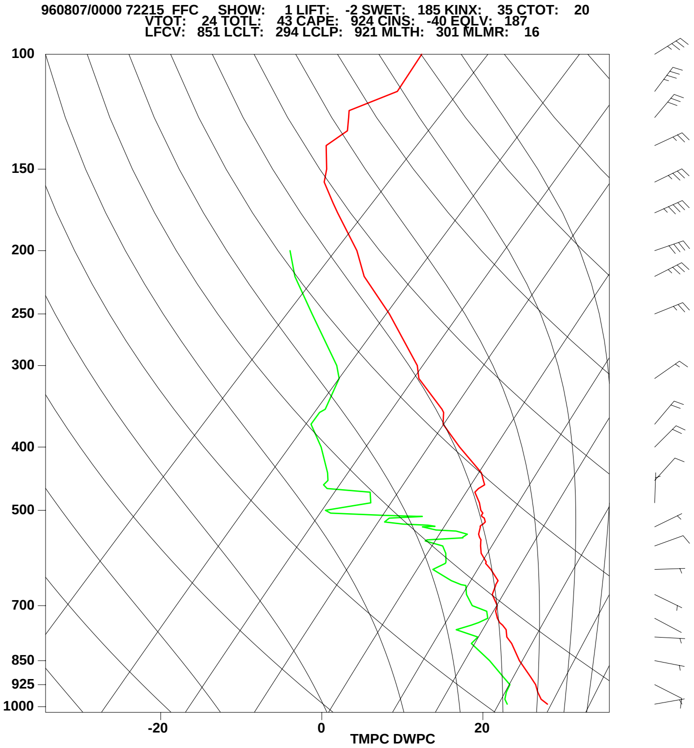

Figure E.19: 0000 UTC 07 August 1996 skew–T / log–P diagram.

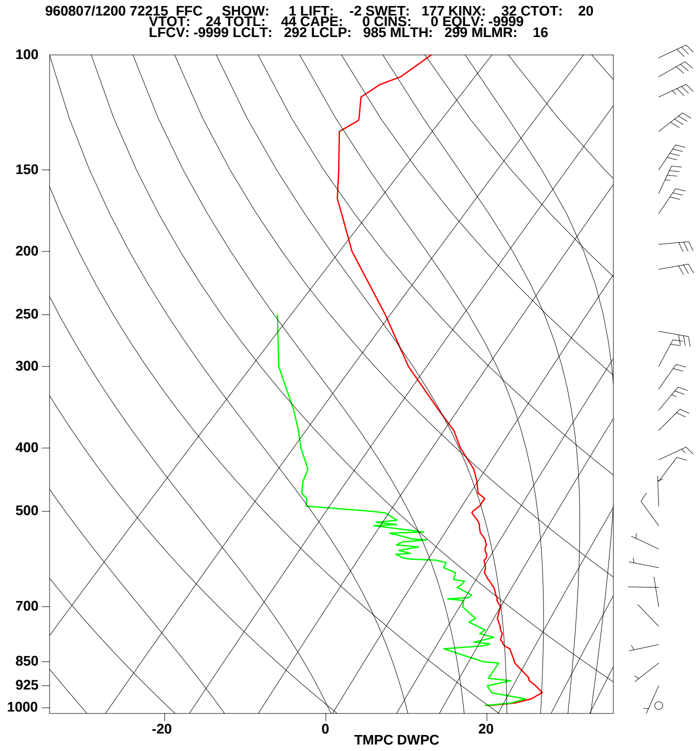

Figure E.20: 1200 UTC 07 August 1996 skew–T / log–P diagram.

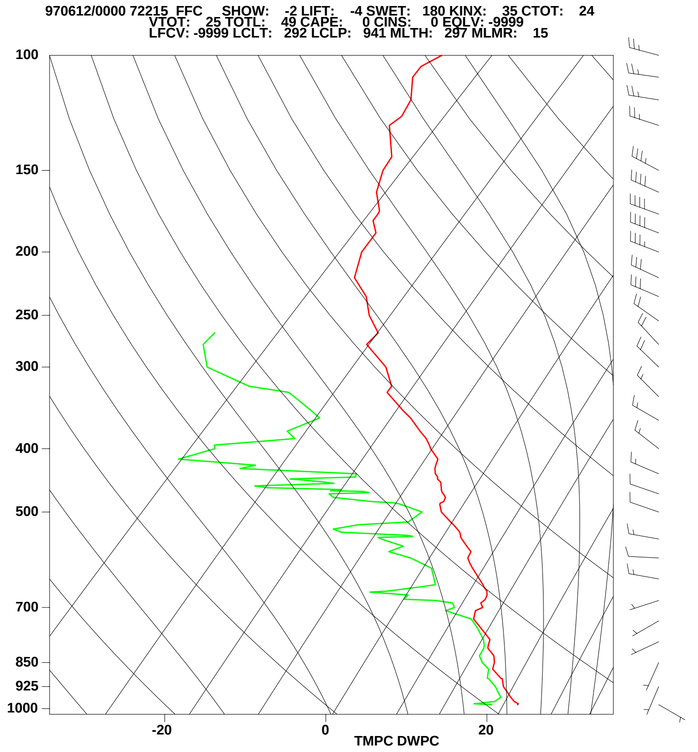

Figure E.21: 0000 UTC 12 June 1997 skew–T / log–P diagram.

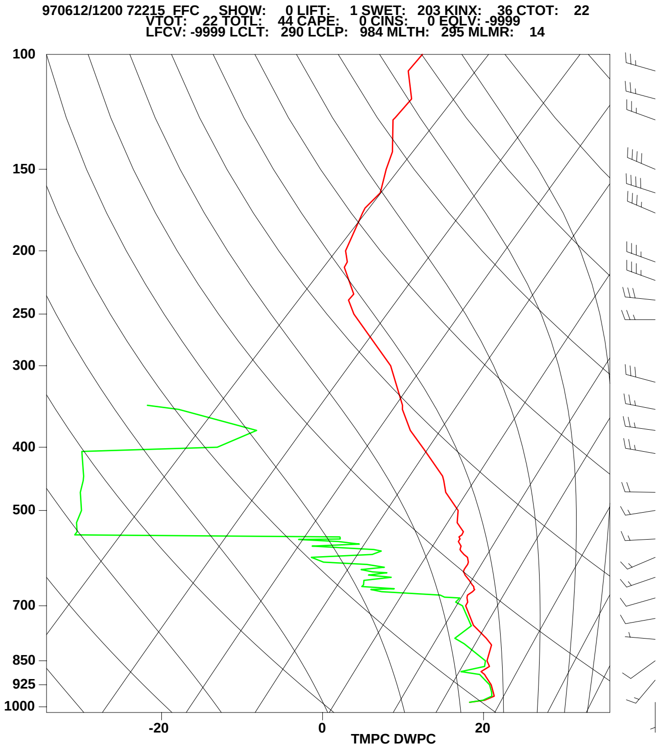

Figure E.22: 1200 UTC 12 June 1996 skew–T / log–P diagram.

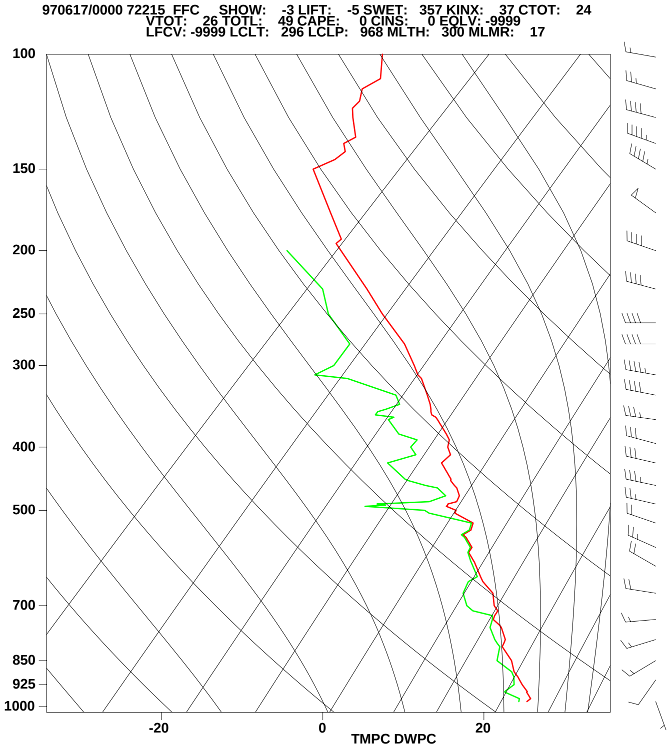

Figure E.23: 0000 UTC 17 June 1997 skew–T / log–P diagram.

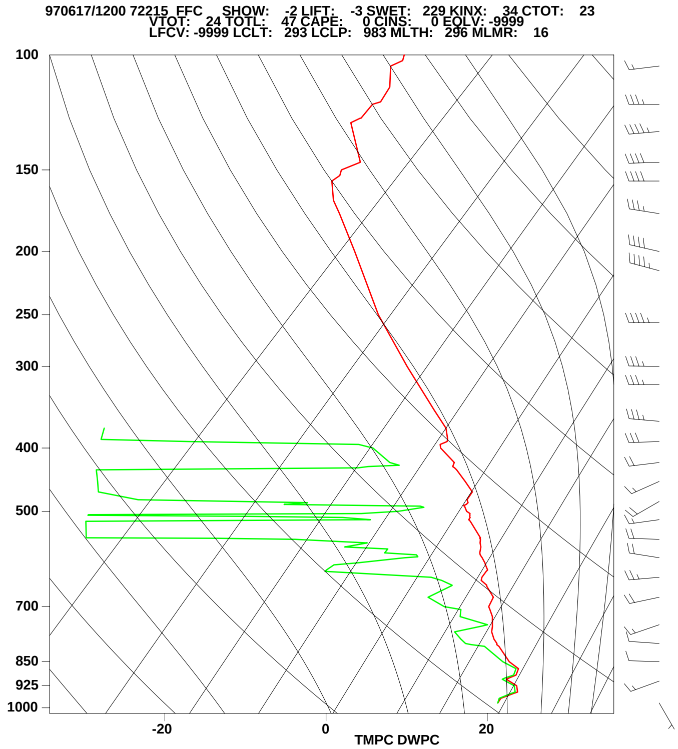

Figure E.24: 1200 UTC 17 June 1997 skew–T / log–P diagram.

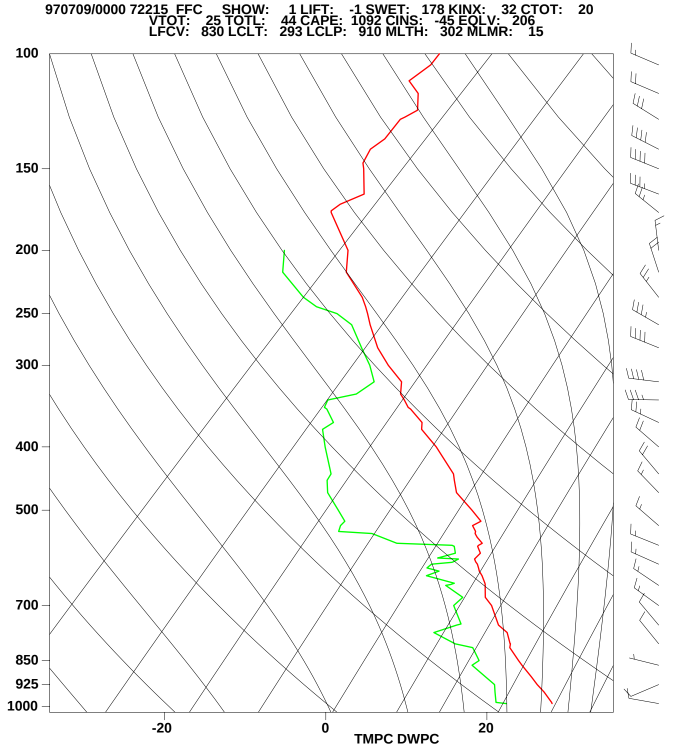

Figure E.25: 0000 UTC 09 July 1997 skew–T / log–P diagram.

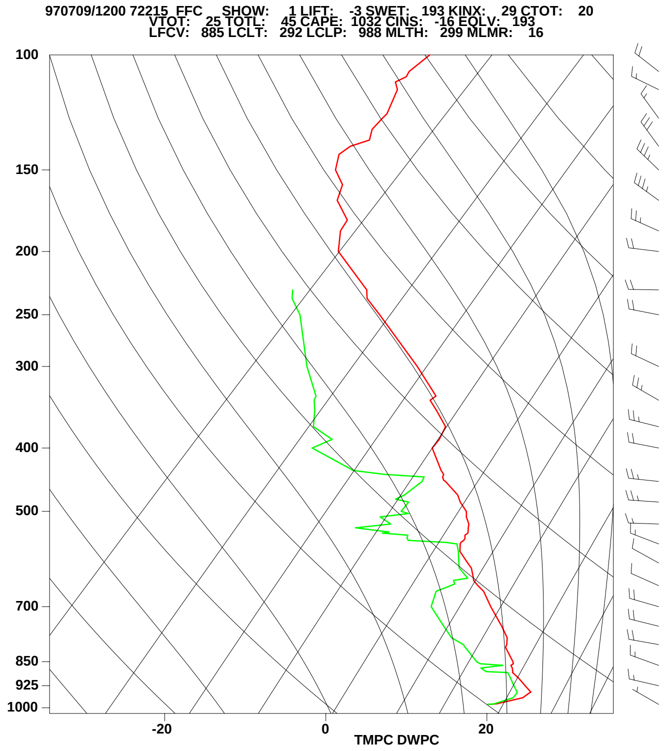

Figure E.26: 1200 UTC 09 July 1997 skew–T / log–P diagram.

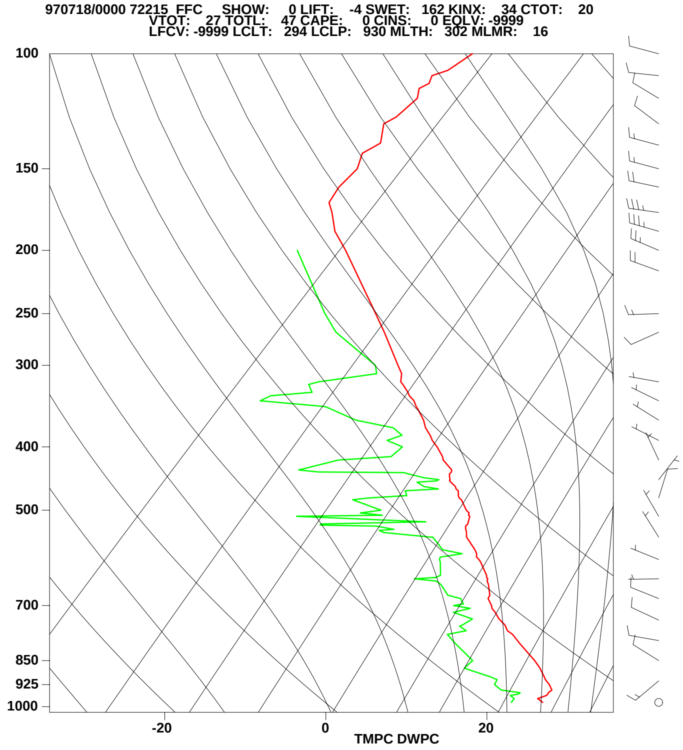

Figure E.27: 0000 UTC 18 July 1997 skew–T / log–P diagram.

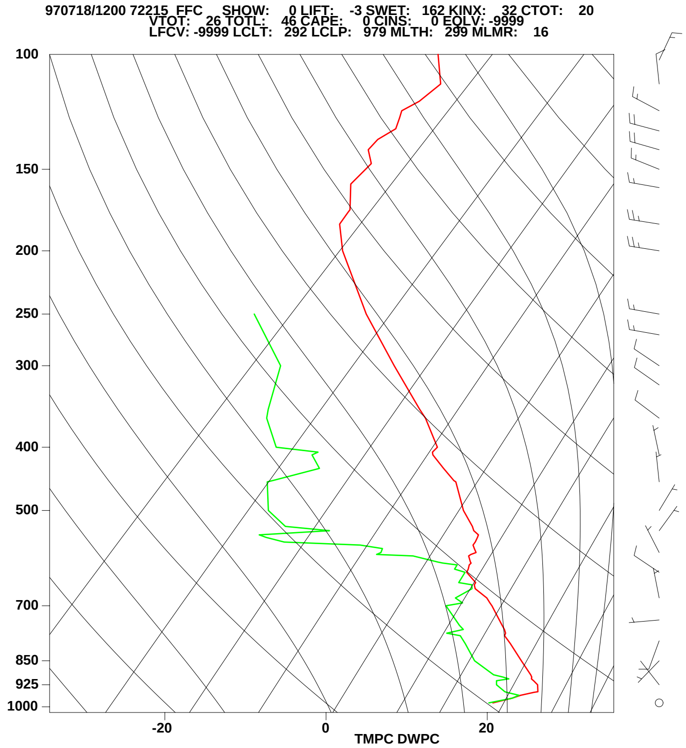

Figure E.28: 1200 UTC 18 July 1997 skew–T / log–P diagram.

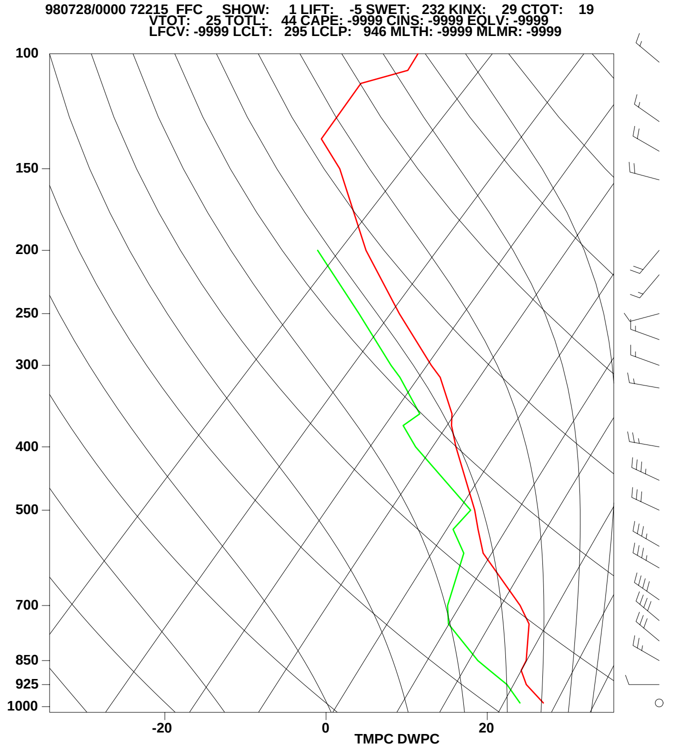

Figure E.29: 0000 UTC 28 July 1998 skew–T / log–P diagram.

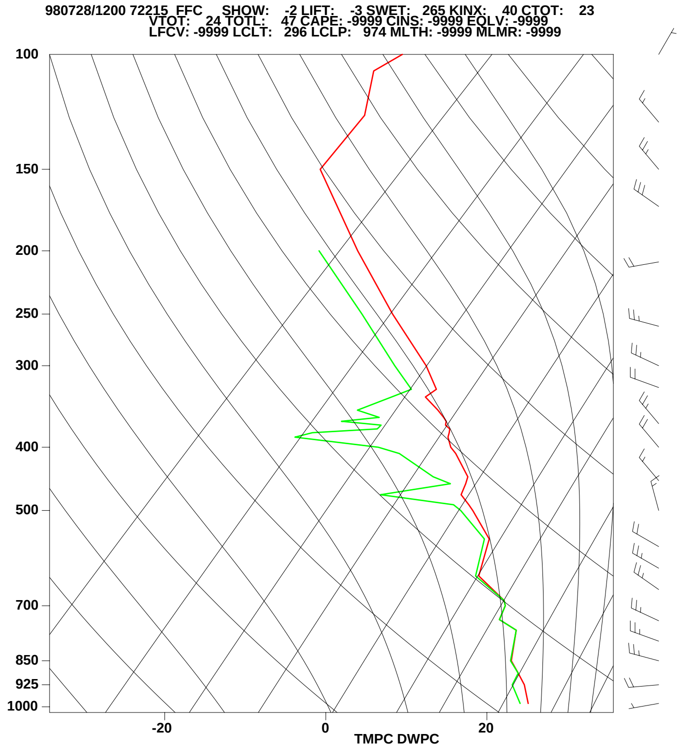

Figure E.30: 1200 UTC 28 July 1998 skew–T / log–P diagram.

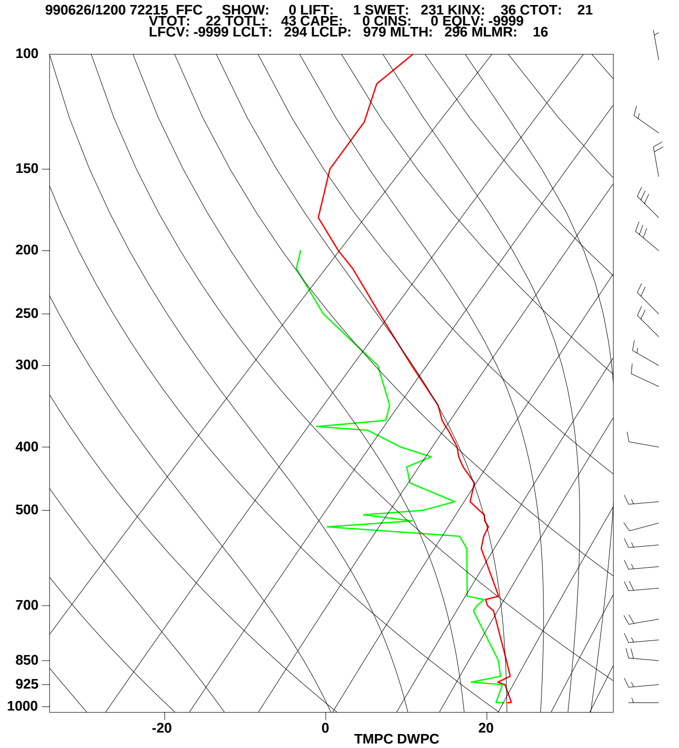

Figure E.31: 1200 UTC 26 June 1999 skew–T / log–P diagram.

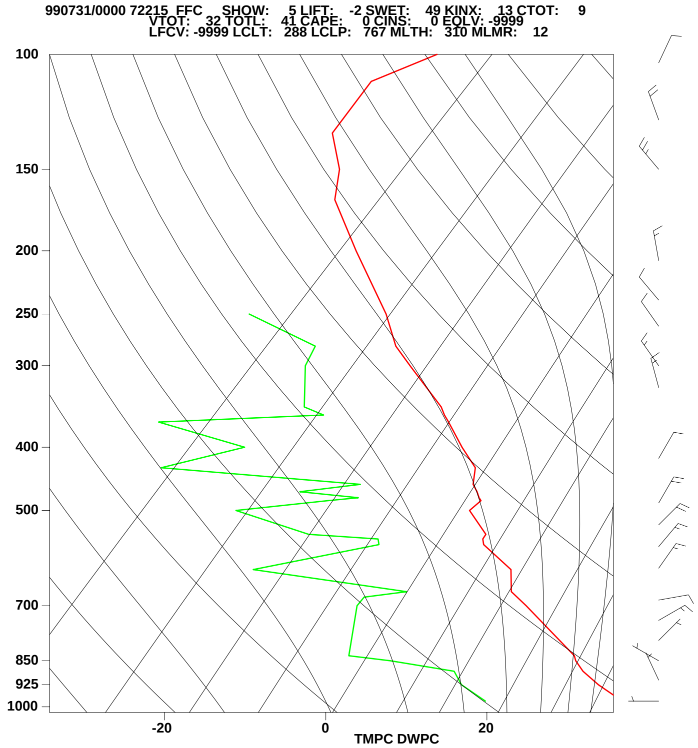

Figure E.32: 0000 UTC 31 July 1999 skew–T / log–P diagram.

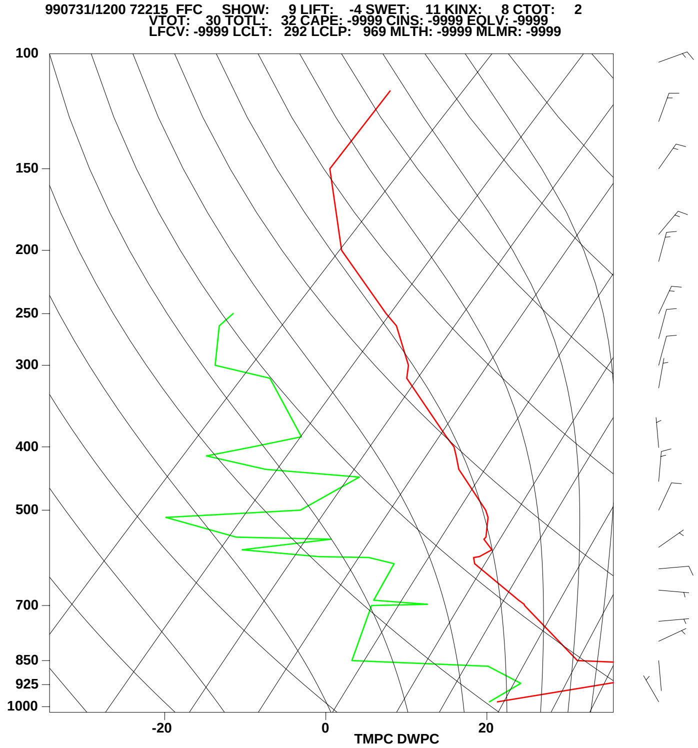

Figure E.33: 1200 UTC 31 July 1999 skew–T / log–P diagram.

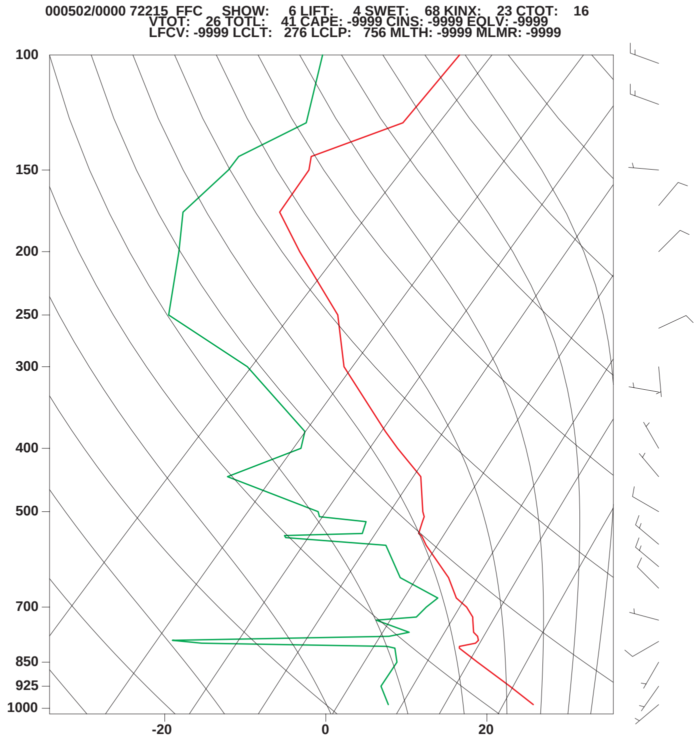

Figure E.34: 0000 UTC 02 May 2000 skew–T / log–P diagram.

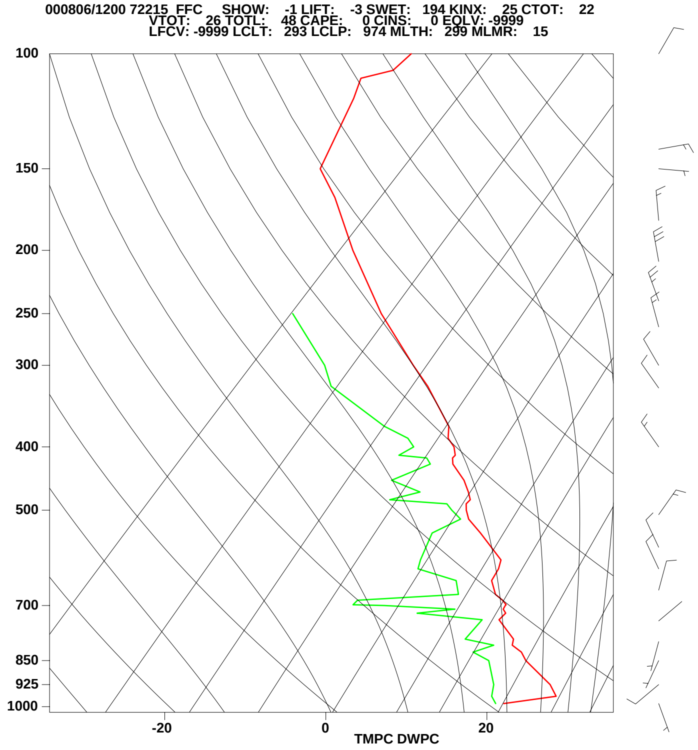

Figure E.35: 1200 UTC 06 August 2000 skew–T / log–P diagram.

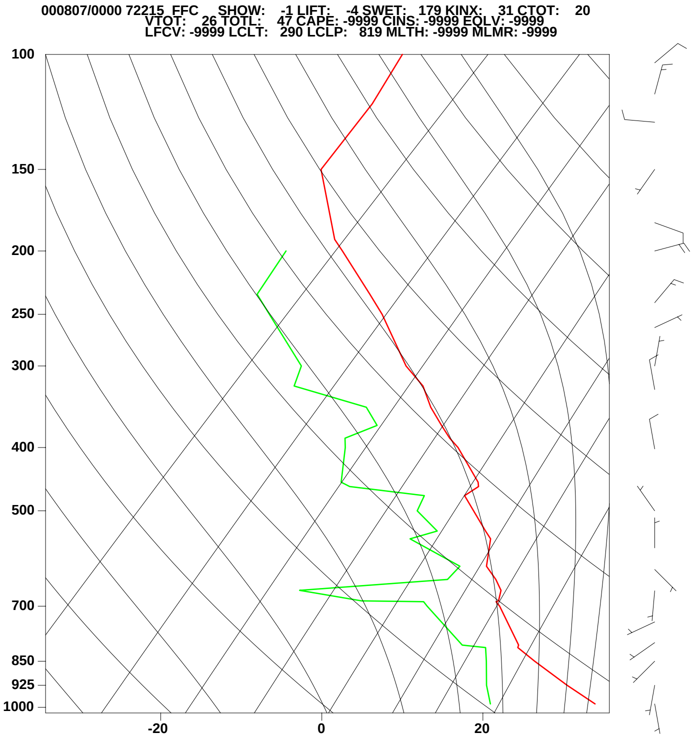

Figure E.36: 0000 UTC 07 August 2000 skew–T / log–P diagram.